UNIVERSITY OF CALIFORNIA, MERCED

SUMOylation is a regulator of regional cell fate and genomic integrity in planarians

by

Manish Thiruvalluvan

A dissertation submitted in satisfaction of the requirements
for the degree Doctor of Philosophy

in

Quantitative and Systems Biology

Committee in Charge:

Professor Kirk Jensen, Chair
Professor Jennifer Manilay, Member
Professor Anna Beaudin, Member
Professor Néstor J. Oviedo, Advisor

2018

The dissertation of Manish Thiruvalluvan is approved, and it is acceptable in quality and form for publication on microfilm and electronically:

Jennifer Manilay

Anna Beaudin

Kirk Jensen, Chair

University of California, Merced

2018

TABLE OF CONTENTS

LIST OF FIGURES

LIST OF ABBREVIATIONS

1. *Smed* – Schmidtea mediterranea
2. DSB – double stranded breaks
3. SUMO pathway – includes the entire signaling pathway, including the SUMO enzymes
4. SUMO - small-ubiquitin like modifier
5. DDR – DNA damage repair
6. DSBs – double stranded breaks
7. ASCs – Adult stem cells
8. SENP – sentrin specific protease
9. SAE1/2 – SUMO activating enzyme subunit 1/2
10. Hh – Hedgehog
11. Ptc – Patched
12. Smo -Smoothened
13. Sfrp1 – secreted frizzled like protein 1
14. Fz4 – frizzled like protein 1
15. AP axis - anteroposterior axis
16. DNA damage and repair – DDR
17. ROS – reactive oxygen species
18. *D. melanogaster* – drosophila melanogaster
19. *C. elegans* - Caenorhabditis elegans
20. BRCA1 – breast cancer associated 1
21. XRCC4 - X-ray repair cross-complementing protein 4
22. Ku70 - Lupus Ku autoantigen protein p70
23. ATM - ATM serine/threonine kinase
24. ATR - ataxia telangiectasia and Rad3 related
25. RANGAP1 - Ran GTPase Activating Protein 1
26. RanBP2 - RAN Binding Protein 2
27. PIAS - protein inhibitor of activated STAT
28. H2Ax - H2A histone family, member X
29. PTEN - Phosphatase and tensin homolog
30. COMET - single cell gel electrophoresis
31. MADD - MAP kinase activating death domain
32. Rb – retinoblastoma protein
33. p53 – tumor protein p53

ACKNOWLEDGEMENTS

First, I want to thank Dr. Nestor Oviedo for believing in me ever since he took me in as an undergraduate and encouraged me to get my PhD when all other paths were closed. He has helped me not only becoming a better scientist, but a better teacher and a better person. I greatly enjoyed my time working with him and sincerely appreciate everything he has done for me. In the same vein, I would like to thank all members of my lab, especially Paul, who has helped me immensely in carrying out experiments. It was my pleasure to work day in and day out with my colleagues who made the tedious process of bench work more enjoyable.

Special thanks to Dr. David Ardell and Melanie LeGro for their work with transcriptomic analysis as this data drove the late stages of my research. I would also like to thank members of my committee, Dr. Jennifer Manilay, Dr. Anna Beaudin and Dr. Kirk Jensen, who stuck with me and helped me finish my doctoral journey. In addition, I would like to thank Dr. Limor Broday and her lab for their expertise in SUMOylation and for helping bring forth and develop this idea into a successful project.

I am extremely grateful to my parents for bringing me to this country and providing me with a once in a lifetime opportunity to pursue higher education. Finally, I want to thank my wife Sandra, who has been at my side for most of my adult life and has encouraged me to pursue and achieve my dreams. When I started my PhD, I was twenty-one and just graduated college. Now, I’m a husband and father to my son Alex. Without her help, I would not have been able to come this far.

CURRICULUM VITAE

Manish Thiruvalluvan
Ph.D. Quantitative and Systems Biology
School of Natural Sciences
5200 N Lake Rd, Merced, CA 95340
(408) 910-9028 | ezmotts@gmail.com

I. EDUCATION

2013 – present Ph.D., Quantitative and Systems Biology, University of California Merced

- Worked with the planarian model system to study stem cell proliferation and regeneration
- Conceived, developed and conducted independent research directed at identifying the molecular mechanism behind differential rates of cancer formation
- Identified epigenetic modifications through UBC9 and the SUMOylation is responsible for regulating regional maintenance of cell survival and DNA damage in the adult body
- Presented my research at various conferences and meetings around the United States
- Dissertation: Role of SUMOylation in stem cell regulation and DNA damage repair in planarians
- Advisor: Nestor J. Oviedo

2009 – 2013 Bachelor of Science, Human Biology, University of California Merced (Cum Laude)

- Dean's List: Awarded four times
- Academic Chair of Hermanos Unidos Organization, 2011-2013
- Leadership position in Tae Kwon Do Club, 2010-2012

2007 – 2011 Stockton Delta College

- Attended part time as a high school student and undergraduate
- Classes Taken: Psychology, Writing, Statistics, Mythology, Music Theory and Speech

II. PUBLICATIONS

1. **Thiruvalluvan, M.**, Barghouth, P. G., Tsur, A., Broday, L., & Oviedo, N. J. (2018). SUMOylation controls stem cell proliferation and regional cell death through Hedgehog signaling in planarians. Cellular and Molecular Life Sciences: CMLS, 75(7), 1285–1301. https://doi.org/10.1007/s00018-017-2697-4

2. Barghouth, P. G., **Thiruvalluvan, M.**, LeGro, M., & Oviedo, N. J. (2018). DNA damage and tissue repair: What we can learn from planaria. Seminars in Cell & Developmental Biology. https://doi.org/10.1016/j.semcdb.2018.04.013

3. Barghouth, P. G.*, **Thiruvalluvan, M.***, & Oviedo, N. J. (2015). Bioelectrical regulation of cell cycle and the planarian model system. Biochim Biophys Acta, 1848(10 Pt B), 2629–2637. https://doi.org/10.1016/j.bbamem.2015.02.024
*equal contribution

III. HONORS, FELLOWSHIPS AND GRANTS

2016 Graduate Summer Research Fellowship, University of California Merced
2015 Graduate Summer Research Fellowship, University of California Merced
2015 Travel Grant, Quantitative and Systems Biology, University of California Merced
2015 Travel Grant, Society for Developmental Biology
2014 Travel Grant, Quantitative and Systems Biology, University of California Merced
2011 Grossman Scholar's Award, School of Natural Sciences, University of California Merced

IV. CONFERENCES AND MEETINGS

2018 Oral Presentation, International Planarian Meeting, Madison, USA
2017 Oral Presentation, Molecular Cell Biology Seminar, Merced, USA
2016 Poster Presentation, Quantitative and Systems Biology Seminar, Merced, USA
2015 Society for Developmental Biology Conference, Yosemite, USA
2015 Poster Presentation, Quantitative and Systems Biology Seminar, Merced, USA
2015 National Planarian Meeting, Chicago, USA
2015 Society for Developmental Biology Conference, Seattle, USA

V. EMPLOYMENT

2013 – 2017 Teaching Assistant, School of Natural Sciences, University of California Merced

- Instructed numerous undergraduate biology courses of at least fifty students
- Developed syllabus and course materials, including weekly lab practicum and administered all grades
- Evaluated laboratory write-ups, graded exam and provided online course materials
- Collaborated to create interesting course plans to meet academic, intellectual and social needs

VI. SKILLS

- Knowledge of wide range of research methodologies: animal husbandry (planarians), RNA interference, RNA isolation, cloning, reverse transcription, immunofluorescence, flow cytometry, PCR, gel electrophoresis, karyotyping, COMET, TUNEL

- Authorized by the Nuclear Regulatory Commission to work with radioactive materials
- Microsoft Office Suite, Adobe Photoshop and Illustrator, Graphpad Prism, Endnote, Zotero and ImageJ
- Operating Systems: Unix, Windows Vista, XP, 8 and 10, MAC OSX
- Regularly supervised exams for undergraduate students and have supervised the undergraduate research projects of 2 final year students.
- Writing grants and presenting reports
- Current and clean driving license
- Can read and speak Spanish; fluent in Tamil and English

VII. PROFESSIONAL MEMBERSHIPS

2015 – present Society for Developmental Biology

VIII. REFERENCES

- Nestor J. Oviedo, Molecular and Cell Biology, University of California Merced; noviedo2@ucmerced.edu
- Kirk Jensen, Molecular and Cell Biology, University of California Merced; kjensen5@ucmerced.edu
- Jennifer Manilay, Molecular and Cell Biology, University of California Merced; jmanilay@ucmerced.edu

ABSTRACT

SUMOylation is a regulator of regional cell fate and genomic integrity in planarians

Manish Thiruvalluvan
Ph.D. in Quantitative and Systems Biology
University of California, Merced
2018

Regional signals along the anteroposterior (AP) body axis influence the growth of normal and neoplastic cells. The regenerative response, cellular turnover and the aggressiveness of proliferative cells are superior in the top-half of the body than in the posterior region. However, the mechanisms underlying regional differences in the adult body have yet to be elucidated. Studies in several model systems have suggested that SUMO modification system may be responsible for regulating the regional survival of cells. Small ubiquitin-like modifier (SUMO) proteins can alter function of other proteins through reversible post-translational modification. SUMOylation has been implicated in a range of processes associated with the regulation of cellular fate decisions during cell cycle progression and apoptosis. The planarian flatworm *Schmidtea mediterranea* is an emerging model organism that allows analysis of stem cell-mediated tissue turnover and regeneration in the context of the whole body. We identify that post-translational modifications through SUMOylation are evolutionarily conserved in the Lophotrochozoan *Schmidtea mediterranea*. Disruption of SUMOylation with RNA-interference of the E2 conjugating enzyme UBC9 lead to regional defects characterized by loss of the posterior half of the body and lethality. In addition, UBC9 RNAi uniformly reduced the number of adult stem cells in planaria, which was linked to an inability for cells to undergo proper cell cycle transition. In addition, the loss of tail phenotype was determined to be caused by a marked increase in cell death specific to the posterior. Further evidence indicates that UBC9-induced regional cell death is due to inhibition of Hedgehog signaling through an early increase in expression of its repressor Patched, a regional-specific cue. Furthermore, UBC9 is essential for planarians to mount a robust regenerative response to injury, suggesting a novel function for the SUMOylation pathway. Our results evaluating UBC9 function in the adult organism uncover that in addition to organ specific and systemic events, SUMOylation also regulates regional cell fate during tissue renewal and regeneration.

Intriguingly, UBC9 downregulation leads to loss of genomic integrity characterized by the appearance of double stranded breaks and abnormal chromosomes throughout the planarian body axis. It was found that UBC9 knockdown restricts nuclear translocation of RAD51, a key regulator of homologous recombination repair. However, some cells in near the head continued to proliferate with DNA damage, leading to a cancer-like state. To

dissect the molecular events driving anterior tissues survival in the presence of DNA damage, we performed RNA sequencing on anterior and posterior fragments from control and UBC9 RNAi animals. Our analysis revealed 37 differentially regulated genes that are specific to the anterior region of UBC9 animals. One of these genes, MADD (MAP kinase activating death domain), is known to act as a negative regulator of apoptosis and is overexpressed in neoplastic cells. In planarians, MADD is predominantly expressed in the nervous system and confined to post-mitotic cells. To better characterize MADD function, we downregulated its expression via RNAi. Knockdown of MADD led planarians to oversecrete mucous, fission excessively and exhibit poor motor function. MADD RNAi animals displayed a regional difference in mitotic activity across the AP axis, where stem cells were lost in the anterior but not in the posterior. In addition, MADD knockdown animals were unable to fully regenerate their cephalic ganglia and displayed reduced mitotic activity after amputation. Additionally, double knockdown of MADD and UBC9 lead to a rescue of the morphological defects associated with the UBC9 phenotype. Superficially, MADD knockdown attenuates the dramatic increase in posterior cell death in UBC9 RNAi animals that leads to posterior tissue loss. Taken together, these findings suggest MADD is a regional regulator of cell death and long-range neural signals play an important role in determining cell fate across the planarian body axis. Furthermore, this finding is critical as it provides validation of our transcriptomic analysis and approach to identify novel regulators of regional tissue maintenance.

1. INTRODUCTION

1.1. Regional signals influence cell fate decisions in health and disease

An adult human replaces billions of cells every single day[1,2]. In order to accomplish this gargantuan task, a delicate balance between cellular division and programmed cell death must be established to maintain tissue stability within tissues and organs. In most cases, adult tissue homeostasis is mediated by resident adult stem cells (ASCs), which can self-renew, differentiate and generate lineage-restricted cellular progeny that carry out tissue specific functions in normal, stressed or aged tissues[3–7]. Therefore, these ASCs drive tissue repair, maintenance and regeneration throughout an organism's lifespan. However, constant renewal can be prone to error and provide recurrent opportunities for tissue atrophy, aging phenotypes and cancer development.

Various signals, both local and systemic, are required for the proper regulation of these stem cells so they faithfully maintain tissue integrity and longevity of the organism[3,8]. One of these essential cues are regional signals along the AP axis that influence cellular fate decisions. Various studies in immunology, regeneration, carcinogenesis, and developmental biology indicate there are patterns of regional differences in cell proliferation across the adult AP body axis[9–13]. These regional differences in cellular proliferation are evolutionarily conserved across a wide range of animals[9]. Studies in the 1980s have shown that mice exposed to carcinogens developed tumors at much faster rate in the anterior region than the posterior region[14,15]. For example, topical treatment with carcinogens and transplanted cancer cells are more aggressive and transform faster when located in the anterior region of the body[15]. In addition, during regeneration, wound induced-cellular proliferation and the healing response are more robust when tissue damage is in the anterior region than in posterior parts of the body[16]. Several general ideas were proposed to explain the basis of this phenomenon, such as increased vasculature near the head and the presence of nervous tissue, but a concrete paradigm uniting signaling mechanisms and region-specific cues has yet to be elucidated.

This phenomenon is not only unique to experimental models but is also evident in human health. Several studies have found that various human cancers exhibit regional preferences when it comes to their location of incidence and proliferative capability. For example, the site of the initial development of melanomas lead to poorer patient survival rates if they arise more relative to the neck and head areas than the rest of the body[17,18]. Other cancers such as pancreatic cancer, colorectal cancer and adenocarcinomas also display this same behavior within the organs in which they develop[19–23]. The discrepancy in the rates of patient survival can be as high as thirty percent across the various cancers types depending on their origin in the human body[17,18]. Despite the central relevance to health and disease, the underlying mechanisms controlling regional

cell fate decisions in the AP axis remain poorly understood. Identifying the molecular mechanisms behind this phenomenon would provide the foundation for the discovery of novel drug targets and development of therapeutic strategies to combat these human cancers. To better understand the mechanisms leading to differential maintenance of cell proliferation, we searched for phenotypes involving regional defects across various experimental models. It was found that disruption of the SUMOylation pathway, a type of post-translational modification, through the downregulation of the UBC9 gene lead to regional abnormalities in multiple animal models[24–26]. Targeting SUMOylation through UBC9 may provide a powerful venue for understanding how regional signals along body axis regulate cell proliferation and tissue homeostasis.

1.2. SUMOylation - a type of post-translational modification

Post-translational modifications of proteins are a key component of the cellular toolkit to alter protein function, activity or localization after their synthesis. More than 500 post-translational modifications are known to date, demonstrating the immense potential of these signals in fine-tuning major and minor biochemical processes within the cell. In some cases, these modifications are due to protein attachments, with ubiquitin being the most well-known protein. In the late 90s, scientists studying ubiquitination discovered a number of enzymes related to ubiquitin that they named small-ubiquitin like modifier (SUMO)[27]. SUMOylation is a type of post-translational modification that alters protein function in numerous ways rather than simply flagging them for degradation[27,28]. SUMOylation has been shown to be evolutionarily conserved from yeast to humans and is now strongly established as one of the key regulatory protein modifications in eukaryotic cells[29–31]. SUMOylation is enriched in the nucleus and has been most intensely studied in this context[32–36]. It is responsible for a myriad of nuclear and chromatin-associated functions, including transcription, DNA Repair, chromatin remodeling, facilitating ordered assembly, intercellular transport, mitosis, macromolecular assembly, protein homeostasis, trafficking, and signal transduction[31,37–40]. A key property of SUMOylation is its reversible nature, which allows it to act as a molecular switch that quickly controls protein activity. This process is thought to be transient as it is extremely difficult to capture proteins in their SUMOylated state as only 5% of proteins are attached to SUMO at any one time[27,28]. In addition, this response seems to be stress related, as SUMOylation is massively upregulated after exposure to DNA damage agents and ROS stress, which in turn causes a reduction in transcription as a whole[41,42].

SUMOylation is a dynamic process that requires the cooperation of several key components to successfully modify proteins and alter their function[29,40] (Fig 1A). Initially, the cell produces an immature version of the SUMO protein, which is 101 amino acids in length and contains a B-grasp ubiquitin fold and a diglycine motif on its C-terminus end, masked by hydrophobic amino acid residues. Several SUMO proteins have been identified in the established literature, with up to four

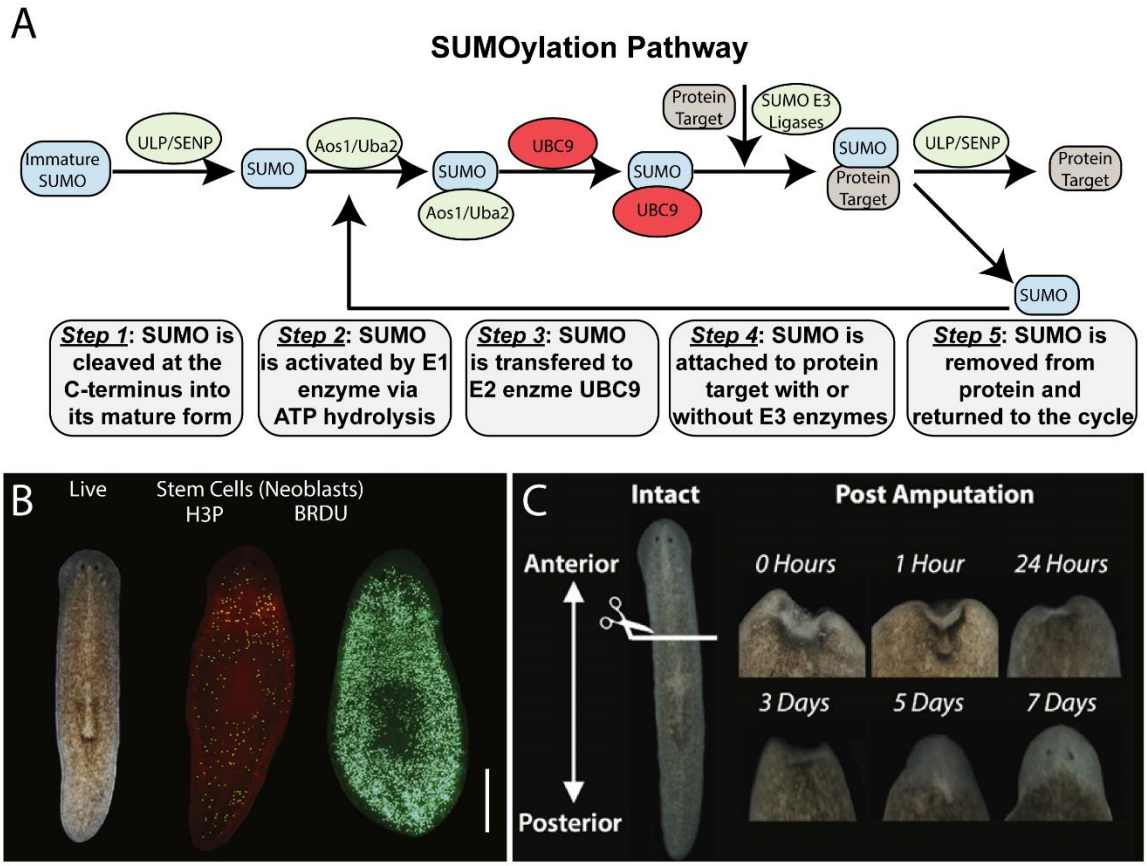

Figure 1: SUMOylation and the planarian model system. A) A general outline of the SUMOylation pathway with the names of all enzymes involved and a brief description of each step of the process. B) Left to right. Live worm, whole-mount immunohistochemistry (WIHC) to stain cells in different parts of the cell cycle, including mitotic cells alone (H3P) and cells entering S phase of the cell cycle (BRDU positive cells, green dots indicate proliferative cells). Scale bars = 200 µm. C) Images of a live worm (left) amputated into three fragments (anterior, trunk and posterior); images on the right show the regeneration of these fragments. Day 1 fragments show proper wound response and blastema formation and by day 7, all fragments have regenerated into completely functional animals.

homologs in humans (SUMO1, SUMO2, SUMO3 and SUMO4)[27]. The consensus is that these proteins specifically target different sets of signaling proteins and thus have different functions within the cell. Thereafter, SUMO proteases or SENPS recognize the immature SUMO and proteolytically cleave the hydrophobic portion of the SUMO C-terminus to reveal the diglycine residues. Once mature, the SUMO protein is activated by the SUMO heterodimer SAE1/SAE2 in an ATP-consuming step that results in the formation of a thioester bond between the glycine of SUMO and the catalytic cysteine 173 on SAE2. After this, SUMO is transferred to the catalytic cysteine on the E2 conjugating enzyme UBC9. At this point, UBC9 can transfer SUMO to a consensus motif surrounding a lysine residue on a target protein. What makes UBC9 crucial to the proper function of this pathway is that it can single handedly determine whether to put SUMO onto another protein or coordinate with E3 ligases to pick its target[43]. Due to this function, UBC9 is known to be the linchpin controlling the SUMOylation pathway and acts as a rate-limiting step for SUMO conjugation[27]. Finally, SUMO attachment to the target protein has a strong impact on its function, as it can affect protein localization, stability, protein–protein interaction, cause conformational changes or act as a hub to form multi-protein complexes[29,40,44]. After the target protein has performed its function, SENPs bind to the SUMO/protein complex and rapidly deconjugate the SUMO proteins, which either rejoin the cycle or are quickly degraded.

Studies across several model systems have demonstrated that SUMO pathway proteins are critical to proliferating cells[45–50]. Knockout of SUMO genes is embryonically lethal and most of our understanding on the regulation of this signaling pathway has been obtained through work mostly performed *in vitro* or during early development[51–53]. In yeast, SUMO depleted cells arrest in G2/M phase, display massive accumulation of DNA with a single nucleus severely impaired in growth and exhibit chromosomal abnormalities[54,55]. Conditional depletion of UBC9 in chicken DT40 cells leads to an increase in the number of cells containing multiple or fragmented nuclei, with most of these cells dying by apoptosis[56]. Moving onto more complex models, UBC9 or SUMO RNAi knockdown experiments in *C. elegans* result in embryonic arrest after gastrulation and massive defects in larval development[57]. In *D. melanogaster*, the UBC9 lethal mutants show attenuated spindle formation and blockage in nuclear import during embryogenesis, limiting cell proliferation[25]. In zebrafish, UBC9 knockout leads to early embryonic death via loss of cartilage progenitor cells and massively increased cell death in the posterior arches[24]. Finally, UBC9 knockout mice embryos fail to expand past the initial stages, although the blastocysts themselves are at least viable for two days before dying[51]. SUMO1 knockout does not produce any credible effects, but SUMO2 is essential for early mouse development[58]. A conditional knockout of UBC9 in the gut of adult mice led to collapse of the proliferative cell compartment and rapid depletion of stem cells[57]. These studies reveal that SUMOylation allows for complex and precise control of cell processes in a wide range of model systems. The striking dependency of proliferating cells

on reversible SUMOylation provides one of the rationales for targeting the SUMO pathway in cancer therapy[59–63].

In addition, mounting evidence suggests SUMO regulation of proliferative cells is dependent on its critical role in DNA damage and repair (DDR). SUMO modification is thought to regulate DDR from the initial sensing stage to the final steps of repair[64–67]. DNA is ubiquitous to life and acts as the molecular blueprint for cells to carry out essential functions. Consequently, its integrity is vital for the survival of the organism[68–70]. For example, SUMO1, SUMO3 and UBC9 have been seen to accumulate at DSB sites within minutes after laser induced DNA damage and lead to a repressed chromatin state[71,72]. Initial sensors of DNA damage such as PARP1 were found to be targets of SUMOylation[73]. In particular, SUMO modification is essential for repair of double stranded breaks (DSBs) through non-homologous end-joining (NHEF) and homologous recombination (HR). Several NHEJ factors must be SUMOylated for proper function, such as the nuclear localization of XRCC4 and DNA association of Ku70[32,74]. One of the initial sensors of DSBs is BRCA1, which must be SUMOylated to bind to sites of DNA damage and to perform its ubiquitin ligase activity[75,76]. In addition, SUMO deconjugation of ATM checkpoint mediator protein MDC1, whose recruitment to damage sites via binding to phosphorylated H2AX, is required to bring about repair involved with RanGAP1 and RanBP2 proteins[77,78]. SUMOylation plays an extensive role in regulating the proper function of RAD51, which is vitally important for strand selection and successful repair via homologous recombination[72,79,80]. SUMOylation facilitates recruitment of RAD51 to the sites of DSB directly via UBC9 and PIAS1/4 and indirectly by SUMOylation RPA and facilitating its exchange for RAD51[33,79,80]. Taken together, these studies suggest a critical role for SUMOylation in maintaining genomic integrity by faithfully coordinating DNA repair allows proper proliferation of stem cell to renew damaged tissues and maintain longevity of the organism.

Through our exploration of the existing SUMO literature, we identified that the SUMO pathway may be crucial for the differential regulation of proliferative cells across the adult body. We noticed that disruption of UBC9 function via gene delete led to AP axis abnormalities and regional defects during embryonic development in *C. elegans*, drosophila and zebrafish[24–26]. As stated before, the SUMOylation cascade requires UBC9 to conjugate the SUMO proteins to target proteins to regulate their function. UBC9 knockdown in *C.elegans* leads to curling of the tail and impaired movement[26]. Drosophila larvae and zebrafish embryos displayed smaller heads and deformed scaling of their body axis[24,25]. These defects are due to decreased cell proliferation or increased cell death in the anterior and a general loss of the native stem cell population. In all three cases, animals do not survive past the early embryonic stages into adulthood, demonstrating that UBC9 is essential for development and survival of the animal. These observations suggested that a UBC9 and SUMOylation could be a potential candidate for understanding the phenomenon underlying regional differences in

cancer proliferation across the adult body. Since inactivation of UBC9 is embryonically lethal, it limits our understanding about the role of SUMOylation in the maintenance and cellular turnover in adult tissues. Furthermore, there has been limited effort to establish the relationship between SUMOylation and regional differences that stem from its dysfunction. To address this problem, we required the use of an alternative model that can bypass the embryonic lethality of SUMO pathway components to better characterize its role in the adult organism.

1.3. The planarian model *Schmidtea mediterranea*

The planarian *Schmidtea mediterranea* (*Smed)* provides unique opportunities to dissect mechanisms controlling cellular decisions in the adult body. They are bilaterally symmetrical, triploblastic animals belonging to the phylum Platyhelminthes[16]. Planarians can reproduce by sexual or asexual means, have a stable diploid state and a relatively small genome[81,82]. They have a complex body plan consisting of brain primordia, ventral cords, protonephridia, digestive system and an all-encompassing mesenchyme that fills the body cavity[16,83,84]. Planarians are well known for their large population of versatile adult pluripotent stem cells called neoblasts (Fig 1B). Planarians utilize their vast pool of neoblasts to maintain a high rate of cellular turnover and tissue homeostasis[84–86]. Since the neoblast is the only dividing cell in the entire planaria, γ-irradiation provides a useful tool to eliminate neoblast and study their function in many different contexts[87,88]. Neoblasts give rise to the 40 different types of cells characterized in their body plan and are themselves a heterogenous pool of cells with varying levels of potency[89–91]. One population of neoblasts, termed clonogenic or NB2 neoblasts, are thought to be truly pluripotent as they can rescue animals who have lost all their proliferative capabilities due to irradiation[87,89]. In addition to maintaining cellular turnover, these stem cells also fuel robust regeneration in the planarian, allowing a fragment approximately 1/273th the size of a normal planarian to regenerate the complete organism[16]. This ability is fueled by increasing the levels of cellular proliferation at wound sites which helps them recover from all manner of injury[81,84,92,93] (Fig 1C). Studying these stem cells can help us identify the role of SUMOylation during cellular proliferation and differentiation at the organismal scale while simultaneously looking at the molecular components underlying SUMO-associated responses.

In addition, *S. mediterranea* has several other characteristics that are extremely useful for studying SUMOylation and understanding its role in the regional maintenance of cell proliferation. Planarians are constitutive adults, meaning they do not age and are seemingly immortal[81]. This allows for investigation of signaling pathways in post-embryonic stages of development as well as study stem cell function. So far, the SUMO pathway function could not be understood in adult organisms due to embryonic lethality of its components, so this could help overcome that limitation. Next, signals controlling their AP axis have been thoroughly characterized, making it possible to pinpoint exactly which cells

are responsible for determining cell fate in a specific part of the body axis[12,94]. Planarians are susceptible to cancer formation, which was clearly shown via the downregulation of the tumor suppressor PTEN[13]. Since the early 2000s, a myriad of molecular tools have been developed to study every aspect of biological function in planarians, ranging from studying stem cells with immunostaining, to assessing DNA damage through COMET and *in situ* hybridization to evaluate expression of specific genes[11,49,87,95,96]. Due to their relatively small size, it is also possible to view effects of certain genes at the organismal level, which is not always possible with traditional model systems[12,97]. They are amenable to RNA interference, allowing for loss of function studies[98,99] as well as pharmacological alterations[100–105]. Furthermore, the genome of *Schmidtea mediterranea* been sequenced and is available as an online resource, along with data published from previous RNA-seq projects, to identify and characterize novel genes[89,90,106–108]. Various studies have shown that signals influencing cellular behavior during adult tissue maintenance, repair and cancer are evolutionarily conserved between planarians and mammals[11,13,94,95]. Taken together, this model systems and the various traits attributed to it make it ideal for the study of SUMOylation and understand its role in regional regulation of cell proliferation. We expect to provide critical insights about the relationship between SUMOylation and the regulation of cell fate along the AP axis, which is a very significant issue that could identify novel drug targets and lead to the development of targeted treatment strategies.

1.4. Research Summary

This dissertation describes my efforts to identify the role of SUMOylation in regulating regional differences in cell proliferation observed in various biological contexts, including cancer. My aim was to identify the role of SUMOylation in tissue homeostasis, cell turnover and regeneration by primarily focusing on characterizing the function of UBC9, the sole E2 conjugating enzyme, in the planarian model system *Schmidtea mediterranea*. Thus, this work can be divided into three distinct parts, each with its own goals and implications. First, we wanted to fully characterize the function SUMOylation in planarians. We established that all components of the SUMOylation pathway are conserved in *S. mediterranea*. Knockdown of UBC9 in planarians results in specific loss of the posterior half of the body while the anterior portion stays intact. Planarians contain pluripotent stem cells termed neoblasts that are essential to maintaining tissue renewal. Our data revealed that loss of UBC9 leads to a gradual and uniform reduction of neoblasts throughout the body. The reduction in the neoblast compartment was attributed both to a general loss in gene expression of markers needed for their maintenance as well as inability to progress past the G1 phase of the cell cycle. However, this finding does not explain tissue loss in the posterior region as all these markers are downregulated evenly across the AP axis. We posited that loss of the posterior region is due to increase in regional cell death. We found that cell death is upregulated after UBC9 knockdown, specifically in the posterior region of planarians, like what similar to other models[24,26]. In addition, we took advantage of

the regenerative capacity of planarians to determine whether SUMOylation plays any role in this process. Planarians are known to be the masters of regeneration and are to repair any damage within seven days. Addressing this gap would not be possible using other traditional models' systems and will provide critical insights behind SUMOylation and tissue homeostasis. We found that UBC9 knockdown stymied regeneration and animals were unable to properly grow and reorganize new tissues after injury, but the specific mechanism behind its attenuation of this process remains to be understood.

Next, we examined the molecular mechanisms by which SUMOylation controls posterior tissue identity as we hypothesized this may be the reason for the degradation and loss of the tail after UBC9 RNAi. Homologs and variants of the Wnt/Beta-catenin pathway form multiple gradients across the planarian AP axis to specify and establish proper tissue polarity[12]. Canonically, the hedgehog (Hh) pathway has been established as key regulator of posterior tissue identify in planarians[109,110]. We hypothesized that an interplay between SUMOylation and Hh signaling pathway is required to maintain posterior tissue identity. Our results indicated that UBC9 knockdown leads to an increase in transcription of repressor Patched (Ptc), a Hh pathway repressor, suggesting UBC9 is required for upregulation of Hh signaling. Next, we performed single and double RNAi experiments with UBC9 and components of Hh signaling Hh to determine the impact on cell proliferation and tissue maintenance. Specifically, we used Hh pathway activators and/or repressors to attempt to rescue the UBC9 phenotype by slowing or stopping the posterior tissue loss. Although we found that double RNAi or Ptc and UBC9 led to partial rescue of the posterior abnormalities, none of the tested conditions ever led to a full rehabilitation of the animal. These findings suggested that multiple mechanisms are be at play to regulate AP axis polarity in the absence of SUMOylation and these underlying factors remain to be investigated.

Finally, we discovered loss of UBC9 function led to systemic loss of genomic integrity in planarians. This finding is in line with what is already known about SUMOylation from study in other experimental models[32,74,78]. Specifically, we noticed ubiquitous levels of double stranded breaks (DSBs) and abnormal chromosomes throughout the planarian body axis. Although we were able to attribute the increase in DSBs to inability of the RAD51 protein to localize to the nucleus to fix DSBs, we were unable to identify why the anterior region continues to survive with an increased load of DNA damage. We hypothesized that SUMOylation is part of a larger molecular network that controls cellular fate decisions across the planarian AP axis. In order to identify novel regulators of anterior tissue survival, we performed RNA-seq analysis on anterior and posterior fragments of control and UBC9 RNAi animals. This approach allowed for identification of 37 differentially expressed genes specific to the anterior region. In order to functionally characterize, we focused on 10 genes that had canonical support for being responsible cell proliferation, cell death or tissue survival. We

performed a loss of function screen on these ten genes in combination with UBC9 knockdown. We found that RNAi of MAP kinase-activating death domain protein (MADD), a regulator of apoptosis, led to loss of posterior tissue in planarians and was been able to revert the UBC9 RNAi induced abnormalities in double RNAi experiments. In the future, we expect to identify additional critical nodes regulating SUMOylation-mediated AP differences in the adult body. This multifaceted approach has provided valuable insight into the role of SUMOylation in adult tissues and the mechanisms through which it can affect stem cell function and tissue maintenance.

2. MATERIALS AND METHODS

2.1. Materials

2.1.1. Organisms

Planarians:
Planarian species used in these experiments was *Schmidtea mediterranea* CIW4. The culture was maintained as previously described[111]. Animals were starved for seven days before performing all experiments except for those pertaining to regeneration, which were amputated a day after being fed.

Bacterial strains:
Two bacterial strains were used for experiments. NEB10-beta Competent E. coli is a derivative of the popular DH10B sourced from New England Biolabs (cat # C3019l) were used for initial cloning. HT115 bacteria was used to generate clones for RNAi by bacterial feeding (supplied by the Reddien lab).

2.1.2. Selection of primers and cloning

Plasmids

Plasmid	Source
pCR-TOPO	Thermo Fisher
pPR244	Reddien Lab
pBluescript	Agilent Technologies

Primers:
Primers were identified and designed using the NCBI Primer BLAST (https://www.ncbi.nlm.nih.gov/tools/primer-blast/). Primers in the form of oligonucleotides were obtained from Eurofins MWG Operon, part of Fisher Scientific.

List of primers and probes used in this study:

Name	Forward Primer	Reverse primer
UBC9	TGGGTGATTATTCGGATGCAGA	GGGTTTCGAAATTTTTCCGCC
SUMO2	GTACAAGGTCAAGATGGAGCAGT	CAGTCTGACTCTGGAACACCT
SUMO3	AGGGTCAAGACGGAGCAGTT	CCGGTCTGGCTTTGGAATACT
SAE1	AGATTGTGGGGCTTAGACGC	CCTCTCGCACATATTCATGGTG
SAE2	CCGTTCAACCACTTTCACCC	TGCTTTCTTTTCCGATCGCC
SENP1	CCAATACCGATTGGGAATCAC	CGGTGCACGGGTAACATGCTG
SENP2	CCAGTGGCTGACGGACAATA	TCCACAGTCGTAACCGTTGT
SENP3	GACACTCCATCAGTTCGGCA	CCAATCCGCCAGACTGACTT
SENP4	AGCTGTGTACTATAAGCGAGGG	TAGAAGTTCTTGCGGAACCC

PIAS1	GCACTGGAATCGCAAACAGG	ACCAAGCAATTCAGCGGCTA
PIAS2	CAGGTAAAGACGGTAGGCGG	TCGTCATTGGTCATTCCGGG
PIAS3	GCCGGAGTTTGCACAACTTAT	CAATTGGTCGGTGGCAGAAG
Rad51	TTTGCAAGGTGGTGTTGAAA	ATCAGCCAACCGTAACAAGG
Rb	ATGGCGGAGTCAATTTCAAC	GCAATTCGAGAACCTCAAGC
p53	CCTGCTTTTAAATCCGACGA	AAGTGTTTTCCGACCACCTG
Smedwi-1	TTTATCGTGACGGTGTTGGA	TTGGATTAGCCCCATCTTTG
Prog-1	GCAGATGACGTGAAACAAGG	TACTTGATTTGGCGGGAGAC
Agat-1	ACCGATTCCAGTTTCGCTTA	TCAATCGCTCCAAAATCTCA
Hedgehog	GCTGGAAAACAGCTACGGTG	ATCACCGGACTGAAGCGAAC
Patched	GATCGGAGCCTTCAACGTCT	ATTCGGATAACGGACGGCTC
Smoothened	TCGTTCTGACGGAGCAGTTC	TCATTGCAGGCATCAGGGAA
Sufu-like	GCGATGAAGAGATGCAGCTTG	AACACGTTTACGCATAGCGG
Sfrp1	ACCCTGTGTAGTAACGTCGG	AATCTGAATGGCATTGCCGC
Gli1	CGTATTACGGATCGACGGGAG	TGTAACGAGTCCCGCATTGT
DRP1	TCGATCTGGTGCGGAAAACA	TCGTCAACGTCTGATTCGTGT
Fz4	GAAGCGAGCAAACGGTTCAG	TCGAGAGGCCGAAAGAAACC

2.1.3. Antibodies, enzymes and other reagents

Antibodies

Name	Host	Dilution	Source
Anti-gamma H2Ax	Human	1:1000	Thermo Fisher
Anti-RAD51	Human	1:500	Abcam
Anti-phosphorylated histone H3 (Ser10)	Rabbit	1:500	Millipore
Anti-arrestin	Mouse	1:10000	Agata Lab
Anti-synapsin	Mouse	1:50	Agata Lab
Anti-tubulin	Mouse	1:100	Abcam
Anti-digoxigenin-AP	Sheep	1:2000	Roche
Anti-Digoxigenin-POD	Rabbit	1:1000	Roche
Anti-Fluorescein-POD	Rabbit	1:1500	Roche
Alexa 488 anti-mouse	Goat	1:800	Invitrogen
Alexa 568 anti-rabbit	Goat	1:800	Invitrogen

HRP anti-rabbit	Goat	1:500, 1:1000, 1:2000	Millipore
HRP anti-mouse	Goat	1_500	Millipore

Enzymes

Name	**Source**
Proteinase K	Invitrogen
Taq DNA Polymerase	Invitrogen
DNase	Promega
T3 RNA Polymerase	Promega
T7 RNA Polymerase	Promega
T3 RNA Polymerase	New England Biolabs
T7 RNA Polymerase	New England Biolabs
RNAsin	Promega
BP Clonase II	Thermo Fisher

Uncategorized Kits

Name	**Source**
SYBR Green PCR Mix	Applied Biosystems
Vectashield	Vector Labs
QIAprep Spin Miniprep	Qiagen
QIAquick Gel Extraction	Qiagen
1 Kb Plus DNA Ladder	Invitrogen
SIGMAFAST NBT/BCIP	Sigma-Aldrich
SuperScript® III First-Strand Synthesis System for RT-PCR	Invitrogen
Tyramide Signal Amplification	Invitrogen
DAPI	Thermo Fisher

RNTPs	Promega

2.1.4. Solutions and Buffers

Planarian Water

Name	**Reagents**
1 x Montjuic Salts	1.6 mM NaCl 1.0 mM $CaCl_2$ 1.0 mM $MgSO_4$ 0.1 mM $MgCl_2$ 0.1 mM KCl 1.2 mM $NaHCO_3$

Bacterial Media

Name	**Reagents**
2XYT, pH 7.0	16g bacto tryptone 10g bacto yeast extract 5g NaCl
LB, pH 7.0	10g bacto tryptone 5g bacto yeast extract 10g NaCl 1L MilliQ Water
Final antibiotic concentrations	 50 µg/mL Kanamycin 100 µg/mL Tetracycline 50 µg/mL Carbenicillin

General Solutions

Name	**Reagents**
10 x PBS, pH 7.2	80g NaCl 2g KCl 14.4g Na_2HPO_4 2.4g KH_2PO_4 1L MilliQ Water
10 X TBE	108g Tris Base 55g Boric Acid 10 mM EDTA 1L MilliQ Water
10% Triton X-100	5 mL 50 mL MilliQ Water

10% SDS	10 mL SDS Fill to 100 mL w MilliQ Water
0.5 M EDTA, pH 8.0	9.31g EDTA 50 mL MilliQ Water
1 M $MgCl_2$	4.97g 50 mL MilliQ Water
5 M NaCl	58.4g 1 L Water
1 M Tris, pH 9.5	121.14g 1 L Water
1% Agarose Gel	.5 g Agarose 50 mL 1X TBE

Fixation Solutions

Name	**Reagents**
HCl Solution	570 µL 10 mL MilliQ Water
Carnoys Solution	6 mL Ethanol 3 mL Chloroform 1 mL Glacial acetic acid
NAC Solution	.5g N-acetyl cysteine 10 mL MilliQ Water
4% fix	1.1 mL 36.5% formaldehyde Fill to 10 mL w MilliQ Water
Reduction Solution	500 mL 1M DTT 500 mL 10% SDS 200 µL NP40 Fill to 10 mL w 1 X PBS
Bleaching Solution	2 mL 30% H2O2 8 mL MeOH

2.1.5. Solutions for *in situ* hybridization

Name	Reagents
Denhardt's solution	10 g Ficoll 400 10 ml polyvinylpyrrolidone 10g BSA
50% Dextran Sulfate	50 g Dextran Sulfate 100 mL Water
1 M DTT	154.3g DTT 1 L Water
Proteinase K	1 µL Proteinase K 100 µL 10% SDS 1 mL 10X PBS Fill to 10 ML w water
Wash Hybe	50% DI Formamide 20% 20X SSC 10% 20% Tween 20 20% Water
Hybe Solution	50% DI Formamide 20% 20X SSC 10% 20% Tween 20 10% Dextran Sulfate 10% Water
MABT	11.6 g Maleic Acid 12.5 mL 20X SSC 1 mL Denhardts 10 mL 10% Tween Fill to 50 mL w Water
Blocking Buffer	9 mL MABT 1 mL Inactivated Horse Serum 0.1g BSA
AP Buffer	100 mM Tris pH 9.5 50 mM $MgCl_2$ 100 mM NaCl
NBT/BCIP	1 NBT/BCIP Tablet 10 mL 10% PVA

10% PVA	100 g Polyvinyl alcohol 1 L Water
80% Glycerol	80% Glycerol 10 mM Tris pH 7.5 1 mM EDTA

2.1.6. Immunohistochemistry solutions

Name	Reagents
PBST	100 mL 10X PBS 3 mL Triton X-100 Fill to 1 L w Water
PBSTB	1.25 g BSA 50 mL PBST
1 M Imidazole	68.1g Imidazole 1 L Water
PBSTI	500 µL 1 M Imidazole 50 mL PBST
Tyramide Solution	1:1000 FITC 1:1000 Rhodamine 50 mL PBSTI
Quench	1% NaN_3 50 mL Water

2.2. Methods

2.2.1. Planarian husbandry

All planarians were grown and raised in water with 1x Montjuic salts. They were fed liver once a week. Animals used for experiments are starved for at least one week.

2.2.2. Identification of orthologs and phylogenetic analysis

Components of the SUMOylation pathway were identified by BLASTing human SUMO protein sequences into available genomic resources for *S. mediterranea*. Identified sequences underwent a six-frame translation using PFAM and

conservation was further confirmed with UNIPROT. The sequences were further verified by Blastn and Blastp in NCBI. The identified sequences were aligned by CLUSTALW with sequences obtained using HomoloGene (http://www.ncbi.nlm.nih.gov/homologene). The phylogenetic tree for UBC9 was constructed using 30 sequences from 30 metazoans and for the SUMO tree we used 31 sequences from 22 metazoans. The sequences were aligned using MAFFT L-INS-I http://mafft.cbrc.jp/alignment/server/. The alignment was manually adjusted to remove large gaps. Phylogenetic analysis was conducted first by determination of the optimal substitution model for each alignment with ProtTest 2.4. We constructed maximum likelihood trees in RAxML version 7.3.2, with the appropriate model of protein substitution using the RaxML GUI front end. The best tree and bootstrap proportions were determined by 1000 iterations using Maximum likelihood + Slow bootstrap (100 runs), and PROTGAMMA+LG options using empirical frequencies. Tree images were generated using FigTree (http://tree.bio.ed.ac.uk/software/figtree/).

2.2.3. PCR amplification and gel electrophoresis

For a 50 µl reaction, add .625 µl of forward and reverse primer, 1 µl of DNTPs, 5 µl of PCR buffer and 0.5 µl of TAQ DNA Polymerase. Next, add 41.74 µl of water and thoroughly vortex all components. Set samples in the thermocycler and choose the following parameters: 94 °C denaturing, 58-65 °C annealing and 75 °C elongation temperatures. While PCR is running, make the agarose gel by adding 0.4g agarose to 40ml of 1x TBE. Heat the mixture in the microwave. Once all agarose is dissolved, remove from microwave and add 2µl of ethidium bromide. Pour mixture into gel mold and let it harden. Once the gel is set, add 1X TBE until the gel is completely submerged. Load well with 3µl of 1 kB DNA ladder and 5µl of PCR product: 2µl of 5X loading dye. Run the gel at 100V 0.05A for 40-60 min. Once complete, image the gel using a UV camera set to the EtBr filter.

2.2.4. Planarian Amputation

Animals were placed on a cold plate and amputated using a razor blade. The head and tail halves were then gathered and placed in planarian water until further use.

2.2.5. Irradiation

Sublethal irradiation of animals (neoblasts will recover) was set to 1250 rads. Lethal irradiation (complete ablation of neoblasts) was set at 6000 rads. A Cesium source was used in both cases and animals were fixed afterwards at fixed intervals[87,112,113]

2.2.6. RNAi by bacteria feeding

Primers with attb flanking sites were generated for the gene of interest. PCR products were generated using cDNA synthesized from RNA of asexual *S. mediterranea* animals. Thermo Scientific VERSO cDNA synthesis kit was used to make cDNA. The gene was cloned into the pPR244 vector using BP Clonase II kit. The newly generated vector was transformed into NEB5a bacteria and then into HT115 bacteria. HT115 bacteria with the vector was grown in 2XYT media until it reached an OD595 of 0.400. 50 uL of 0.1M IPTG was added and bacteria were incubated for an additional 4 hours. The media was pelleted at 5000 rpm for 5 min and mixed with 25 uL of calf liver and fed to planarians. RNAi feeding times were adjusted for each experiment time.

For UBC9 RNAi, planarians were fed UBC9 dsRNA expressing bacteria every 3 days for a total of six feedings. All experiments were performed after 25 days of RNAi starting from the first day of feeding. For double knockdown experiments involving SUMO2 and SUMO3, 5 ml of bacteria for each gene was grown as before and mixed together before centrifugation. This pellet was once again mixed with 25 uL of calf liver and fed to the planarians. For RAD51 and UBC9 double knockdown, a total of three RAD51 microinjections were administered over three consecutive days and then the animals were fed with UBC9 dsRNA expressing bacteria 4 times every 3 days. For Hh/PTC and UBC9 double RNAi, animals were fed 6 times with Hh/Ptc and then 6 times with UBC9 and fixed. For double RNAi experiments involved MADD and UBC9, MADD was 3 times, then UBC9 3 times and then one more time for each gene. Animals were fixed 7-10 days after last feeding.

2.2.7. Fixation protocols

NAC Fixation

Pick 20-50 planarians and place in 20 ml scintillation vial. Remove all planarian water and add 5% NAC solution. N-acetyl cysteine (NAC) is a mucolytic (gets rid of mucous and kills the animals). Rotate vials @ RT for 10 min. Remove NAC solution and add 4% fixative. 4% fixative is a cross-linking fixative. Rotate vials @ RT for 15-20 min. Remove 4% fixative and rinse 2X with .3% PBSTx. Add 37°C preheated reduction solution and leave vials in 37°C water bath for 10 min, agitating occasionally. Reduction was carried out in a water bath with intermittent gentle agitation (specimens are fragile at this step). Reduction aids with permeabilization to allow probe penetration of pre-pharyngeal region. Remove the reduction solution and rinse 2X with .3% PBSTx. Add 1:1 (MeOH: 0.3% PBSTx) solution. Rotate @ RT for 7 min. Replace 1:1 (MeOH: 0.3% PBSTx) solution with 100% MeOH. Rotate @ RT for 7 min. Rinse 1x with 100% MeOH and store vials in -20°C for at least 1 hour or long term for up to several months. Replace MeOH with bleaching solution and leave vials under direct light @ RT overnight. Bleaching step removes pigment from the animal and increases permeabilization

to help with visualization of the signal. Remove bleaching solution and rinse 2X with 100% MeOH. Use immediately or return specimen to -20°C.

Carnoy's Fixation

Pick 20-50 planarians and place in 20 ml scintillation vial. Make the appropriate fixing solutions and leave in ice to become cold before fixation. Remove all planarian water and add 5.7% HCl solution. Leave on ice for 5 min. Remove HCl solution and add Carnoy's solution. Leave on ice for 2-3 hours. Remove the Carnoy's solution and rinse 1x with RT 100% MeOH. Add cold 100% MeOH and place in -20°C for at least 1 hour or long term. Remove the MeOH and add 6% H2O2 solution. Place under a light source overnight or until completely bleached. Remove the bleaching solution and rinse 2x with 100% MeOH. Use immediately or place in -20°C for long term storage.

2.2.8. RNA extraction

Collect worms in a 1.5 mL microcentrifuge tube and remove as much water as possible. Add 500 µL of Trizol reagent and homogenize thoroughly. Add another 500 µL of Trizol. Add 266 µL of chloroform to the tube and centrifuge at 11000 rpm for 15 min. Extract the clear layer and deposit into a new tube. Add 667 uL of isopropanol and centrifuge again at 11000 rpm for 10 min. Remove the supernatant and add 1 mL of cold 100% ethanol. Centrifuge at 7500 rpm for 5 min. Remove the supernatant and air dry for 5 min in a fume hood. Add 15 uL of RNAse free water. Aliquot into small tubes and store in the -80° freezer.

2.2.9. Planarian cell dissociation

Planarians were amputated, whole or A/P, into small pieces using a razor, resuspended in cold calcium, magnesium-free (CMF) media and placed on a rocker for 30 minutes at 4°C in the dark. Cells were forced through a 20-micron filter and centrifuged at 1500 rpm followed by resuspension in 1ml of CMF media before cell counting.

2.2.10. Immunocytochemistry

Planarians were killed in 5.7% 10N HCl solution and fixed in Carnoys solution for 2 hours on ice. Planarians were replaced with cold 100% MeOH and placed in -20°C. Worms were bleached overnight in 6% H2O2 solution. Worms were then rehydrated in series from 100% MeOH to 100% PBST and stained as previously described. Primary antibodies: α-H3p 1:250 (Millipore Cat# 05-817R), α-synapsin, 1:100 (Developmental Studies Hybridoma Bank); and activated caspase-3, 1:500 (Abcam ab13847); Secondary antibodies: Goat anti-mouse Alexa488, 1:400 (Invitrogen Cat# 673781) for α-synapsin, α-arrestin, acetylated tubulin, Goat anti-rabbit Alexa568, 1:800 (Invitrogen Cat# 11036) for H3P, HRP-conjugated Goat

anti-rabbit antibody (Millipore Cat# 12-348) with TSA-Alexa568 anti-HRP for caspase-3 (1:2000).

Dissociated cells were pipetted onto glass slips and left to anneal for 30 min in the dark. After, the slips were transferred to a glass beaker and fixed in Carnoys solution for two hours on ice. Carnoys solution was replaced with 100% methanol and transferred to -20°C for 1 hour. Samples were then rehydrated using mixtures of 75%, 50% and 25% Methanol in PBST. After final rehydration with 100% PBST (PBS + 0.3% triton), the cells were blocked in PBST containing bovine albumin serum (BSA) for 4 hours RT and primary antibody added overnight: α-RAD51 1:500 (Abcam ab109107). Wash 6 X 10mins in PBSTB and replace with secondary antibody overnight: 1:500 HRP-conjugated Goat anti-rabbit antibody (Millipore Cat# 12-348). Wash 6 X 10mins in PBSTB. Add TSA-Alexa488 in PBSTI 1:1000 for 20 minutes. Wash 6 X 10mins in PBSTB. Add DAPI (0.1ug/1mL) for 15mins and mounted using VECTASHIELD® Mounting Medium.

2.2.11. RNA probe synthesis

Make a T3 and T7 mix for each gene (make a master mix for multiple genes) that you will generate probes for. Each mix consists of 4 µl PCR product, 5 µl 5X trans buffer, 2.5 µl of 10X DIG RNA mix, 1.5 µl of RNAsin, 1 µl of T3 or T7 RNA Polymerase and 11 µl of water. Incubate samples at 37°C for 1 hour. Add an additional 1uL of either T3 or T7 polymerase and incubate at 37°C for 1 hour. Add 1uL DNase 1 and incubate at 37°C for 15 min. Add 2.7 uL of 5M LiCl and 54 uL of 100% EtOH to each tube. Immediately place tubes in -80°C or dry ice for 15 min. Spin tubes @ 14,000 rpm at 4°C for 20 min. Remove as much supernatant as possible without disrupting the pellet and resuspend the pellet in 50 uL of deionized formamide. Store in the -20°C freezer.

2.2.12. *In situ* hybridization

Protocol was adapted from previously established literature[97,114].

<u>Day 1</u>

Transfer NAC fixed worms from glass vials into a 24 well plate. Replace 100% MeOH w/ 1:1 100% MeOH: 0.3% PBSTx and incubate samples for 5 min. Replace 1:1 100% MeOH: 0.3% PBSTx w/ 100% 0.3% PBSTx and incubate samples for 5 min. Remove 0.3% PBSTx and treat w/ Proteinase K solution for 10 min. Replace Proteinase K solution w/ 4% formalin and fix for 10 min. Rinse 2X w/ 0.3% PBSTx. Incubate samples w/ 1:1 Wash Hybe: 0.3% PBSTx for 15 min. Replace 1:1 with Wash hybe and place in rotator @ 56°C for 2 hours. Prepare riboprobes in Hybe solution and heat them @ 72°C for 2 min. Return the probes to 56°C. Replace prehybe w/ riboprobe mix. Cover top of wells with aluminum seal and tape the outside. Incubate in rotator @ 56° for at least 16 hrs.

Day 2

Remove riboprobes and store at -20°C for re-use if possible. Perform the following washes w/ preheated solutions in the 56°C rotator: 2 x 30 min washes w/ Wash Hybe, 2 x 30 min washes /w 1:1 Wash hybe, 3 x 20 min washes w/ 2X SSC + 0.1% Tx and 3 x 20 min washes w/ 0.2X SSC + 0.1% Tx. Move to RT for final wash. Wash 2 x 10 min w/ MABT. Block for 1 hr in MABTB. Dilute appropriate antibody in MABTB and incubate samples overnight @ 4°C while rocking.

Day 3

Remove antibody and discard. Rinse 2X w/ MABT. Perform 6 x 20 min washes w/ MABT. Develop worms as per selected development procedure. For NBT/BCIP Colorimetric development: Equilibrate w/ 2 X 5 min washes in AP Buffer and 5 min in AP Buffer (5% PVA). Suspend an NBT/BCIP tablet in 10 mL of 10% PVA and add to wells to initiate development. When stain has reached appropriate levels, rinse 2X in 0.3% PBSTx. Fix in 4% paraformaldehyde fixative for 30 min. Rinse 2X in 0.3% PBSTx. If desired, use 100% EtOH for 10 min @ RT to get rid of background staining in NBT/BCIP animals. Clear samples in 80% glycerol overnight in 4°C and mount them onto slides. For Tyramide Amplification Fluorescent development: Incubate samples in 300 uL of FITC/CY3 tyramide solution for 30 min. Add 6 uL of .15% H2O2 directly into the tyramide solution. Cover the well plate and incubate for 45 min. Rinse 2X w/ PBSTx. Add 300 uL of peroxide quench and incubate for 45 min. Rinse 2x with PBSTx. For double FISH, incubate in appropriate ab overnight and repeat previous steps. Clear samples in 80% glycerol overnight in 4°C and mount them onto slides. If background is high, perform 1 hr incubation in $CuSO_4$ solution to get rid of autofluoresence. Re-clear in 80% glycerol and mount.

2.2.13. Quantitative PCR (qPCR)

Quantitative real time PCR (qPCR) was performed as previously described[11,115]. The ubiquitously expressed gene H.55.12e (UDP Glucose) was used as the control. Each individual experiment consisted of triplicates per condition and experiments were independently repeated at least twice. RNA was extracted from anterior and posterior region of animals (>20 per condition) and converted to cDNA using the Verso cDNA synthesis kit. Gene expression is expressed of fold change in comparison to the control. Average gene expression at each time point was generated from each triplicate and divided by the average of the control for that experiment.

2.2.14. Protein Extraction and Western Blot

Animals were dissociated until no tissue fragments were visible and incubated in 1× RIPA buffer (Cell Signaling Technologies, 9806) with protease inhibitors (Roche Complete Mini Protease Inhibitor Cocktail, 04693124001; 1 mM PMSF; 1 mM DTT) for 30 min on ice. Volume-tomass ratio for this was as follows: 10 large, dissociated planaria were incubated in 300 µl of 1× RIPA and protease cocktail mixture. Samples were spun at 20,817 g for 15 min at 4°C. The supernatant was transferred to a new tube and immediately placed on ice. A 25 µl aliquot of the supernatant was used to measure protein concentration. The remaining solution was mixed with equal volumes of 2x Laemmli buffer (4% SDS, 10% 2-mercaptoethanol, 20% glycerol, 0.004% bromophenol blue, 0.125 M Tris-HCl) and incubated at 95°C for 5 min (or boiled at 100°C) to denature and reduce. Protein lysates were stored at -20°C. A Bio-Rad protein assay was used to determine protein concentration.

Western blot Protein lysate aliquots of 40 µg were heated at 80°C for 5 min and loaded in 12.5-15% SDS-PAGE gel along with a molecular weight marker (Bio-Rad, 1610375). Samples were transferred to a 30 s methanol-activated PVDF membrane (Bio-Rad, 162-0175) overnight in 1x Tris-glycine transfer buffer [25 mM Tris base, 192 mM glycine, 10% (v/v) methanol, pH 8.3] at 4°C. The membrane was blocked with 5% milk for 1 h and incubated in the primary antibodies overnight at 4°C on a rocker. Primary antibodies: anti-tubulin (1:500; Sigma, 081M4861), anti-RAD51 (1:5000; Abcam, ab109107) and anti-caspase (1:5000; Abcam, ab13847). The membrane was washed three times for 30 min prior to the addition of the secondary antibodies: HRP-conjugated goat anti-rabbit antibody (1:2000; Millipore, 12-348) for anti-RAD51 and anti-caspase, HRP-conjugated goat anti-mouse antibody (1:2000; Invitrogen, G21040) for anti-tubulin. The membrane was washed three times for 30 min and developed using HRP substrate (Millipore, WBLUF0100).

2.2.15. COMET Assay

Frosted microscope slides were coated with 1% normal melting point agarose (NMPA) in 10× PBS and dried overnight. Dissociated cells were resuspended in 10 ml CMF followed by incubation at 37°C for 2 hours. Cells were centrifuged at 664 g for 2 min and resuspended in 100 µl of 0.5% low melting point agarose (LMPA) made in 10× PBS per 50,000 cells. The mixture was loaded onto coated 1% NMPA dried slides and allowed to dry at 4°C until the agarose solidified. Slides were incubated overnight in a Coplin jar at 4°C with 89% lysing solution (2.5 M NaCl, 100 mM EDTA, 10 mM Trizma base, 8 g pelletized NaOH in dH2O; filtered and pH 10.0), 10% DMSO and 1% Triton X-100. Medium was then replaced with neutralization buffer (0.4 M Tris base in dH2O, pH to 7.5) for 5 min and kept at 4°C. The neutralization buffer was then removed, and slides were placed into an electrophoresis chamber at 4°C filled with 1× electrophoresis buffer (10 N NaOH and 200 mM EDTA in dH2O, pH 13) and the sample was allowed to equilibrate for 15 min. The current was adjusted to 12 V for 30 min at 4°C. Next, slides were transferred back into the Coplin jar and equilibrated for 5 min in neutralization

buffer. Samples were fixed with cold 100% ethanol for 5 min and stained with a 1:10 ratio of SYBR gold into 1× TE buffer (10 mM Tris-HCl and 1 mM EDTA, pH 7.5). A standard 'DNA damage scale' was built as reference based on different doses of gamma irradiation on whole worms. The scoring scheme is based on a rank from 0 to 2, where a score of 0 showed little DNA damage and 2 is visualized as a disbursed tail, indicating extensive DNA damage[11,116,117].

2.2.16. Flow cytometry

Flow cytometry was performed as described in previous literature[87,88]. Briefly, 1x106 cells from dissociated planaria were stained with DNA marker Draq5 (eBioscience, 65-0880-96) at a 1:500 dilution in CMF media for 30 min at room temperature in the dark. Incubation with calcein (Invitrogen, C3100MP) diluted 1:500 in CMF medium for 10 min at room temperature was sufficient to stain live cells. BD FACSDiva software was used for initial gating and samples were either analyzed using a LSRII flow cytometer (BD Biosciences) or sorted using an ARIAII flow cytometer (BD Biosciences). Lethally irradiated planaria were used to approximate the gates for X1 and X2 populations and/or gated as previously described. Final gating of cell populations was performed using FlowJo software (www.flowjo.com). Cell cycle analysis was performed using either Draq5 (1:500 diluted in CMF media) or DAPI (0.1 µg/ml). Draq5-stained populations were gated for cell cycle using live Draq5-positive populations and FlowJo software. Staining of apoptotic cells was performed using 1×105 cells from dissociated planaria immersed in 100 µl binding buffer (BioLegend, 422201) and stained with 5 µl Annexin V (Pacific Blue; BioLegend, 640918) and 5 µl 7-AAD Viability Staining Solution (PECy5; BioLegend, 420404). Labeled cells were incubated at room temperature for 15 min. The samples were immediately analyzed using an LSRII flow cytometer (BD Biosciences).

2.2.17. Karyotyping

Protocol adapted from previous literature[118]. Animals were karyotyped at by placing animals in 0.05% colchicine overnight and fixing for 15 minutes in 3:1 ethanol and acetic acid. Animals were then treated for 2 minutes in 1N HCl at room temperature (RT) then for 6 minutes at 60°C. HCl was replaced with acetic orcein for 15 minutes. Animals were then treated for 5 minutes each in 60% acetic acid then 1:1:1 lactic acid, acetic acid, and water. Specimens were placed on a Superfrost Plus glass slide (VWR), squashed with a siliconized coverslip (Hampton Research), and allowed to settle overnight. Slides were frozen in liquid N2, coverslips removed with a razorblade, and submerged in cold ethanol mixed with dry ice. Slides were warmed to RT, air dried, stained with 0.5 µg/ml propidium iodide for 30 minutes, rinsed with water, and mounted in Vectashield.

2.2.18. Planarian datamining

Data from multiple published RNA sequencing projects were gathered from Planarian SCS: https://radiant.wi.mit.edu/app/ and Planarian Digiworm: https://digiworm.wi.mit.edu/

2.2.19. Imaging and Data Processing

Animal behavior and digital pictures were recorded using a Nikon AZ-100 multizoom microscope and NIS Elements AR 3.2 software. Area measurements were calculated with ImageJ. Brightness and contrast were adjusted with Adobe Photoshop. Neoblasts were counted and normalized to the area (mm^2) using ImageJ. Caspase-3 signal was quantified by measuring levels of fluorescence using ImageJ.

2.2.20. Statistical Analysis

Data are expressed as mean ± standard error of the mean (SEM) or fold change ± SEM. Statistical analyses were performed in Prism, GraphPad software Inc. (http://www.graphpad.com). Two-way ANOVA was used to determine significance due to multiple conditions that exist within each experiment (ant/post, days 10,15,25, etc.). Power analysis was used to determine if sample size was adequate to establish robustness of the statistical analysis.

2.2.21. RNA Sequencing and Differential Expression Analysis

Control and UBC9 RNAi animals were amputated across the pre-pharyngeal and RNA was extracted from each set of fragments. Triplicated analysis was performed for each condition that consisted of at least 20 animals each. RNA library was prepared and sequenced on the Illumina HiSeq 4000 platform at the DNA Technologies Core at the UC Davis Genome Center. Samples were indexed and pooled for multiplexing. All samples were analyzed by a Bioanalyzer for quality control before sequencing. Trimmed fastq files were assessed for quality control and mapped to the recently published complete Schmidtea mediterranea genome dd_Smed_v6 from the PlanMine database[119]. The Bioconductor package Rsubread was used to map reads to the reference genome using a robust and efficient seed-and-vote algorithm followed by the featureCounts algorithm to assign counts. The raw counts data were normalized and filtered for genes with log2 counts-per-million (CPM) greater than 0.5. Sample variation was assessed for quality. A customized pipeline using the limma package and voom transformation for precision weights was developed to identify differentially expressed genes was developed.

3. RESULTS

3.1. SUMO pathway components are conserved in the planarian *Schmidtea mediterranea*

To understand the relationship between SUMOylation, UBC9 and regional differences in cell proliferation, we used the planarian model organism *Schmidtea mediterranea* to circumvent limitations previously described in more traditional models. First, we wanted to determine if SUMOylation and its components are conserved in planarians, as it has found to be in various other model systems[24,52,56,120–123]. The SUMOylation pathway is cyclical in nature and can be broadly summarized in five steps: SUMO maturation, activation, conjugation, attachment and its removal from the target protein (Fig 1A)[27]. Our analysis of the established *S. mediterranea* genome allowed us to identify homologs of all components of the general SUMOylation pathway[106,107,119]. A summary of all *Smed* homologs and how they compare with homologs from other models can be found in (Fig 2A)[28]. Consistent with other organisms, there is only one homolog for the SUMO E2 conjugating enzyme UBC9 (*Smed*-UBC9, henceforth UBC9)[27,124].

Studies have shown that abrogating UBC9 function is enough to stop a wide range of protein SUMOylation as it is acts as the rate limiting step. Interestingly, our analysis of the planarian SUMO homologs determined that the two SUMO are actually homologs of SUMO-2/3 and not SUMO-1. This is in stark contrast with one of the nearest cousins of planarians, *C. elegans,* which only code for a homolog of SUMO1[120,125]. Other SUMO pathway components such as SENPS, E1 and E3 enzymes were redundantly expressed, which was to be expected. Phylogenetic and structural analysis of UBC9 across different species confirms its evolutionarily conserved, which in the case of planarians is 73% identical to its human counterpart (Fig 2B-C). Specifically, UBC9 shared the critical cysteine residue that is crucial to its ability to bind SUMO proteins (Fig 2C). These results suggest that the SUMO pathway is evolutionarily conserved in *S. mediterranea*, but the extent of its functional homology remains to be determined.

3.2. UBC9 is required for regional tissue maintenance

To functionally characterize the role of SUMOylation and UBC9 in *S. mediterranea*, we performed loss of function analysis by feeding planarians with dsRNA expressing bacteria mixed with liver six times every three days. Animals were left to starve 7 days after the last feeding and were fixed for experiments 25 days after the first dsRNA feeding (25dpf) (Fig 3A). Animals subjected to UBC9 RNAi exhibited macroscopic signs of tissue degradation, characterized by darkening of the epithelia in the post-pharyngeal region, followed by formation of lesions and complete loss of their tail by day 25 (20%) (Fig 3B-C). After 25 dpf, the experimental group undergoes rapid tissue deterioration, begins to lyse and eventually die (Fig 3C). We noticed that UBC9 RNAi animals were also unable

A

SUMO Components	Yeast	Humans	Planarians
Small ubiquitin-related modifiers	Smt3p	SUMO-1, SUMO-2, SUMO-3, SUMO-4	SUMO-2, SUMO-3
Activating enzyme (E1)	Aos1p-ba2p	Aos1 (Sae1)-UBA2 (Sae2)	SAE1, SAE2
Conjugating enzyme (E2)	Ubc9p	UBC9	UBC9
Ligating Enzyme (E3)	Siz1p, Siz2p, Mms21p, Zip3p	PIAS1, PIAS3, PIASxa, PIASxb, PIASy, Mms21	PIAS1, PIAS2
SUMO Protease	Ulp1p, Ulp2p	SENP1, SENP2, SENP3, SENP4, SENP5, SENP6, SENP7	ULP1, ULP2, ULP3

B

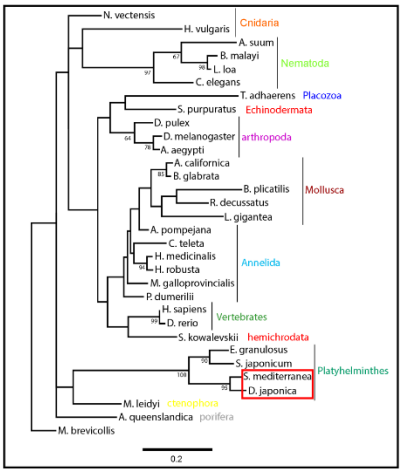

C

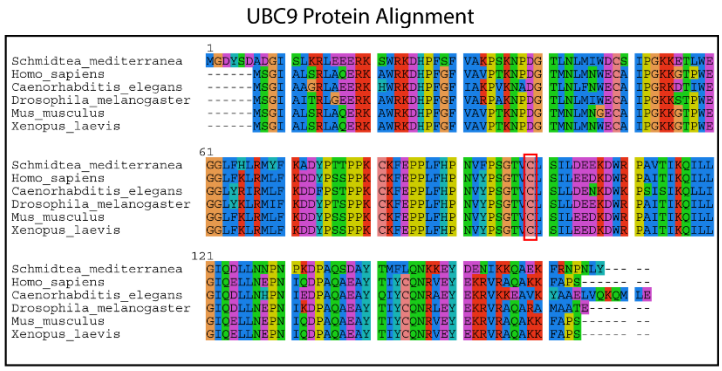

Figure 2: The SUMOylation pathway is conserved in the planarian model *Schmidtea mediterranea*. A) A list of SUMO pathway genes found in humans and their homologs in yeast and *S. mediterranea*. B) Phylogenetic relationship among primates and invertebrates based on the protein sequences of UBC9. Maximum likelihood method was based on the JTT matrix-based model. The percentage of trees in which the associated taxa clustered together is shown next to the branches. The tree is drawn to scale, with branch lengths measured in the number of substitutions per site. Branch support is under 5000 Bootstrap replicas. Red box highlights the two planarian models. C) Protein alignment of planarian UBC9 and homologs found in humans (NP_003336.1), mice (EDL06246.1), Drosophila (NP_476978.1), C. elegans (NP_001023158.1) and Xenopus (NP_001080758.1). Human and planarian UBC9 protein sequences are 73% identical and the catalytic cysteine at 93 is conserved across all species (red box).

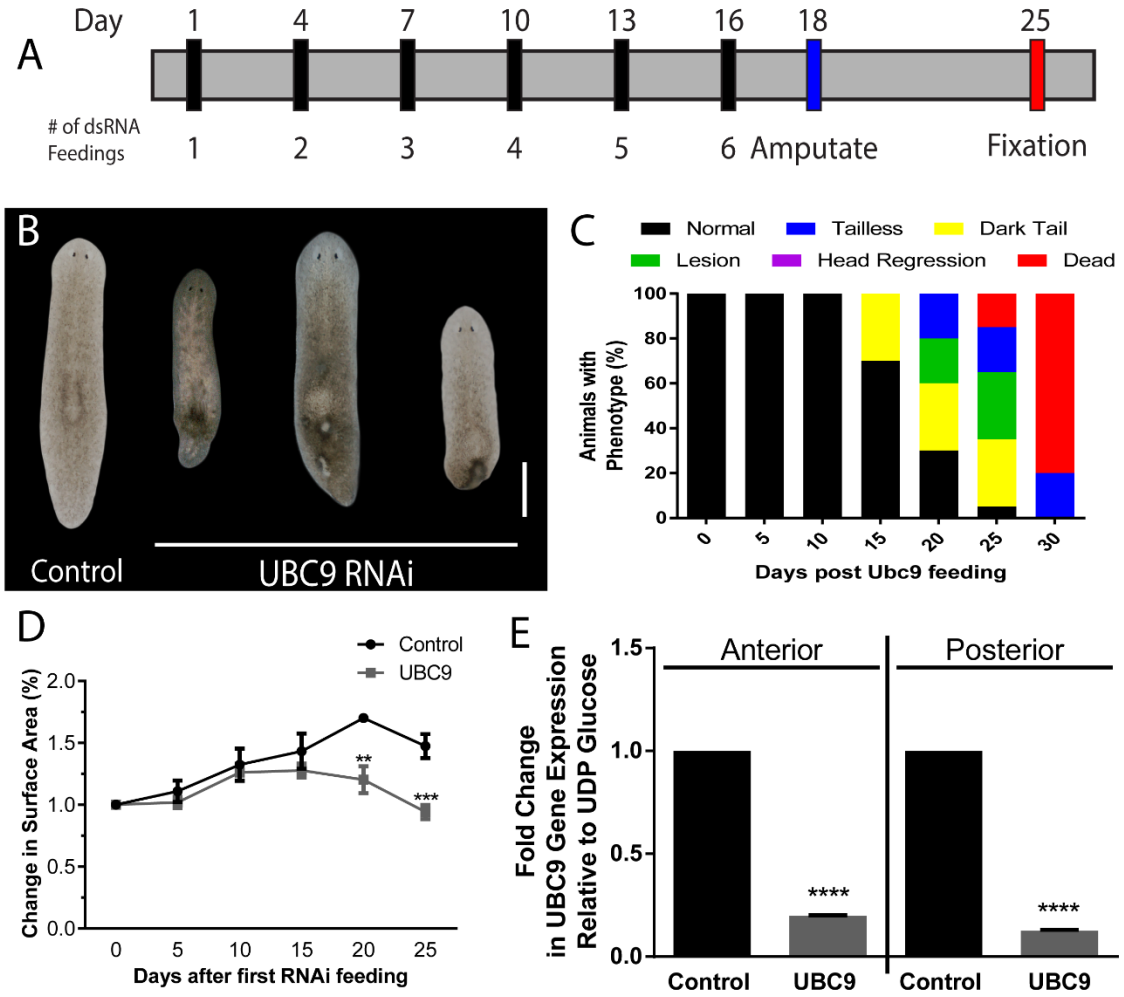

Figure 3: UBC9 is required for regional tissue maintenance. A) RNAi schedule based on feeding with bacterially expressed dsRNA to knockdown UBC9 expression. All controls were fed either UNC22 or GFP. Black bars represent feeding days, green bar represents amputation and red represents fixation. B) Representative images of control and UBC9 RNAi animals 25 dpf. The arrows indicate different abnormalities including dark tail, lesions, and tail loss. n = 75 total animals used in three biological replicates. C) Histogram illustrates the progression of the UBC9 phenotype based on macroscopic abnormalities observed in “B”. D) Change in surface area over the 25-day RNAi time course in controls and UBC9 RNAi animals. The experiment involves 15 animals per time point and three biological replicates. E) Levels of UBC9 gene expression measured with qPCR. Data obtained from triplicates per experiment of at least two biological replicates. ** p<.01; *** p<.001; **** P<0.0001; two-way ANOVA. Scale bar = 200 µm.

grow in response to nutritional status (Fig 3D). Animals fed with liver began to show signs of degrowth as early as 15 dpf and this was followed by a large decrease in surface area toward the end of the experiment, which could be due to the loss of tail that occurred in 35% of the animals. The reason for the early decrease in animal size could be two-fold: 1) animals are unable to eat due to lack of a proper digestive system and/or pharynx or 2) genes required for neoblasts maintenance are no longer being transcribed. To further validate the regional loss of tissue, we wanted to reject the idea that the RNA interference was partial or uneven. Despite the tissue loss being restricted to the posterior region, qPCR experiments revealed that UBC9 gene expression was effectively downregulated throughout the whole organism at 25 dpf (Fig 3E). These observations are in concert with data collected from other model systems, suggesting UBC9 regulation of regional cell fate is conserved in planarians.

3.3 UBC9 is actively expressed by the stem cell compartment

UBC9 RNAi animals exhibited regional loss of tissue characterized by loss of tail and persistence of the head. Previously established literature suggests any loss on tissue integrity in planarians is due to a dysregulation of neoblast function as these cells are critical to maintaining and replenishing damaged tissues. Previous studies in the field of SUMOylation have shown that UBC9 is responsible for maintenance of stem cell populations in various contexts and tail loss could be due to loss of stem cells in the posterior. To further characterize UBC9 function in planarians, we evaluated its spatial genetic distribution within the planarian via *in situ* hybridization. We found that UBC9 is ubiquitously expressed throughout the organism, in a pattern of expression similar to many conserved stem cell markers[87,98,114] (Fig 4A). Previously established studies demonstrated that expression of genes associated with stem cells are abolished 2 days after lethal irradiation (6K rads), providing an assay to test if a gene may be responsible for neoblast function[87].

To comprehensively test this hypothesis, we subjected control and UBC9 RNAi animals to lethal rounds of radiation and fixed them every day for seven days and examined the change in UBC9 gene expression. Interestingly, UBC9 expression is dramatically reduced 24 hours after lethal irradiation, which is known to eliminates planarian neoblasts and remains at that level 7 days post-irradiation (dpi) (Fig 4A). In addition, we detected strong UBC9 expression surrounding the pharynx and the periphery of the brain at 7 dpi (Fig 4A). Persistence of its expression after long term irradiation suggests UBC9 may also play an important role in differentiated tissues. Distribution of UBC9 expression among neoblasts and post-mitotic cells was further confirmed by qPCR (Fig 4B). Furthermore, the single cell analysis also reveals that UBC9 expression is present across all neoblast subclasses and in a subset of differentiated cells including neural, epidermal, and gut (Fig 4C). Together, these findings suggest that UBC9 is mainly expressed in neoblasts, but it is also present in post-mitotic cells.

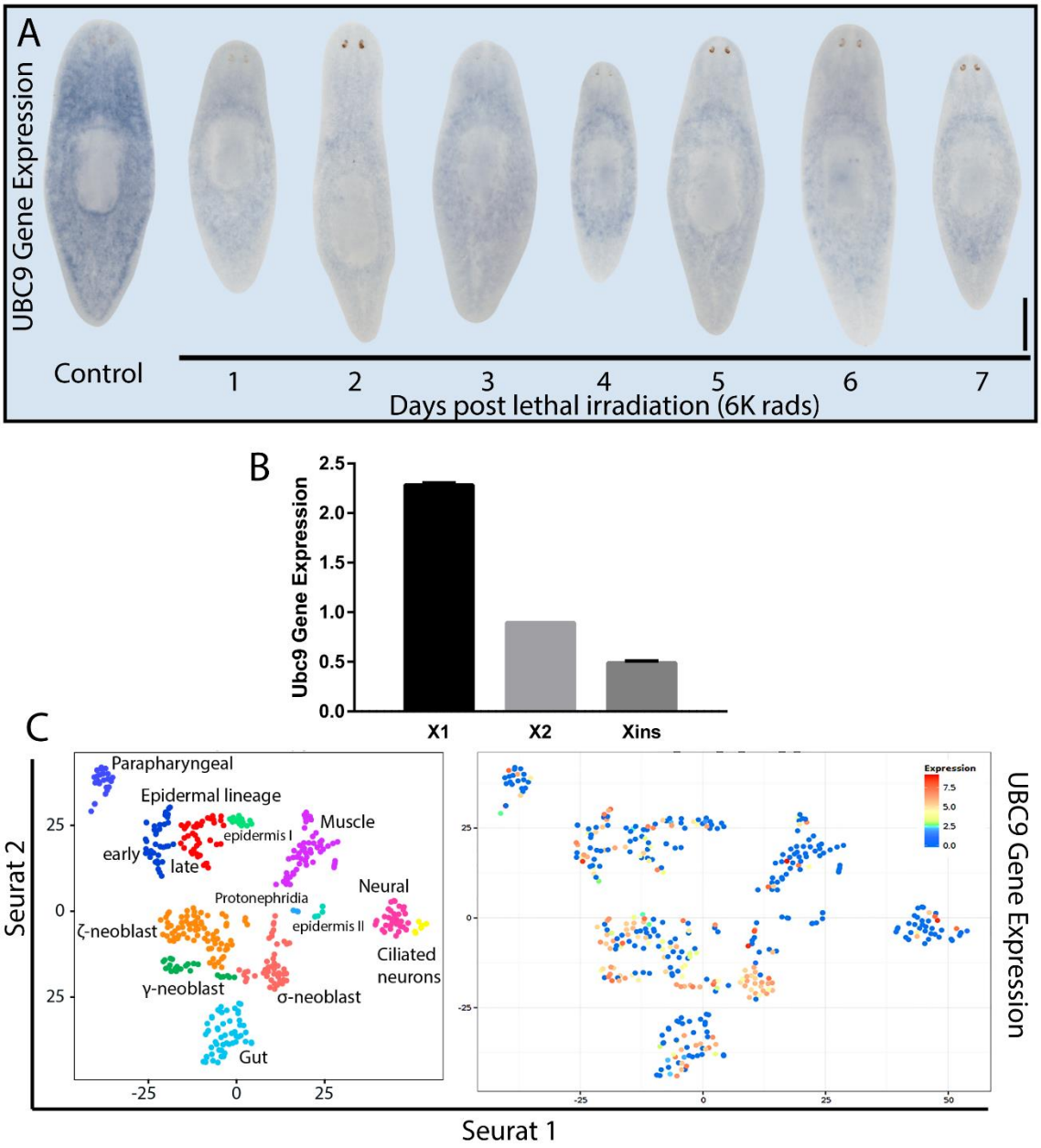

Figure 4: UBC9 is actively expressed by the stem cell compartment. A) *in situ* hybridization using antisense probe against UBC9. Gene expression is found ubiquitously distributed along the AP axis (left) and is dramatically reduced 24 hours after lethal exposure to gamma irradiation (6K rads) and remained at that level for 7 days post-irradiation. Experiments involved three biological replicates with 10 animals per experiment. Scale bar = 200 µm. (B) UBC9 gene expression levels in different cell populations (X1: proliferative cells, X2: early post-mitotic progeny, and Xins: late post-mitotic progeny) determined by qPCR. (C) t-SNE plot of single cells displaying clusters of neoblasts and differentiated cells (left), along with the overlaid UBC9 expression (right). The respective reference for the level of expression based on the colored gradient scale blue to red (low-high, respectively). The gene expression data was obtained from the planaria single-cell database hosted by the Reddien Lab (https://radiant.wi.mit.edu/app/)[89].

3.4 UBC9 is required for proper stem cell function and cell cycle transition

We hypothesized that loss of proper tissue architecture is primarily driven by changes in neoblast function, which are known to drive all aspects of planarian homeostasis. Neoblasts are the only proliferative cells in planarians and thus, we evaluated the presence of proliferative cells by whole-mount immunostaining against phosphorylated histone-3 (H3P), a marker for mitosis, after UBC9 RNAi[126–128](Fig 5A). These experiments revealed a three-fold reduction in H3P+ cells in the experimental group but residual mitotic activity remained (Fig 5B). The macroscopic regional effects are visible by day 15 after UBC9 RNAi (Fig 5C), but the mitotic decrease is noted by day 20-25 post-RNAi. This suggests that posterior tissue loss follows depletion of planarian neoblasts. To evaluate whether there was a regional reduction in mitotic activity, we separately quantified H3P+ cells in the anterior and posterior regions. Each animal was split into two parts along the AP axis, considering the pre-pharyngeal as the anterior region and the remaining tissue including the pharynx as the posterior region (Fig 5B). Such delimitation was made to account for the dramatic reduction in the tail region in the phenotype. This analysis demonstrated that mitotic activity was halved along both the anterior and the posterior regions, suggesting neoblast ablation is not driving the specific loss of tail tissues. Finally, control and UBC9 RNAi animals were subject to BRDU staining, which can label cells in S phase. Animals were soaked in BRDU infused water for 1 hour and chased for 4 hours. We can see a uniform loss in BRDU foci after UBC9 knockdown, similar to what we see with the mitotic marker H3P (Fig 5D).

Since we observed a reduction of cells in both the S phase and M phase, we deduced that UBC9 may be responsible for proper cycle transition past the G1 phase. Previous studies have demonstrated that cell cycle blockage is a prominent feature of UBC9 depletion in other experimental models[54,55,129,130]. To test this hypothesis, we analyzed the effects of UBC9 downregulation on cell populations and cell cycle dynamics by using flow cytometry (FACS). Control and UBC9 RNAi animals were amputated in half and the anterior and posterior parts were separated and pooled. Cells from each half were isolated by dissociation and processed for subsequent FACS analysis. First, we examined cellular populations associated with neoblasts (X1) and early and late post-mitotic progeny (X2 and Xins, respectively)[87,131]. There was an overall reduction in the proliferative X1 population across the AP axis, which was four times lower in the posterior region of the experimental group (Fig 6A). The decline in the X1 cells is consistent with the reduction in mitotic activity (Fig 5A). In addition, UBC9 RNAi shows concomitant increase in post-mitotic cells in the anterior and posterior region, suggesting that these cells now make up more of the planarian cell population. Furthermore, we found that UBC9 RNAi leads to an increase of cell in G1 phase (74.1 vs 81.1) and a decrease in S and G2/M (13.9 vs 6.02) phases of the cell

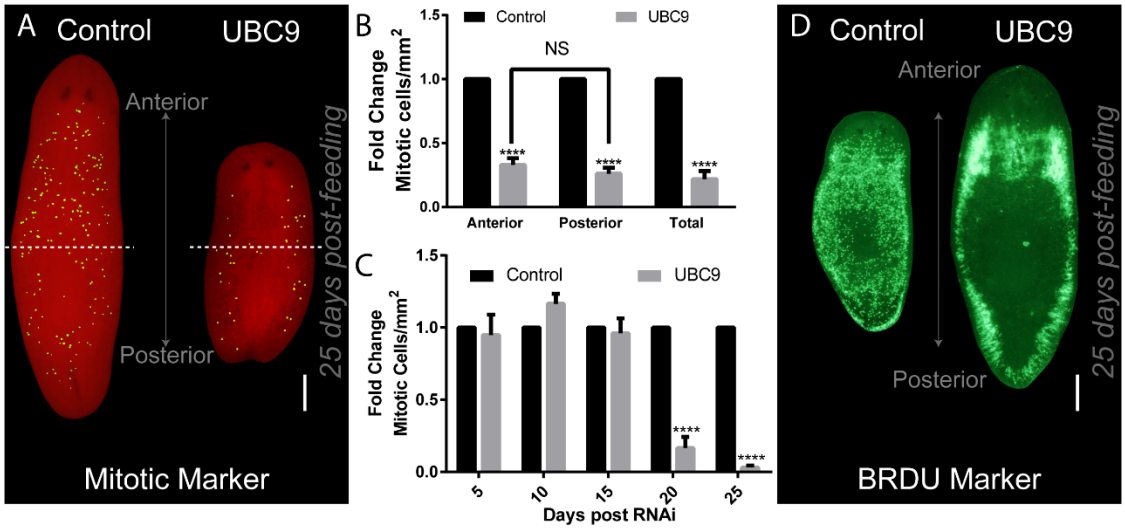

Figure 5: UBC9 is required for neoblast proliferation. A) Spatial distribution of mitotic activity in whole mount immunostaining against phospho-histone H3 (Ser10) (H3P) at 25 dpf UBC9 RNAi. Dashed line divides anterior and posterior regions of the animal. B) Fold change mitotic counts obtained independently from the anterior or posterior regions. Mitotic levels involved three biological replicates and more than 40 animals. C) Time course of mitotic activity along the AP axis, expressed as fold change in reference to the control at each time point. D) Representative images of control and UBC9 RNAi animals immunostained against BRDU marker, depicting cells in S phase. ** p<.01; *** p<.001; **** P<0.0001; two-way ANOVA. Scale bars = 200 µm.

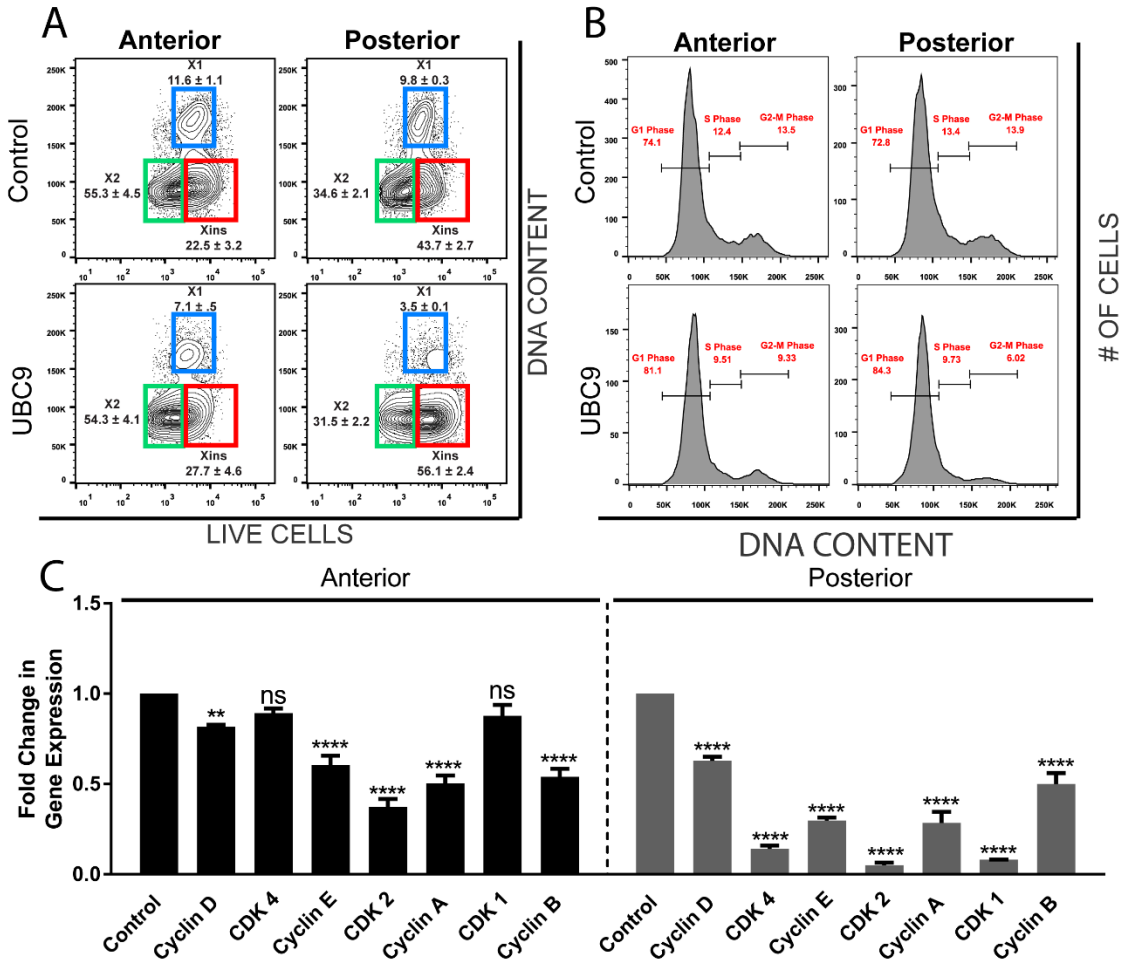

Figure 6: UBC9 is responsible for proper cell cycle transition. A) FACS analysis using DRAQ5, a nuclear dye and Calcein, a live cell marker, in either anterior or posterior regions of control and UBC9 RNAi animals 25 dpf. Blue, green and red squares represent X1, X2 and Xins populations, respectively. B) Cell cycle analysis using DRAQ5 DNA dye in AP regions of control and UBC9 RNAi animals 25 dpf. Red numbers represent percentage of cells at different phases of cell cycle. All FACS analysis performed with more than 10,000 cells and results are representative of three experiments with about 40 animals total. C) Gene expression levels of various cell cycle markers necessary for proper G1, S and G2/M transition in AP regions of control and UBC9 RNAi animals 25 dpf. Gene expression portrayed as fold change normalized to control. ** p<.01; *** p<.001; **** P<0.0001; two-way ANOVA.

cycle uniformly across the AP axis (Fig 6B). This data further validates our previous observations with whole mount immunostaining against H3P and BRDU (Fig 6A, D). Furthermore, the expression levels of genes that are evolutionarily conserved and commonly associated with G1, S and G2/M transitions were significantly decreased in UBC9 RNAi animals (Fig 6C). Together, these results suggest that UBC9 is required for maintenance of neoblasts and proper cell cycle transition.

3.5 UBC9 is necessary for maintenance of neoblasts and postmitotic cells

In addition to its role in cell cycle control, UBC9 is also required for maintenance of genes that specify the proliferative and postmitotic cell compartments in planarians. Whole mount *in situ* hybridization against markers for X1, X2 and Xins cells (*smedwi-1*, *Smed*-prog-1 and *Smed*-AGAT-1, respectively) demonstrated the expression levels of these genes were severely downregulated after UBC9 RNAi (Fig 7A). This was further corroborated by qPCR analysis against all three gene markers, which showed gene expression is halved across the whole-body axis (Fig 7B). Interestingly, the dramatic reduction in the expression of post-mitotic markers in the tail region and their persistence in the anterior region may imply that UBC9 may regulating regional tissue maintenance (Fig 7A). Since AGAT-1 is a general differentiation marker, we wanted to identify if UBC9 is responsible for maintenance of a specific differentiated organ systems in planaria. We performed *in situ* hybridization for the nervous marker (innexin-3), protonephridia (innexin-10) and digestive tract (innexin-9) (Fig 7C).

While neither the nervous system or protonephridia was affected by loss of UBC9, the digestive system was found to be completely missing. We previously identified that UBC9 RNAi animals are unable to consume food and grow in size (Fig 3D). It is possible that this is due to their loss of digestive tract, which inhibits the planarian ability to extract nutrients from food sources. However, it is still unclear whether they can uptake food as that requires proper pharynx function, which has yet to be tested. Interestingly, there is already precedent for UBC9 regulation of the gut as seen with mice where specific knockdown of gene expression lead to the collapse of gut proliferative cells and intestinal branches[57]. This relationship between UBC9 and the gut requires further investigation. Nonetheless, these findings, combined with the FACS analysis, demonstrate that UBC9 is required for proper function of stem cells and the maintenance of differentiated tissues.

3.6 Downregulation of SUMO pathways components recapitulates UBC9 RNAi phenotype

Next, we tested whether RNAi of other planarian SUMO pathway homologs lead to gross morphological defects observed with UBC9 RNAi. Since the other components were redundant and had multiple homologs, we devised a new double RNAi feeding time course to effectively downregulate multiple genes at a time.

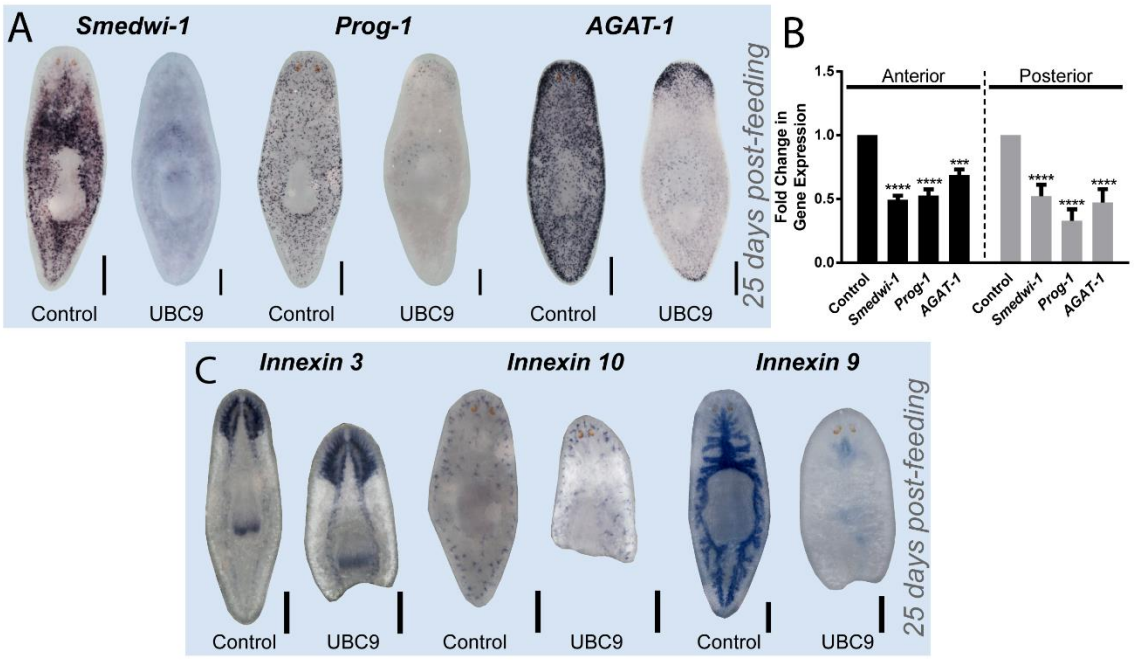

Figure 7: UBC9 is required for the maintenance of proliferative and post-mitotic cells. A) Whole mount *in situ* hybridization pictures probing against markers of neoblasts and post-mitotic progeny *smedwi-1*, Prog-1 and AGAT-1 in control and UBC9 RNAi animals 25 dpf. B) Levels of gene expression of *smedwi-1*, Prog-1 and AGAT-1 expression shown as fold change normalized to control in UBC9 RNAi animals 25 dpf. C) *in situ* hybridization against markers for nervous system, protonephridia and digestive tract reveal that UBC9 has an important role in maintaining gut differentiation. ** p<.01; *** p<.001; **** P<0.0001; two-way ANOVA. Scale bars = 200 µm.

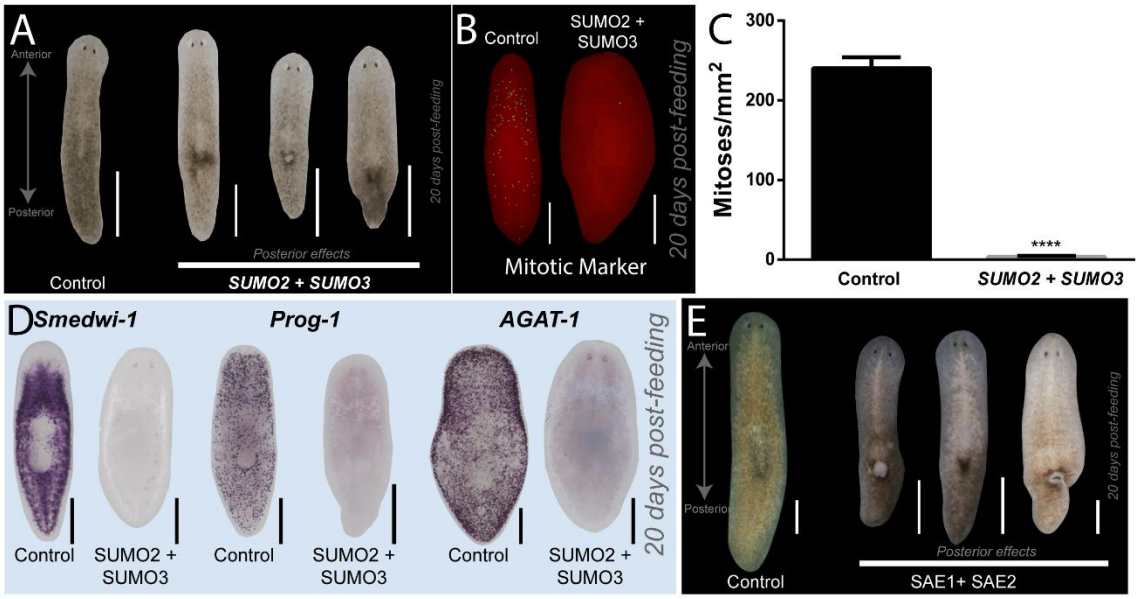

Figure 8: Downregulation of SUMO pathway components recapitulates UBC9 RNAi phenotype. A) Representative images of control and SUMO2 + SUMO3 RNAi animals. Percent indicate phenotype distribution at 20 dpf. B) Whole mount immunostaining against H3P reveals systemic reduction in neoblasts in SUMO2/3 RNAi 20 dpf. n>40, biological replicates = 3 C) Quantification of H3P+ foci in anterior and posterior in control and SUMO2/3 RNAi animals 20 dpf. Mitotic number is H3P+ foci divided by surface area in mm^2. D) Whole mount *in situ* hybridization pictures probing against *smedwi-1*, prog-1 and AGAT-1 in control and SUMO2 + SUMO3 RNAi animals 20 dpf. E) Representative images of control and SAE1 + SAE2 RNAi animals. n>15, replicates = 3. **** p<.0001; two-way ANOVA. Scale bars = 200 µm.

First, we performed RNAi of the two SUMO homologs in the *S. mediterranea* genome, which we termed *Smed*-SUMO2 and *Smed*-SUMO3 (SUMO2/3). We followed the same knockdown schedule as for UBC9, except we combined bacterial pellets from the two different genes. Initially, we found that individual RNAi of each component did not lead to behavioral or gross morphological defects, probably due to compensatory roles. However, SUMO2/3 double RNAi did produce regional defects like those noted after UBC9 RNAi (Fig 8A). Performing SUMO2/3 RNAi led to accelerated tail loss in a fraction of the animals (i.e. 15% animals, 20 dpf) (Fig 8A). The remaining animals gradually underwent regional tissue loss and eventually died. One interesting note is that double knockdown of the SUMO proteins accelerated the tail loss phenotype we first observed in UBC9, suggesting that these transcripts have shorter half-lives.

In addition, we evaluated mitotic activity after SUMO2/3 RNAi to see if it is similar to UBC9 RNAi. We found that SUMO2/3 RNAi dramatically reduced the number of proliferative cells across the animal with no differences between anterior and posterior (Fig 4B-C). We did not observe any differences in mitotic activity in anterior and posterior regions. In addition, SUMO2/3 are also important for maintenance of potency and differentiation as these markers are completely ablated after their downregulation as evidence by *in situ* hybridization against the markers for the three planarian cell compartments (X1, X2 and Xins) (Fig 8D). Furthermore, this regional tissue loss was phenocopied by double RNAi of SUMO E1 activating enzyme components SAE1 and SAE2. Double knockdown of these genes also led regional loss of posterior tissues and loss of proliferative cells (Fig 8E). However, dysregulation of numerous SENPs and E3 ligases did not lead to any macroscopic phenotypic effects. This may be because there are numerous homologs for each of these pathway components in planaria and it may require uniform downregulation of all homologs to present any external phenotypes. Collectively, these results suggest that regional defects and systemic neoblast dysfunction are specific to disruption of SUMOylation through RNAi of UBC9 and/or SUMO2/3. For simplicity and consistency, our analysis of the SUMO pathway will remain focused on the UBC9 knockdown model to identify the various mechanisms driving homeostatic aberrations along the AP axis.

3.7 UBC9 knockdown leads to regional increase in cell death

Initially, we observed gross morphological changes in UBC9 RNAi animals such as lesions or darkened tissue restricted to the posterior region. Our analysis of mitotic activity and markers associated with stem cell maintenance revealed that neoblasts are ablated evenly across the body axis after UBC9 RNAi (Fig 5B). Thus, these findings do not explain why UBC9 RNAi lead to specific loss of planarians tails. Tissue homeostasis is defined by a fine balance between cell proliferation and death. Several studies in the planarian field have linked these outward phenotypes to an increase in cell death[11,132,133]. To investigate the cause of regional tissue loss after UBC9 RNAi, we analyzed cell death through whole-mount

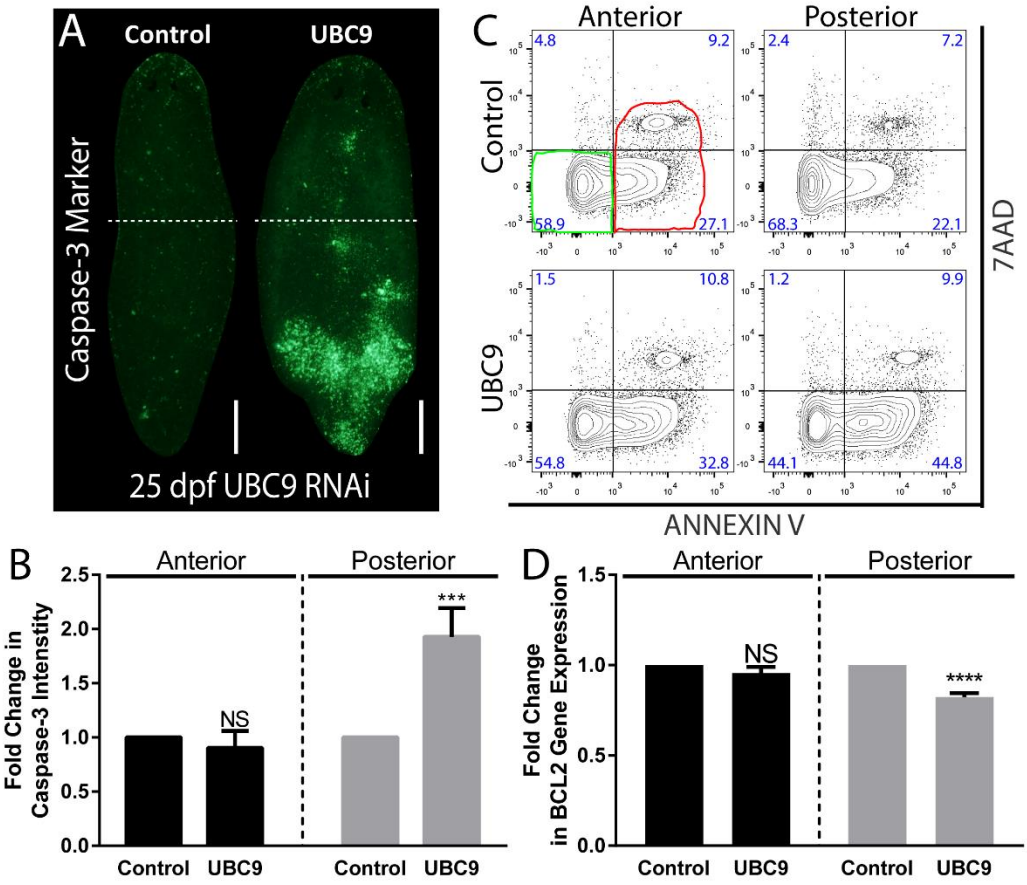

Figure 9: UBC9 knockdown leads to regional increase in cell death A) Whole mount immunostaining against caspase-3, a marker for cell death, in control and UBC9 RNAi animals. About 65% of experimental animals showed similar caspase-3 signal distribution at 25 dpf. Immunostainings involved three biological replicates and more than 40 animals. B) Intensity of capase-3 signal from anterior to posterior (white line) of control and UBC9 RNAi animals. Intensity signal quantification involved three biological replicates and more than 20 animals. C) FACS analysis staining against Annexin V, a marker for apoptosis, and 7AAD, a cell viability marker, in AP regions of control and UBC9 RNAi animals 25 dpf. Annexin V-/7 AAD- quadrant includes viable cells (outlined green). Annexin V+/7 AAD– and Annexin V+/7 AAD+ indicate cells that are in early and late (necrotic) stages of cell death, respectively (outlined red). Blue numbers in each quadrant indicate the percentage of cells with that staining profile. Data is representative of two experiments with n>40 each. D) Fold change of BCL2 gene expression in anterior and posterior regions normalized to control group. *** p<.001; two-way ANOVA. Scale bars = 200 µm

immunostaining and FACS. First, we performed immunostaining on control and UBC9 RNAi animals with antibody against caspase-3, a well-established marker for apoptosis that has been previously characterized in planarians[134–139]. We noticed a general increase in cell death throughout the animal, with a striking increase in caspase-3 expression in the posterior region by 25dpf (Fig 9A). In some instances, cell death signal was associated with cellular clusters, limiting our capacity to manually count dying cells. Instead, we chose to quantify the signal by generating an intensity profile of the fluorescence from anterior to posterior body axis. We found the intensity to be higher in UBC9 RNAi, with a two time increase in cell death in the posterior region (Fig 9B).

In addition, UBC9 RNAi-induced cell death distribution was further analyzed by FACS using Annexin V, a marker for apoptosis[88]. Cells from anterior and posterior fragments of control and UBC9 RNAi animals were dissociated and were processed for FACS analysis. The results demonstrated that there are more annexin V+ cells present throughout the animal after UBC9 knockdown, with a markedly increased expression in the posterior region (Fig 9C). These results are consistent with regional cell death found in immunostaining using caspase-3 antibody. Furthermore, gene expression of BCL2, a survival signal marker, is importantly reduced in the posterior region when compared to the anterior region[132,140](Fig 9D). This change in gene expression suggests that UBC9 may responsible cell survival via direct and indirect means. It may be possible that UBC9 and SUMOylation are affecting a large range of signaling pathways to maintain a state of survival in the posterior region that is lost when the gene is absent. Taken together, our findings demonstrate that UBC9 is essential for regional cell survival and tissue maintenance.

3.8 Regional defects after UBC9 RNAi are mediated through repression of Hedgehog signaling pathway

We have established that UBC9 knockdown is characterized by an imbalance in the processes that maintain tissue homeostasis, leading to loss of neoblasts and increase in cell death. However, it remains unknown what mechanism(s) underlie the region-specific cell death driving posterior tissue loss after UBC9 RNAi. We hypothesized that UBC9 mediated tail loss may be due to attenuation of signaling related to maintenance of posterior tissue polarity, which is responsible for both the specification and survival of the tail region. Posterior tissue identity in planarians is regulated by the evolutionarily conserved Hedgehog (Hh) pathway (Fig 10A). Specifically, regional determination of the posterior tissue is established through Patched (Ptc)-mediated signaling of Hh[109,110]. In addition to its role in AP axis specification, Hh signaling in planarians is also required for ciliogenesis, regeneration and more recently, neural and glial function[141,142]. Previously, amputation of Hh RNAi animals lead to abnormal tail regeneration characterized by half tails and no tail formation whereas its upregulation via Ptc

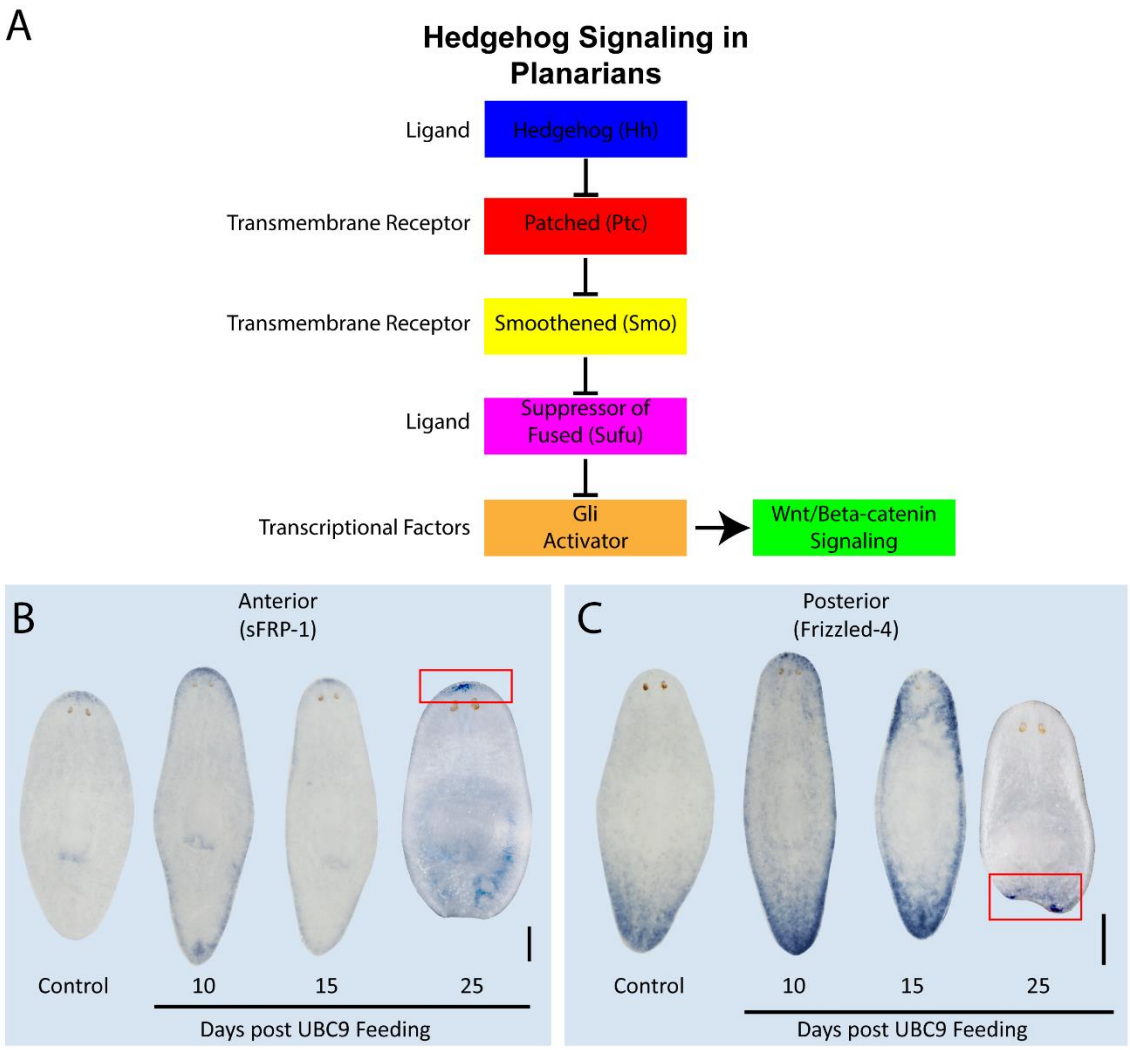

Figure 10: Planarian posterior polarity is maintained by the Hedgehog signaling pathway. A) Diagram depicts how the Hedgehog signaling pathway operates within *Schmidtea mediterranea* based on previous work[107,108]. B) Whole mount *in situ* hybridization expression of sfrp-1 (anterior polarity marker) in control and 10, 15 and 25 dpf UBC9 RNAi animals. C) Whole mount *in situ* hybridization expression of fz4 (posterior polarity marker) in control and 10, 15 and 25 dpf UBC9 RNAi animals. Red arrows indicate abnormal gene expression. Scale bars = 200 µm.

RNAi led to ectopic eye formation and double heads[109]. However, it is still unknown whether this pathway is necessary for regional information in uninjured animals. These observations prompted us identify whether the UBC9 regulates tail identify via Hh signaling.

Previous literature has established region-specific markers that can be used as readouts to determine if tissue polarity is properly established[12,109]. Specifically, polarity can be assayed in planaria via gene expression analysis of the anterior and posterior polarity markers, secreted frizzled protein 1 (sfrp1) and frizzled-like protein 4 (fz4), respectively. These genes are part of the Wnt/Beta-Catenin pathway, which falls under the jurisdiction of Hh signaling. We assayed for the expression of these genes via *in situ* hybridization before and after UBC9 RNAi. Strikingly, the expression of both fz4 and sfrp1 was dramatically altered in uninjured UBC9 RNAi animals, while it remained unchanged in the control group. The expression of sfrp1 was elevated and appeared ectopically in the lateral and tail regions at day 10 when compared to control animals (Fig 10B). The pattern and level of expression of srfp1 decreased to wild-type levels at day 15 but then dramatically increased by day 25, when the tail is lost (Fig 10B). Inversely, fz4 appeared ectopically in the head and lateral cells at day 10 but was strongly elevated at day 15 (Fig 10C). However, by day 25, fz4 expression return to the tail, but was lower than of the control (Fig 10C). This suggests that downregulation of UBC9 may lead to state of anterior identify in the posterior region, instructing the animals to destroy their tails as it is misinterpreted as being in the wrong place. These data are consistent with an effect of repression of Hh signaling on posterior specification.

Suppression of Hh pathway may be due to a downregulation of Hh signaling or an upregulation of one of its suppressors. To test this hypothesis, we analyzed the gene expression of the inhibitor Ptc, activator Hh and downstream regulator Smoothened (Smo) at early and late phases of the UBC9 phenotype via *in situ* hybridization. Ptc expression shows a steady increase in days 10 to 25 that is more than double at late phases of the phenotype (Fig 11A). Hh expression increases steadily until day 15 days post UBC9 RNAi (Fig 11B). At 25 dpf, Hh expression returns to basal levels (Fig 11A). Interestingly, the changes in Hh expression mirror fz4 expression, providing further credence for loss of posterior identity (Fig 10C). Smoothened remained downregulated at all time points, suggesting UBC9 is indirectly reducing gene expression by attenuating Hh signaling upstream. Furthermore, these changes in spatial gene expression were further validated by qPCR analysis, which clear showed the rise and fall of Hh expression over the course of UBC9 RNAi as well as the steady increase in Ptc expression (Fig 11C). This suggests that depletion of UBC9 drives the pathway off equilibrium, leading to abnormal fluctuations in gene expression that ultimately depresses Hh signaling and posterior identity.

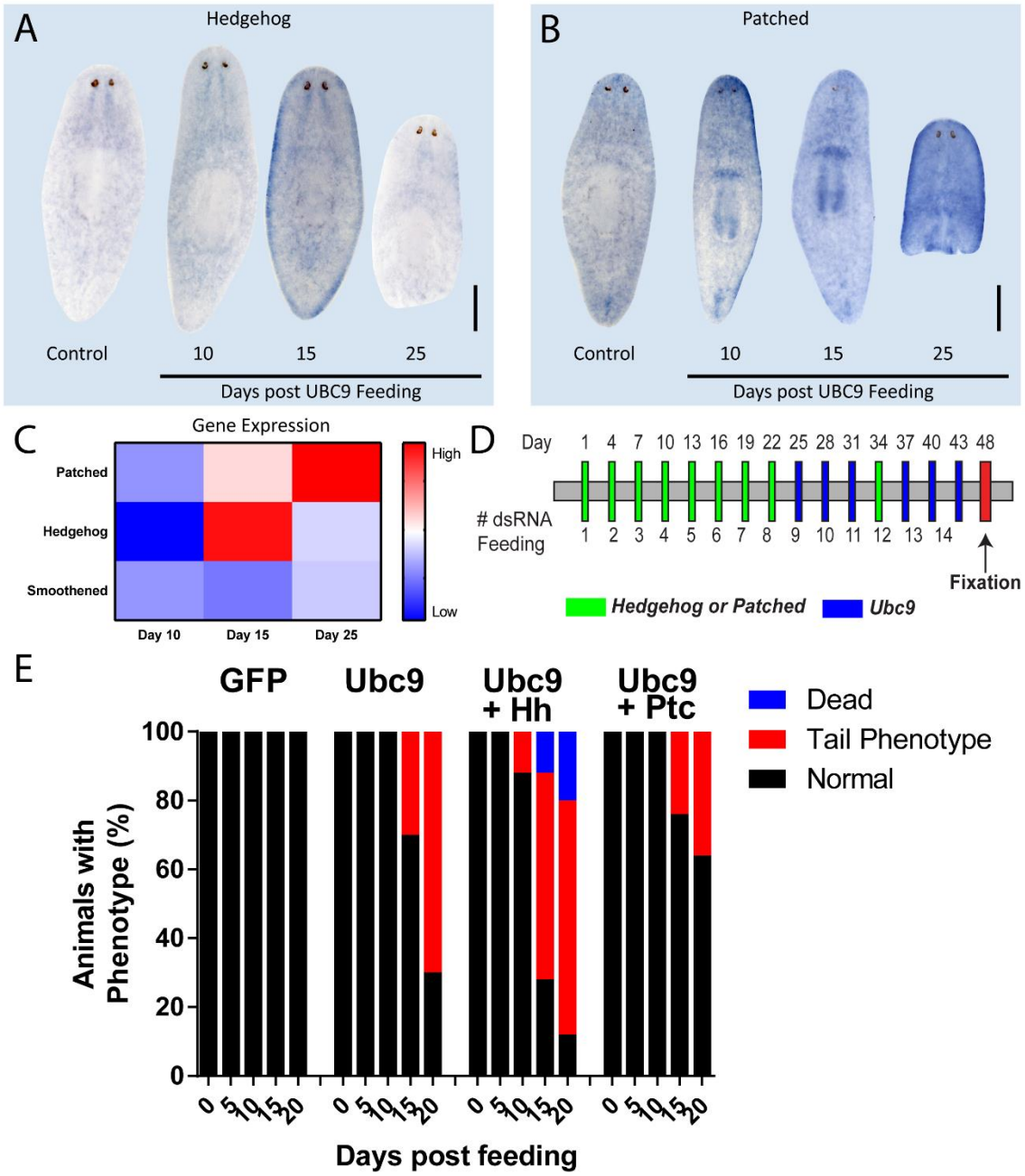

Figure 11: Regional defects after UBC9 RNAi are mediated through a repression of Hedgehog signaling. A) Whole mount *in situ* hybridization expression of Hedgehog in control and 10, 15 and 25 dpf UBC9 RNAi animals. B) Whole mount *in situ* hybridization expression of Patched in control and 10, 15 and 25 dpf UBC9 RNAi animals. C) Gene expression levels of Patched, Hedgehog and Smoothened after UBC9 RNAi animals at 10, 15 and 25 dpf. Gene expression is given in fold change normalized to control. D) RNAi schedule based on feeding with bacterially expressed dsRNA to perform double knockdown of Hedgehog or Patched and UBC9. All controls were fed either UNC22 or GFP. Black bars represent feeding days and red represents fixation. E) Histogram depicts occurrence of tail abnormalities in Hedgehog + UBC9 and Patched + UBC9 animals. Data is representative of n=30 animals consisting of three biological replicates. Scale bars = 200 µm.

To further examine the role of the Hh pathway in mediating the loss of posterior tissue homeostasis in UBC9 RNAi animals, we performed double RNAi experiments involving Ptc, Hh, and UBC9. We engineered and assayed various RNAi strategies and determined the most consistent results by first knocking-down either Ptc or Hh followed by UBC9 in a 40 days schedule that included a total of 14 feedings with dsRNA (Fig 11D). Animals subjected to double RNAi Hh and UBC9 displayed similar phenotypic dynamics as UBC9 alone. However, animals died earlier than normal as the double knockdown was lethal for 20% of the animals by day 20 (Fig 11E). The increased phenotypic effects after Hh + UBC9 RNAi suggest synergistic/parallel contribution between these factors. On the contrary, simultaneous downregulation of Ptc and UBC9 rescued the number of defects observed in the posterior region that appeared by day 20 (Fig 11E). Taken together, these results imply that UBC9 mediated regional tissue loss is at least partially mediated by its regulation of Ptc expression. However, since double RNAi was unable to rescue the UBC9 phenotype, it is possible that other signaling pathways involved with posterior polarity may be affected. This hypothesis remains to be investigated.

3.9 Loss of UBC9 leads to defects in regeneration and attenuation of the cephalic ganglia

Previous studies have shown that knockdown of Hh and Ptc results in abnormal tail and head regeneration, respectively. We reasoned that if UBC9 RNAi leads to deregulation of the Hh pathway, then amputation would result in deficient tail and brain regeneration as previously observed. Planarian regeneration is tightly coordinated response that leads to the complete rejuvenation of an animal seven days after injury. The response involves a substantial increase in cell proliferation in the early phase, cell death in the later phase and the established of an unpigmented blastema at the site of amputation from which new organs/tissues will form[90,132]. This response is well documented within planarians and allows us to dissect UBC9 control over this process and identify any novel functions. Initial datamining of UBC9 expression from the single cell RNA-seq database confirms that UBC9 is upregulated close to these proliferative mitotic peaks post amputation and responds differently according to the type of wounding (Fig 12A). Control and UBC9 RNAi animals were amputated pre- and post-pharyngeally at 18 dpf, which is an early stage of the phenotype where most animals still retain posterior tissue but fluctuations in both Ptc expression and the downstream Hh components (fz4 and sfrp1) are detected (Fig 10B-C). Animals were then set aside in a dark place and allowed to regenerate for seven days (7 dpa). At this time, all blastema formation was assed and quantified (Fig 12B).

We found that UBC9 RNAi animals formed small anterior blastemas and lacked any sign of posterior blastema formation (Fig 12C-D). This is comparable to what we observed in uninjured knockdown animals. To further examine the mechanism limiting regeneration, we assayed the mitotic response after amputation. This revealed that UBC9 RNAi animals can sense injury but respond

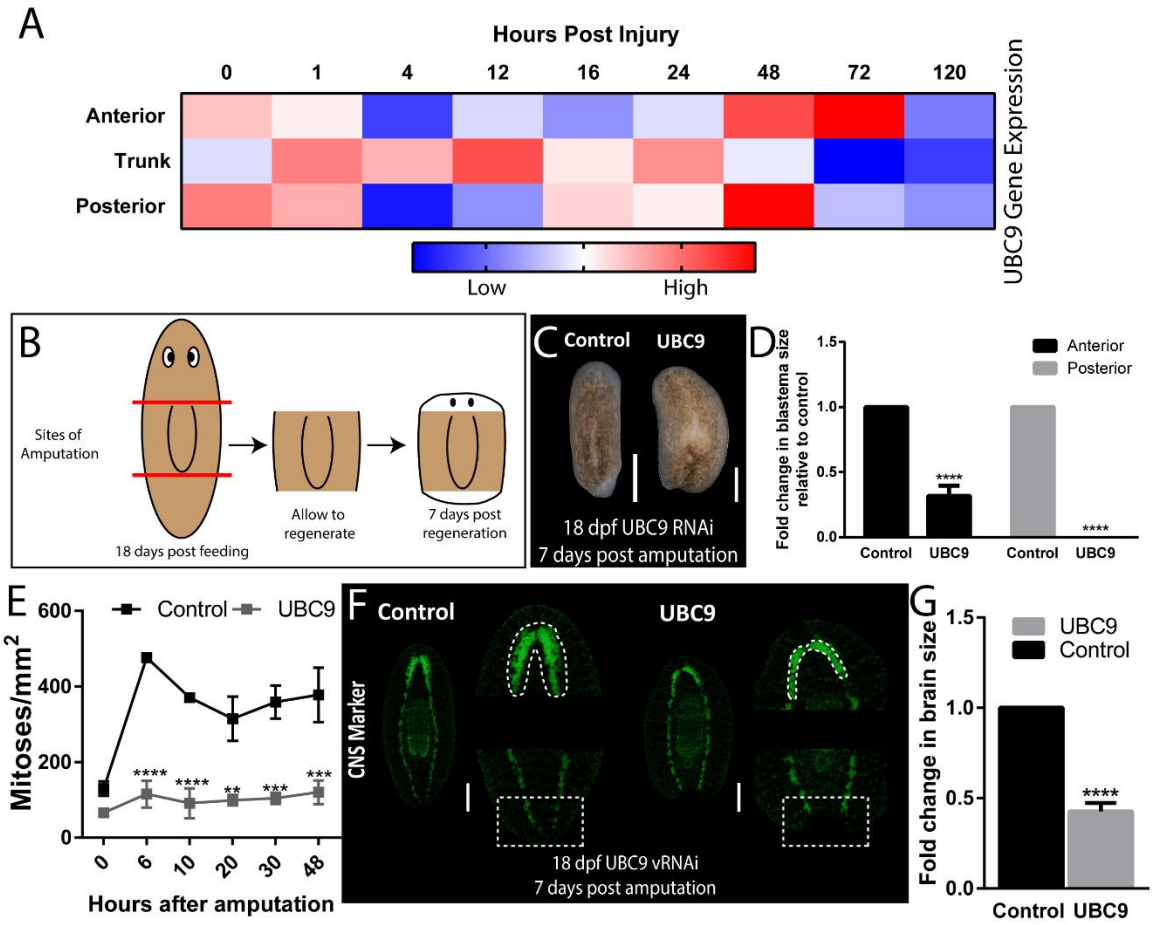

Figure 12: UBC9 is required for proper regeneration. A) UBC9 expression changes during regeneration following amputations along head, tail and both. Data derived from the Reddien single cell database[88]. B) Schematic representation of regeneration experiments on control and UBC9 RNAi animals 18 dpf. C) Live pictures of control and UBC9 RNAi 18 dpf animals 7 days post amputation (7dpa). D) Blastema size in control and UBC9 RNAi animals expressed as fold change relative to control. In all experiments used more than 30 animals in three biological replicates. E) Trunk fragments generated from control and UBC9 RNAi 18dpf animals were fixed at 0, 6, 10, 20, 30 and 48 hours post amputation. Mitotic cell numbers were determined via H3P staining and expressed as H3P+ foci divided by surface area in mm^2. Three biological replicates with more than 15 animals per time point were used. F) Whole mount immunostaining against SYNORF-1 (synapsin), a marker for the nervous system, in control and UBC9 RNAi 18 dpf 7DPA. Green signal denotes the planarian central nervous system and insets provide detailed amplification of anterior and posterior ends including brain and tip of the tail, respectively. White dotted lines underscore differences between control and experimental group regarding brain morphology (top) and ventral nerve cords (bottom). More than 20 animals were stained in three biological replicates. G) Regenerated brain size obtained from determination of surface area in both control and experimental group. ** p<.01; *** p<.001; **** P<0.0001; two-way ANOVA. Scale bars = 200 µm.

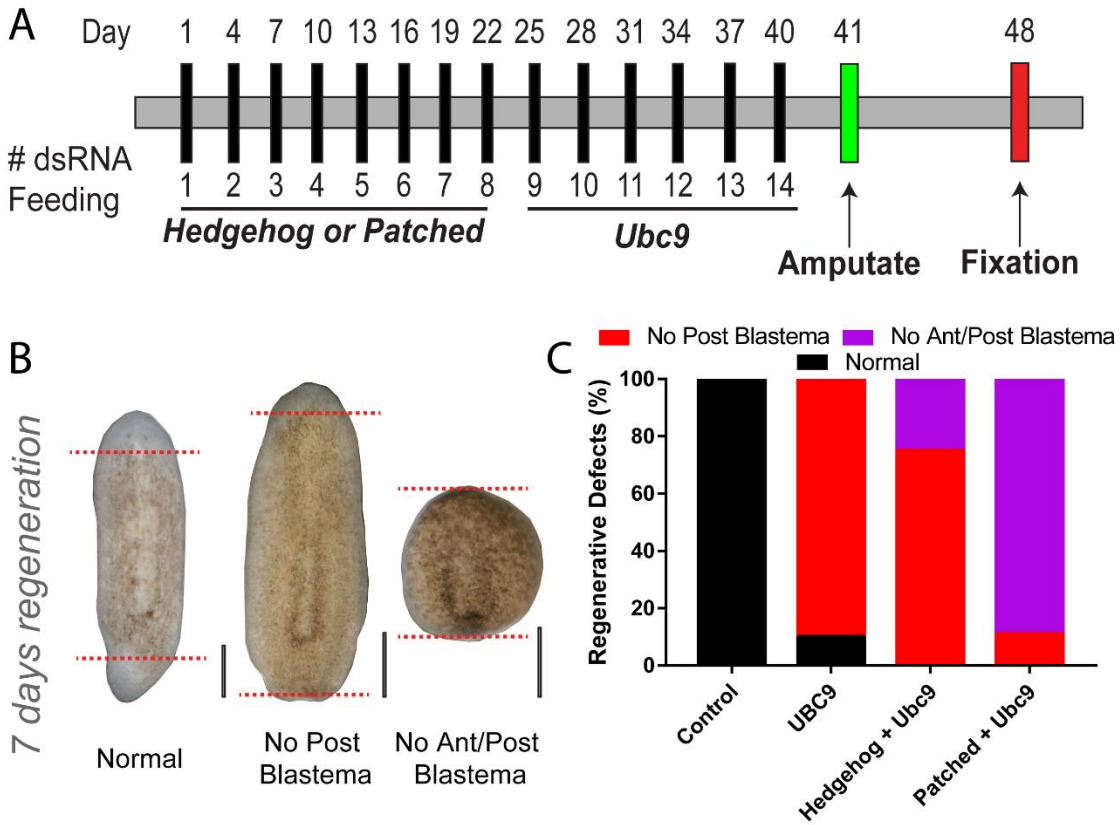

Figure 13: Double knockdown of Patched and UBC9 eliminates blastema formation A) RNAi schedule based on feeding with bacterially expressed dsRNA to perform double knockdown of Hedgehog or Patched and UBC9. All controls were fed either UNC22 or GFP. Black bars represent feeding days and red represents amputation. B) Representative images of defects observed after control, UBC9 and double RNAi conditions. n > 30, N=3 C) Histogram depicts occurrence of regenerative defects in control, UBC9, Patched + UBC9 and Hedgehog + UBC9 animals 7 days after amputation. Scale bars = 200 µm.

with limited mitotic capability, which can be explained by the role UBC9 as a regulator stem cell function (Fig 12E). Interestingly, amputation is able to temporarily alleviate the stem cell suppression that is prevalent in UBC9 knockdown animals, but this effect is temporary (Fig 12E). One study demonstrated that amputation temporary reignites mitotic activity lethally irradiated planarians but causes them to die faster than expected, suggesting the same mechanism is engaged. Next, we considered whether regeneration of the nervous system was compromised after UBC9 RNAi. Two main observations were made: (1) the size of the regenerated brain was reduced by half, consistent with compromised neurogenesis (Fig 12F-G) and (2) ventral nerve cords were truncated, likely due to lack of posterior regeneration[141,142] (Fig 12F). The effects described so far may be due to the inhibition of Hh signaling that follows UBC9 RNAi. To test this, we performed similar amputation experiments on double RNAi animals (Fig 13A). The regenerative outcome of these double knockdowns between Ptc, Hh, and UBC9 revealed that 100% of animals subjected to double RNAi Ptc + UBC9 or Hh + UBC9 presented lack of posterior blastema formation (Fig 13B-C). This observation is in accordance with the posterior homeostasis synergistic/parallel effects (Fig 13C). In addition, during regeneration, the anterior defects were more prevalent in the Ptc + UBC9 RNAi (over 90% of the animals), whereas 35% of the Hh + UBC9 showed regenerative defects in the anterior end as in single UBC9 RNAi (Fig 13C). These results demonstrate that UBC9 is required for posterior blastema formation and organogenesis following injury.

3.10 UBC9 is required for maintenance of genomic integrity

As the UBC9 phenotype mimicked RAD51 phenotype, further analysis was focused on assessing the role of UBC9 in genomic integrity during tissue renewal[11]. The phenotype of RAD51 RNAi is characterized by regional loss of posterior tissue and an increase in DNA double stranded breaks (DSBs) throughout the planarian body[11]. It was reported that these defects were due to apoptosis caused by faulty DNA repair machinery and unchecked DNA damage. In addition, we found that cells from UBC9 knockdown animals were unable to transition past the G1 phase, which may be due to inability to pass the DNA damage checkpoint (Fig 6B). To characterize DNA damage in UBC9 RNAi animals, we utilized a multi-pronged approach to assess genomic integrity: (1) COMET assay, (2) karyotyping and (3) immunostaining against markers required for early DNA damage response and repair through homologous recombination (HR). First, we performed the COMET assay, which was adjusted to detect DSBs. Upon UBC9 RNAi, a transient increase in DNA DSBs was identified throughout the animal by day 10 RNAi and progressively increased over the time course (Fig 14B). Our results also demonstrated this increase in DSBs was equally distributed along the AP axis, suggesting a general loss of genomic integrity (Fig 14B). In addition, the presence of DSBs was accompanied by a two-fold increase in chromosomal abnormalities, detected by karyotyping (Fig 14C-D). Detected abnormalities ranged from deletions, fusions and dicentric chromosomes that

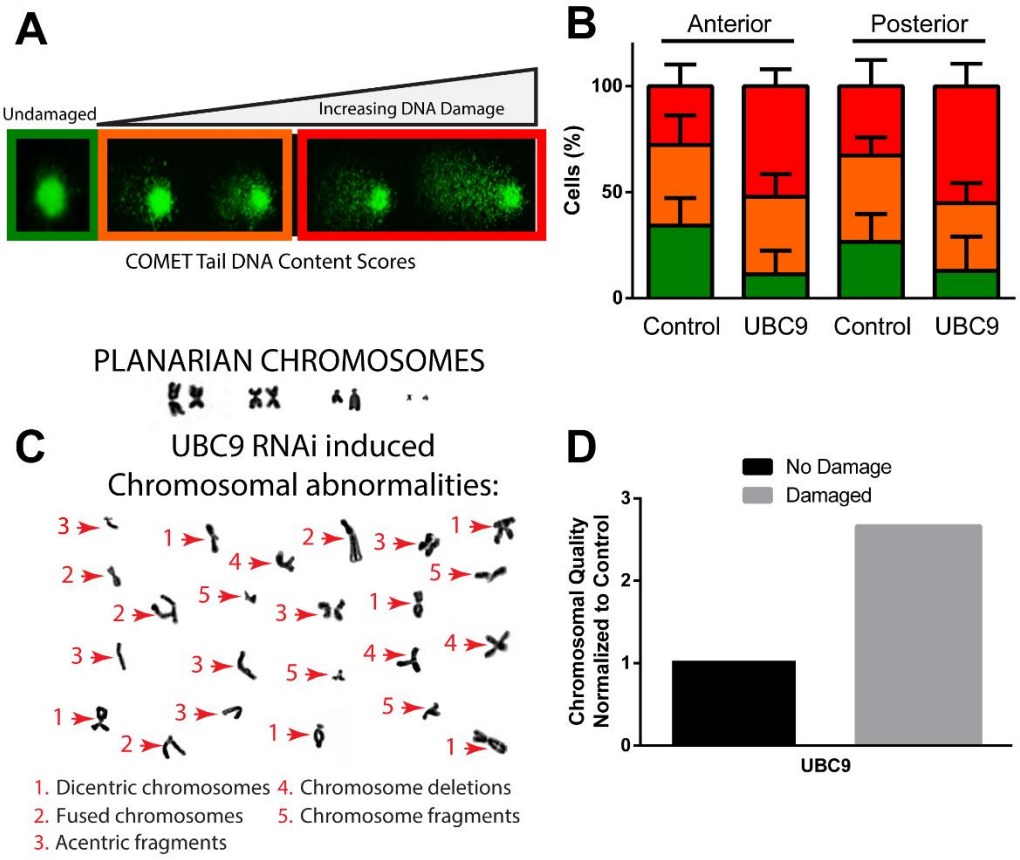

Figure 14: UBC9 is required to maintain genomic integrity along the anteroposterior axis. A) COMET visual scoring used to identify DSBs based on length of the tail. Undamaged (green), moderate damage (orange) and extremely damaged DNA (red). B) Downregulation of UBC9 leads to systemic accumulation of DNA damage as early as day 15 when compared to controls which increases to a maximum at day 25. No difference exists between damages DNA in anterior and posterior. C) Visualization of abnormal chromosomes observed after UBC9 knockdown. D) Chromosome quality (not damage and damaged) normalized to control and UBC9 RNAi 25 dpf animals, N=2.

affected four pairs of chromosomes in *S. mediterranea*. These data suggest that UBC9 is required for faithful maintenance of signaling pathways that mediate DSB repair and chromosomal segregation during mitosis.

Next, we set out to determine whether cells after UBC9 knockdown are able to detect and repair DSBs. Several human specific antibodies against DNA repair proteins such as gamma H2Ax and RAD51 have been found to be compatible with planarians[11,49,143]. Interestingly, UBC9 RNAi animals experienced an increase in gamma H2AX protein expression in the anterior and posterior regions (Fig 15A). These results indicate that intrinsic cellular mechanisms such as ATM/ATR are able to detect DSBs but are incapable of initiating a repair response to fix the damage[11,144–148]. In addition, the spatial distribution of DNA double stranded breaks can be visualized with whole mount immunostaining using antibodies against gamma H2Ax (Fig 15A). Next, we found that RAD51 protein expression was also increased in the experimental group (Fig 15B). Western blot analysis confirmed the increase in RAD51 signal after UBC9 RNAi (Fig 15C-D). Interestingly, increase in signal intensities for both antibodies were consistently displayed in clusters in the pre-pharyngeal and post-pharyngeal area for 70% of the animals. The reason behind why they manifest in clusters is unknown, but it suggests that some cell populations are more susceptible to DNA damage than others. Increase in gamma H2Ax and RAD51 levels demonstrates that the mechanism for sensing DNA damage is active after UBC9 RNAi but the animals are still unable to repair the damage.

3.11 UBC9 facilitates nuclear transport of RAD51 to repair double stranded breaks

Several studies suggest that SUMOylation and UBC9 are an integral part of intracellular transport, especially between the cytosol and the nucleus[43,149–153]. Specifically, UBC9 is required for the nuclear transport of RAD51 after DNA damage has been sensed both directly and indirectly[36,51,80,154,155]. To test this hypothesis, we developed an assay to visualize whether RAD51 protein is actually in the nucleus or the cytoplasm. Exposure to a sublethal dose of gamma irradiation (1250 rads) induces DSBs, to which cells respond to by increasing RAD51 protein expression in their nucleus[11]. They found that nuclear translocation is at a maximum after 5 days post irradiation. Since RAD51 expression is increased, but DNA damage is still present, we hypothesized that RAD51 is not able to translocate to the nucleus to perform its function. Control and UBC9 RNAi animals were exposed to sub-lethal irradiation and the cells were harvested after 5 days to evaluate RAD51 sub-cellular location. Immunostaining for RAD51 on cells revealed that the RAD51 protein in unable to localize to the nucleus to bind to damaged DNA, thus preventing DNA repair (Fig 15E). This experiment revealed that RAD51 nuclear localization was observed in most of the control cells (~80%) whereas a smaller fraction of cells (31%) in the experimental group exhibited the same behavior (Fig 15F). In summary, these data indicate that the function of

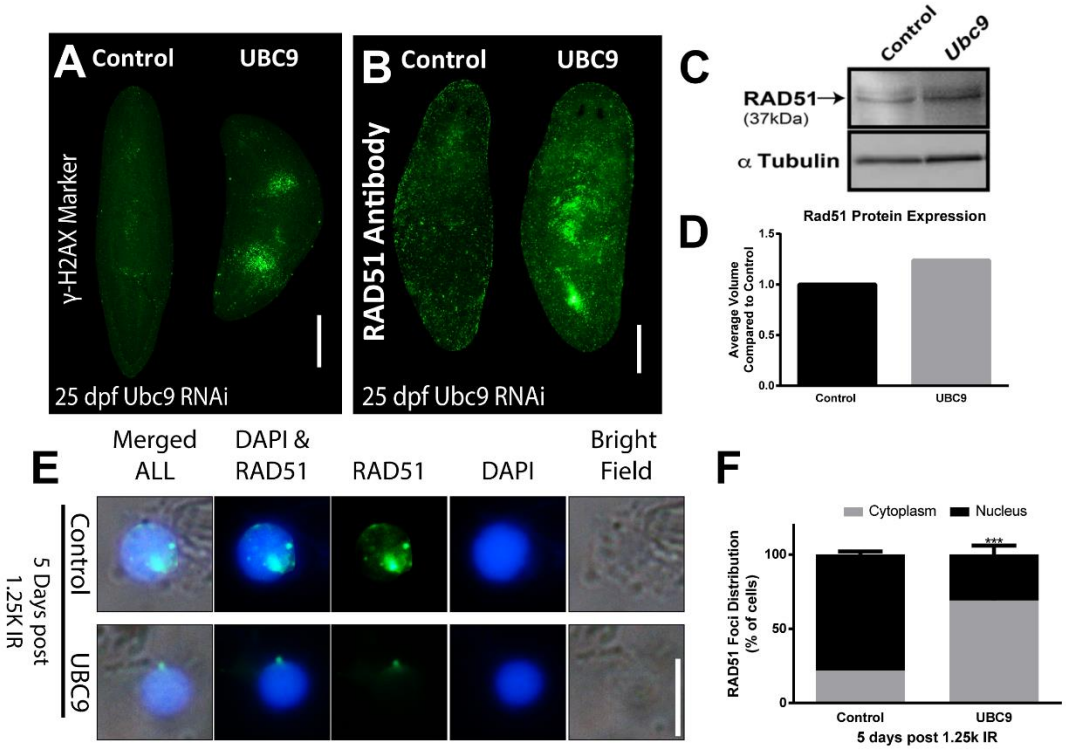

Figure 15: UBC9 facilitates nuclear transport of RAD51 to repair double stranded breaks. A) Whole mount immunostaining against gamma H2AX antibody in control and UBC9 RNAi animals 25 dpf n=20 and N=2 B) Whole mount immunostaining against human RAD51 antibody in control and UBC9 RNAi animals 25 dpf. n=15, N=2 Scale bars = 200 µm and images are representative of approximately 70% of the animals in each condition. C-D) Western-blot and subsequent quantification for RAD51 in control and UBC9 RNAi animals. Alpha tubulin was used as an internal control. Protein was extracted from n>30 animals. E) Spatial distribution of RAD51 immunostaining (green) in reference to the cell nucleus (stained with DAPI, blue) in control and UBC9 RNAi 18 dpf and 5 days after sub-lethal irradiation (1.25k rads). RAD51 subcellular localization to the nucleus is at a maximum at this point in time. Scale bar = 10 µm. F) Quantification of cells with RAD51+ foci in the nucleus and cytoplasm in control and UBC9 RNAi. ***p < 0.001; two-way ANOVA.

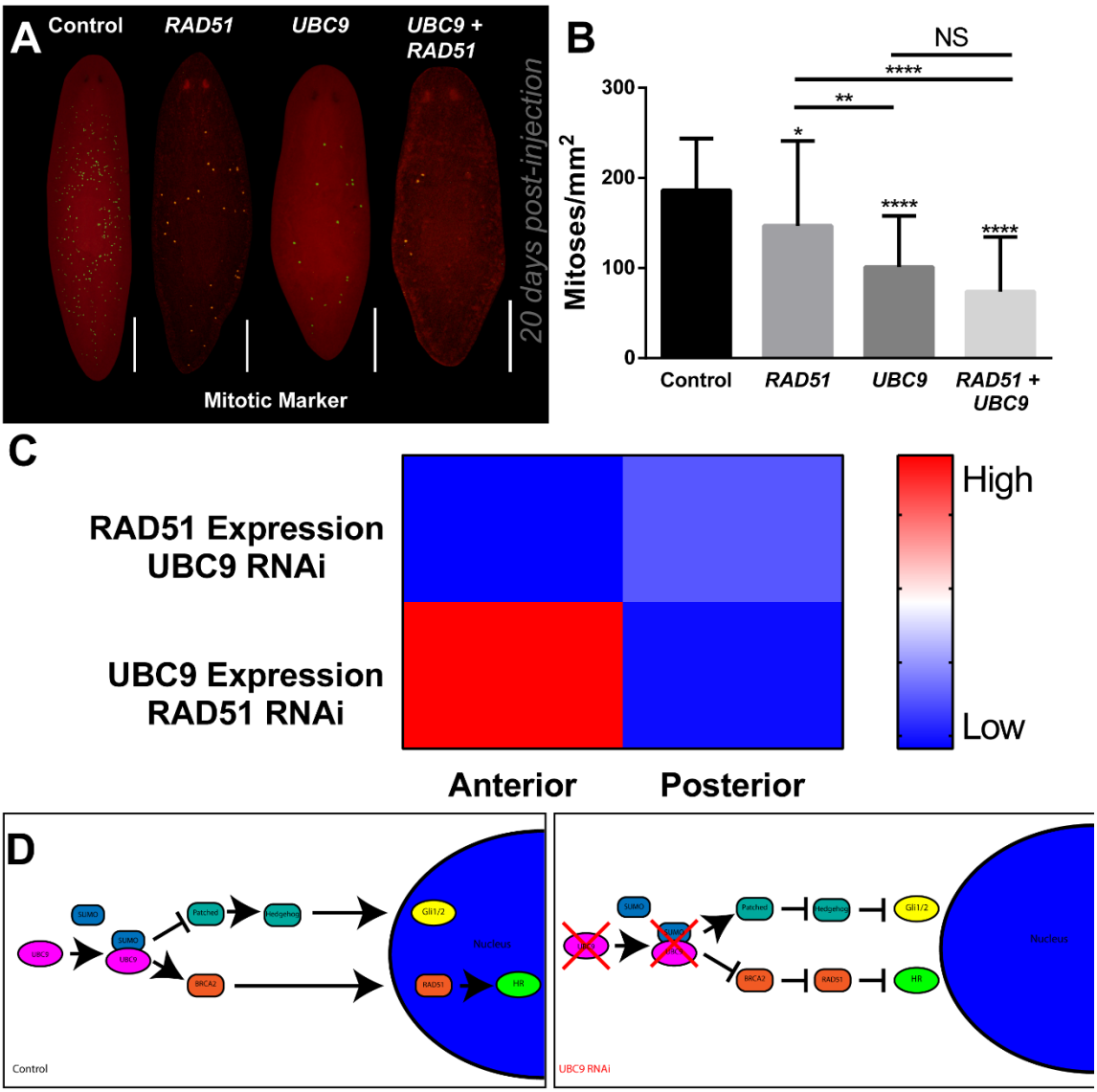

Figure 16: UBC9 and RAD51 work synergistically to maintain tissue homeostasis. A) Representative images of H3P+ foci in control, Rad51 RNAi, UBC9 RNAi and Rad51 + UBC9 RNAi 20 dpf. B) Quantification of H3P+ foci in whole animal after each previously mentioned RNAi. Mitotic number is H3P+ foci divided by surface area in mm2. N>20, replicates=2. C) UBC9 gene expression shown as fold change normalized to control in Rad51 RNAi animals 30 days post injection. Rad51 gene expression shown as fold change normalized to control in UBC9 RNAi animals 25 dpf. D) Diagram depicting UBC9 as an upstream regulator of Hedgehog and homologous recombination pathway. Patched upregulation when UBC9 is turned off leads to attenuation of Hh signaling and loss of posterior polarity, UBC9 controls RAD51 translocation directly by affecting nuclear transport of RAD51 or via regulation of BRCA2. ***p < 0.001; ****p < 0.0001; two-way ANOVA. Scale bars = 200 µm.

UBC9 in maintenance of DNA integrity and RAD51 localization is conserved also in *S. mediterranea*.

Since UBC9-mediated regional cell death follows a similar pattern as RAD51 knockdown model and presents with DNA damage, we wanted to explore the complex interplay between these signaling pathways. We devised double RNAi experiments similar to the previous scheme with Hh signaling. These experiments revealed that RAD51 and UBC9 synergistically reduced mitotic activity throughout the animal (Fig 16A). This was corroborated by quantitative analysis of H3P positive foci (Fig 16B). Within the same time frame, UBC9 downregulation leads to a more significant loss in mitotic activity than RAD51 alone. However, when you combine them together, it leads to largest decrease in mitotic activity but insignificant when compared to UBC9 alone (Fig 16B). This suggests that RAD51 loss of function contributes minimally to the UBC9 phenotype. Furthermore, this finding is supported by the observation of RAD51 gene expression after UBC9 RNAi. RAD51 expression is suppressed across the anterior and the posterior region of UBC9 RNAi animals whereas UBC9 is specifically upregulated in the anterior region in RAD51 RNAi animals (Fig 16C). This observation suggests that UBC9 upregulation may be partly responsible for the continued proliferation of neoblasts with DNA damage in the anterior of RAD51 RNAi animals. These effects of UBC9 upregulation on continued cell survival remain to be investigated. Taken together, these results suggest that the SUMO pathway and UBC9 is upstream of RAD51 and regulates regional planarian cell fate in multiple ways (Fig 16D).

3.12 RNA sequencing reveals MADD as a novel regulator of neoblast function

So far, we have established that UBC9 is required for regional maintenance of tissue homeostasis through the regulation of Hh signaling. In addition, UBC9 knockdown leads to loss of genomic integrity and increased accumulation of DNA damage throughout he animal, specifically by blocking RAD51 nuclear translocation. Though the posterior region deteriorates after loss of UBC9 function, the anterior region persists, and cells continue to undergo mitosis with DNA damage (Fig 5A). The mechanism behind survival of anterior tissues after UBC9 RNAi is unknown. We hypothesized that SUMOylation must be working in tandem with other conserved signaling pathways to lead to survival of cells with anterior fates. To answer this question, we decided to perform RNA sequencing to gain a better understanding of the genetic landscape required to maintain anterior tissues with DNA damage. We aim to build a molecular network through which we can identify the mechanisms underlying regional differences in cellular proliferation across the AP axis.

In order to perform the transcriptomic analysis, control and UBC9 knockdown animals were generated via RNAi as described earlier. The animals were amputated at the pre-pharyngeal border to separate the anterior and posterior compartments. This ensures that we will help us narrow down and

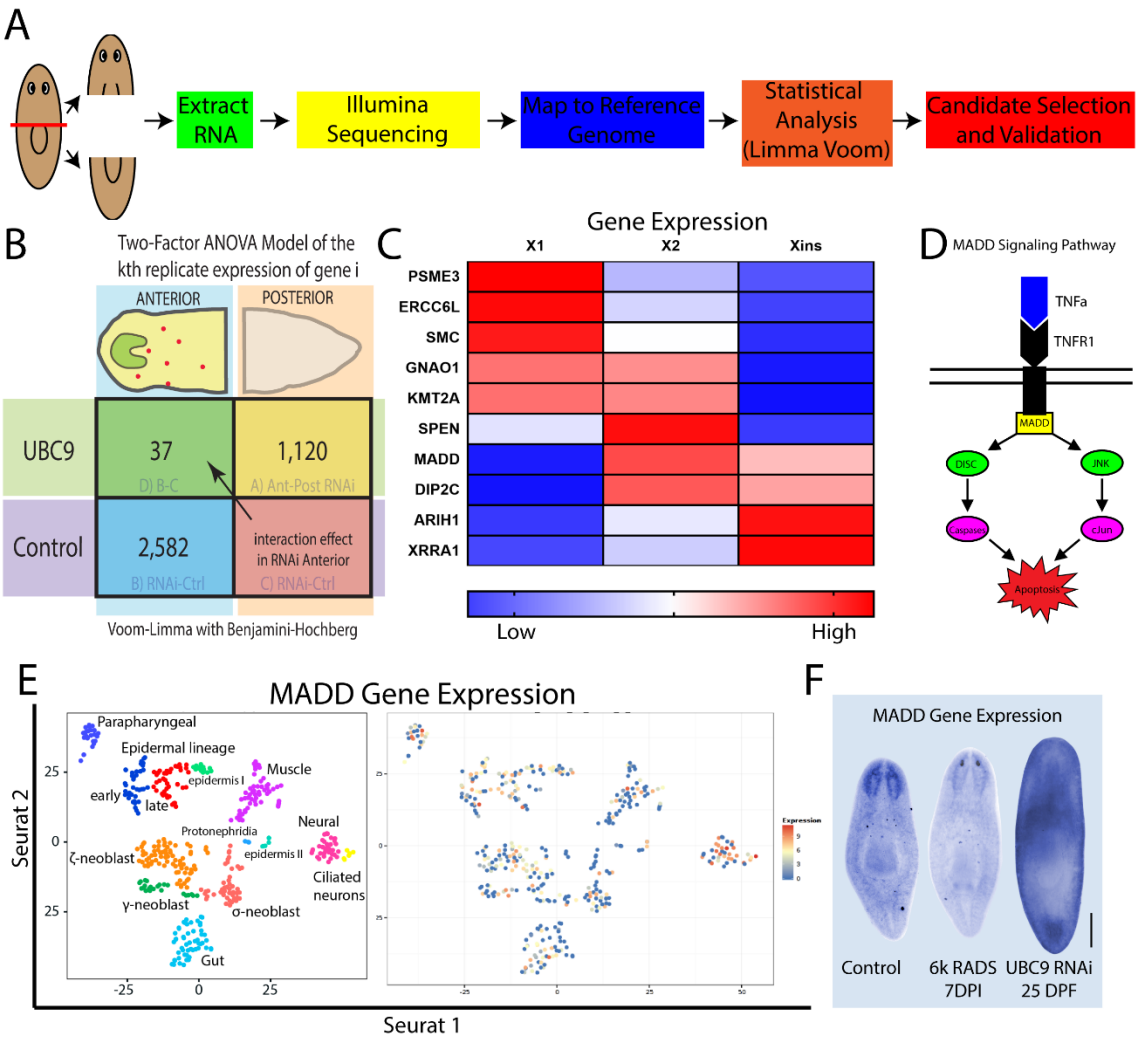

Figure 17: Transcriptomic analysis of UBC9 knockdown model identifies MADD as a potential regulator of neoblast function. A) Schematic diagram detailing how the RNA seq analysis was performed. B) Model depicts transcriptomic data generated using the Voom-Limma pipeline with a Benjamini-Hochberg false discovery rate of 1%. Number in blue indicates genes differentially expressed between control and UBC9 RNAi animals. Number in yellow portrays genes differentially expressed between the anterior and posterior region of UBC9 RNAi animals. Orange box uses statistical analysis similar to two-way ANOVA to determine the interaction effect between blue and yellow boxes. Green box indicates the number of genes that are differentially expressed specifically in the anterior region of UBC9 RNAi animals. C) 10 genes that are differentially regulated in anterior on UBC9 RNAi animals categorized into their expression in three planarian cell populations. D) Schematic representation of MADD signaling as a regulator of cell death. E) Data acquired from the single cell RNA seq database shows MADD is expressed in the neoblast subclasses, epidermis and especially in the neural lineage[89]. F) *in situ* hybridization of MADD gene expression in control, lethally irradiated (6k rads) and UBC9 RNAi animals. n>15, N=3. Scale bars = 200 µm.

identify the responsible genes further down the line. The anterior and posterior fragments were pooled separately, and RNA was extracted and sequenced (Fig 17A). Next, the resulting transcriptomic reads were aligned to the *Schmidtea mediterranea* reference genome[106,107]. The raw transcript counts were statistically analyzed, and differential expression was determined by using the Limma-Voom modelling platform, which is specially designed for analyzing complex experiments with a variety of experimental conditions, such as looking at the anterior vs posterior regions of control and UBC9 RNAi animals (Fig 17B). Through this approach, we identified 37 differentially regulated genes that were specifically enriched in the anterior (green box) (Fig 17B). Next, we narrowed down these candidates to 10 genes by only focusing on genes with literature support for cell proliferation, cell death or cell survival. A heatmap of these 10 genes was generated according to their expression in neoblast and post-mitotic populations within planarians (Fig 17C). These genes were expressed differentially across all stem cell compartments in planarians, revealing the large signaling network that must coexist with different cell types to establish a niche that is amenable for cells to cycle with DNA damage.

Our next step was to validate our RNA sequencing analysis by looking at gene expression of each candidate via *in situ* hybridization and identify if any of them can rescue the UBC9 phenotype. One candidate of interest was the MAP kinase-activating death domain protein (MADD). MADD has been shown to be regulator of apoptosis and it is highly expressed in cancerous cells[156–164] (Fig 17D). Expression profiles collected from the planarian single RNA-seq database illustrated that although MADD is expressed throughout various cell populations like neoblasts and epidermal cells, it is mostly concentrated among the neural lineage, suggesting a role in nervous function[108] (Fig 17E). To validate this data, we examined that MADD gene expression in planarians via *in situ* hybridization and determined that it was specific to the nervous system, but with sparse expression throughout the mesenchyme (Fig 17F). Its expression is persistent even after 7 days post lethal irradiation, which is enough to abolish neoblasts, validating our RNA-seq analysis that MADD is mostly expressed in post-mitotic cells and terminally differentiated cells with some expression in the neoblast population (Fig 17F). Additionally, we looked at MADD expression after UBC9 RNAi and found its expression to be dramatically increased throughout the animal, which confirms what we expected from the RNA-seq analysis.

In order to further characterize MADD, we performed loss of function analysis via RNAi (Fig 18A). MADD knockdown resulted in animals who fissioned excessively, with as much as 80% of animals having at least undergone one round of fission and many animals fissioning multiple times by the end of the RNAi time course (Fig 18B-C). Fissioning usually follows when an animal grows too big to support its biomass, thus it will eventually separate its head and body fragments in a process called fission. It is also the primary means of reproduction in asexual animals. The resulting tail fragment regenerates the entire body as an artificially

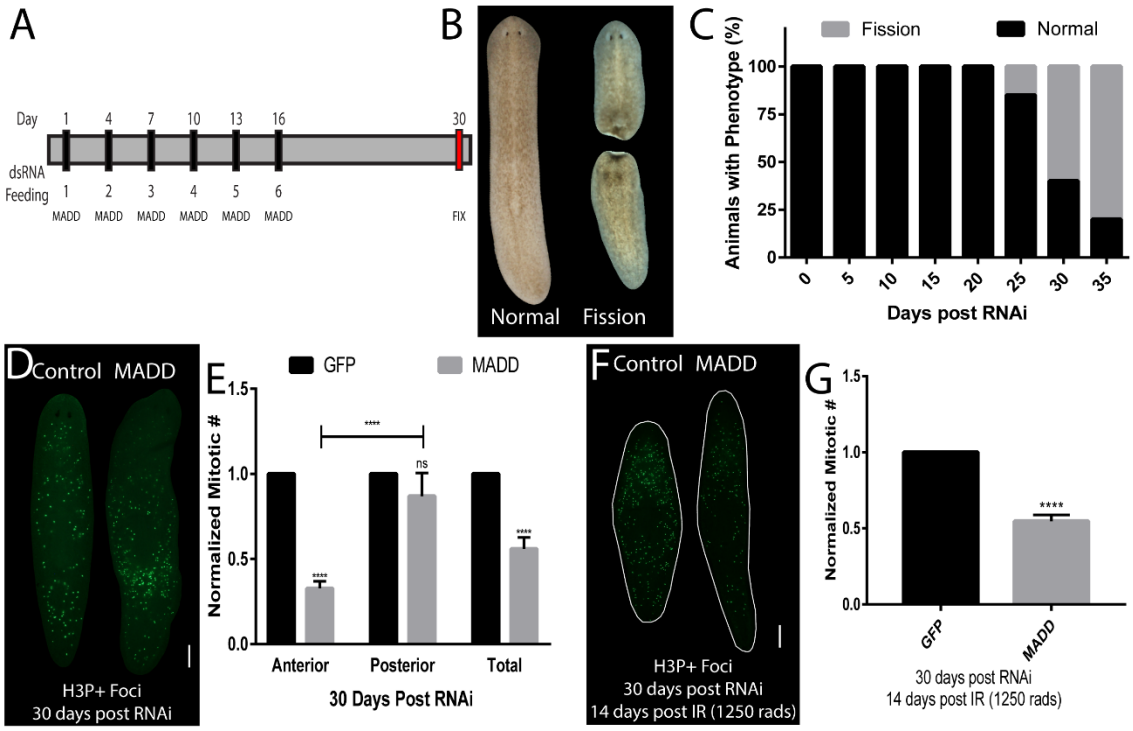

Figure 18: MADD regulates fissioning behavior and neoblast maintenance. A) Schematic for MADD gene knockdown. Animals are fed every three days over a total of six feedings and fixed for experiments. B) Representative images of a normal and fissioning planarians. C) Phenotypic frequencies of fissioning behavior in MADD RNAi animals. By day 30, almost 70% of MADD RNAi animals have undergone at least one round of fission. In addition, all animals display improper gliding behavior and secrete excessive mucous. n=40, N=3 D) Immunostaining against mitotic marker H3P in control and MADD RNAi animals. E) Quantification of mitotic activity expressed as fold change in control and MADD RNAi animals. Mitotic activity is lower in the anterior than the posterior of MADD knockdown animals. n=30, N=3. F) Immunostaining against mitotic marker H3P in control and MADD RNAi animals after sublethal irradiation. G) Quantification of mitotic activity expressed as fold change in control and MADD RNAi animals. MADD is responsible for neoblast repopulation after neoblasts have been exposed to irradiation. ***p < 0.001; ****p < 0.0001; two-way ANOVA. Scale bars = 200 µm.

amputated tail fragment would do, and the body fragment regenerates a tail, resulting in two whole planarians. Fissioning behavior in planarians is thought to be controlled by the brain through excretion of some unknown signaling molecule that displays an AP gradient, high in the anterior to low in the posterior[165–169]. Our finding suggests that MADD may be directly or indirectly responsible for the secretion of this molecule. In addition, 100% of animals also secreted excessive amounts of mucous and displayed poor motor function, exemplified by scrunching rather than smooth gliding in the water[170,171]. Previous data suggests that defects in movement may be due to improper ciliogenesis[115], but this hypothesis remains be tested in MADD knockdown animals.

Next, we assessed the molecular events driving this phenotype by looking at mitotic activity. Immunostaining experiments with H3P revealed a significant decrease in mitotic cells in the anterior, but not in the posterior of MADD RNAi animals (Fig 18D). We quantified the number of H3P positive foci and determined that while mitotic activity was reduced in MADD knockdown animals than controls in general, loss in stem cell activity seems to be restricted to the anterior region (Fig 18E). This result is very interesting since it is directly opposite to what we observed in the RAD51 knockdown model and the interaction between will require further study. Finally, we identified whether MADD is required for neoblast maintenance. It was previously shown that sublethal irradiation depletes neoblasts in planarians, but they recover over a period of 7-14 days[93,172]. We posited that dysregulation of any gene needed for neoblast maintenance would slow down or half the recovery of these stem cells. We subjected control and MADD RNAi animals to sublethal irradiation 1 day after the last RNAi feeding and looking at the mitotic activity 14 days after irradiation. We observed a general loss in H3P+ foci uniformly across the animal and this was further corroborated by foci quantification (Fig 18F-G). Taken together, these findings suggest a novel role for MADD as regulator of neoblast maintenance and function in planarians.

3.13 Knockdown of MADD rescues UBC9 phenotype by reducing cell death in the posterior

One of our initial goals with this RNA sequencing approach was to identify and characterize genes that were differentially regulated in the UBC9 knockdown model that could potentially rescue the regional defects associated with it. Data supporting rescue of the UBC9 phenotype would not only provide credence to the sequencing analysis but provide further insight into the molecular landscape through which SUMOylation controls cell fate decisions in the AP axis. To this end, we performed double RNAi knockdown of MADD and UBC9 via bacterial feeding similar to previous schedules (Fig 19A). Our initial phenotypic assessment of the four RNAi conditions led us to uncover defects we labelled anterior abnormality, posterior abnormality, anterior and posterior abnormalities and fission fragments (Fig 19B). As previously noted, UBC9 RNAi animals from this altered feeding schedule still display posterior abnormalities (90%) while MADD RNAi animals still

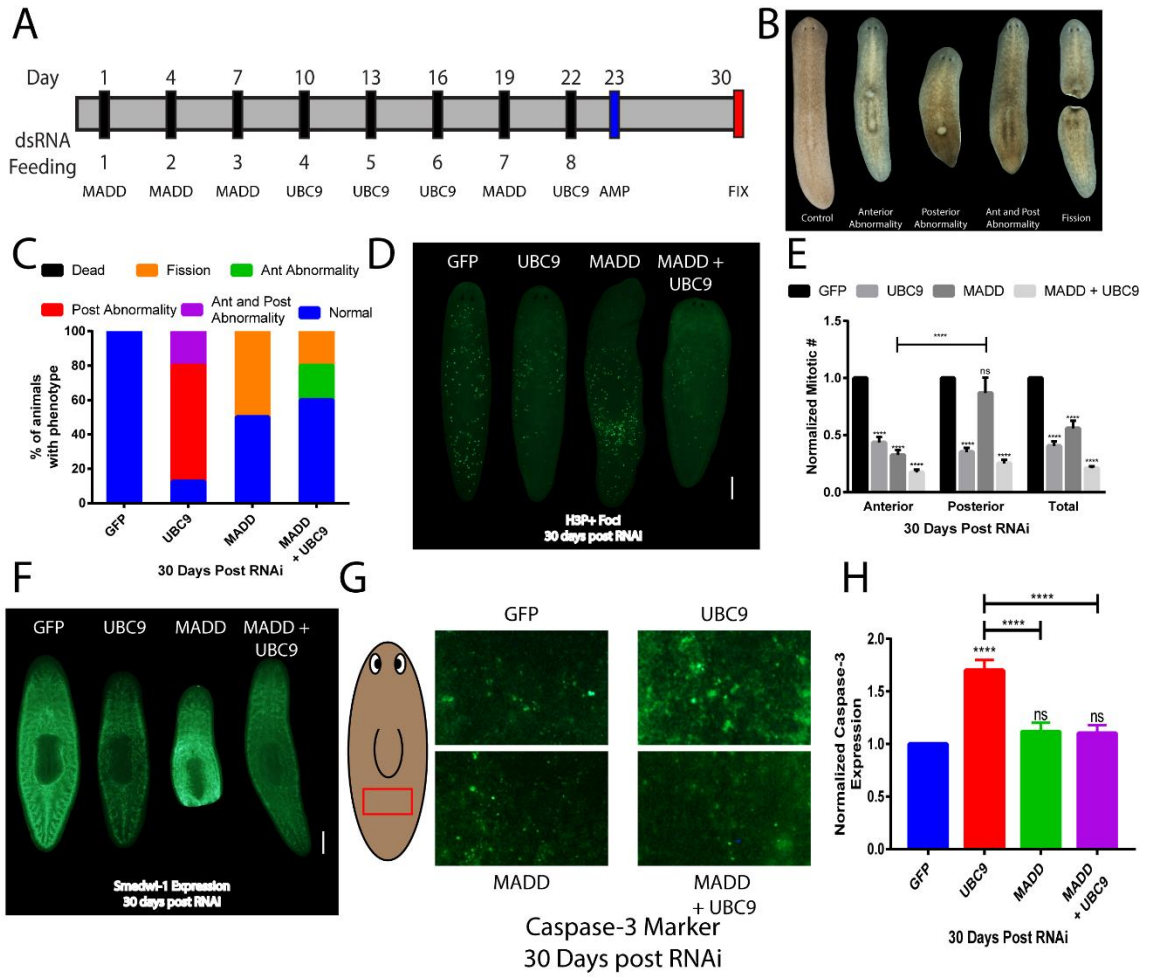

Figure 19: Knockdown of MADD rescues UBC9 phenotype by reducing cell death in the posterior. A) Schematic for double knockdown of MADD and UBC9. B) Representative images of planarians with phenotypes. C) Graph displays phenotypic frequencies in control, MADD, UBC9 and double RNAi animals. 80% of UBC9 RNAi animals have poster abnormalities whereas none of the double RNAi animals do. n=30, N=3 D) Immunostaining against mitotic marker H3P all RNAi conditions. E) Quantification of mitotic activity expressed as fold change in all RNAi conditions. Mitotic activity is uniformly lower in the double knockdown animals than UBC9 RNAi alone. F) *in situ* hybridization against stem cell marker *Smed*wi-1 in all RNAi conditions. G) Animal represents section where fluorescence intensity reading was taken as displayed by the red box. H) Representative images of caspase-3 signal in the post pharyngeal region of all RNAi conditions. I) Quantification of caspase-3 fluorescence intensity in all four RNAi conditions. n > 15, N=2 ***p < 0.001; ****p < 0.0001; two-way ANOVA. Scale bars = 200 µm.

fission excessively, demonstrating the success of the new protocol (60%) (Fig 19B-C). Interestingly, when MADD was combined with UBC9, it rescued the posterior abnormalities and somehow caused the appearance of anterior abnormalities (Fig 19C). Simultaneously, UBC9 halts the fissioning in MADD knockdown animals (Fig 19C). It is possible that fissioning may require an increase in mitotic activity, which will be severely depleted in the absence of UBC9, does leading to our observation. The reversal of the UBC9 phenotype suggests MADD may act as a molecular switch for regulating stem cell fate in the presence of DNA damage.

Next, we looked to further understand the molecular events driving this reversal by first assessing for the mitotic activity. UBC9 RNAi alone results in uniform loss of neoblasts, whereas MADD RNAi animals display reduced mitotic activity in the anterior while the posterior remains the same, as expected (Fig 19D). Strikingly, we saw a uniform depletion of cycling cells in the double RNAi condition, albeit a somewhat lower mitotic activity than UBC9 alone (Fig 19D). This was further corroborated by *in situ* hybridization against neoblast marker *smedwi-1* (Fig 19F). Similar to what we established with UBC9, this suggested that the phenotypic reversal caused by MADD may be dependent on its regulation of cell death as opposed to cell proliferation. To test this hypothesis, we assayed for cell death using the marker caspase-3, specifically in a small portion in the posterior where we previously established cell death occurs in UBC9 RNAi animals (red box) (Fig 19G). We observed that while there were no significant differences between control and MADD RNAi animals, we saw a significant decrease in caspase-3 positive foci in the double knockdown animals when compared to UBC9 alone (Fig 19H). To verify, we quantified the levels of fluorescence intensity and determined that MADD RNAi was able return the levels of cell death in the UBC9 condition back to basal levels (Fig 19I). Taken together, these data suggest novel roles for MADD as regulator of regional cell proliferation and as a negative regulator of apoptosis. The underlying molecular mechanisms driving both the increased fissioning and the decrease in posterior specific cell death remains to be investigated.

4. DISCUSSION

Studies have demonstrated that regional signals contribute to cell fate decisions in the adult body[9,11,14,15,49]. There is a tendency for cells near the anterior portion of the body to have a superior proliferative response and this is especially applicable to cancer[9,10]. Despite its relevance in human health[17,18], the mechanism underlying this regional difference remains poorly understood. Recent scientific literature suggests that the posttranslational modification via SUMOylation may be a potential candidate driving this phenomenon[24–26]. Post-translational modification (PTMs) with small ubiquitin-like modifier (SUMO) is a key regulator of various cellular processes in eukaryoyes[27]. A major challenge facing the study of the SUMO pathway and its components is the fact that its complete abrogation is embryonically lethal, which hampers our capacity to understand the systemic contribution of SUMO pathway at post-embryonic stages[51–53]. To circumvent this limitation, studies in *S. mediterranea* will provide unique opportunities to analyze PTMs through SUMOylation during simultaneous renewal of many tissues and regeneration in the context of the adult body. This is critical because non-Ecdysozoan protostomes include the largest number of animal phyla across metazoans and the study of members of this group will complement information obtained in more traditional model systems[173–175].

In this work, we examined the detailed molecular mechanism regulating regional cell fate during tissue renewal and regeneration in the UBC9 knockdown model. We established that SUMOylation is evolutionarily conserved in *S. mediterranea*, a member of the under studied group of Lophotrochozoans. The lack of redundancy of UBC9, the sole E2 conjugating enzyme, in the planarian genome recapitulates its evolutionarily conservation in the regulation of the SUMO pathway across eukaryotes. This is further evidenced by the close relationship in the protein sequence between human and planarian UBC9. Specifically, we demonstrated that UBC9 is instrumental in controlling cell cycle, stem cell renewal and adult tissue homeostasis. We establish UBC9 is an upstream regulator that exerts control over Hedgehog signaling to mediate regional cell fate decisions and anteroposterior polarity. In addition, UBC9 function is required to facilitate DNA repair and maintain genomic integrity as it is responsible for the subcellular translocation of RAD51 into the nucleus, an essential component of homologous recombination. Finally, through RNA sequencing, we identified MADD as a novel regulator of cell death in the presence of genomic instability induced by UBC9 knockdown and is part of the large molecular landscape through which SUMOylation maintains adult tissue homeostasis.

4.1 SUMOylation is required for proper cell function and tissue homeostasis in planarians

The role of UBC9 in regulating stem cells depends on the context and the experimental models in which the studies are performed[47,56,176,177]. For example,

UBC9 function is required for embryonic stem cell survival in vitro and reprograming of induced pluripotent cells but UBC9 function is not pertinent to the maintenance of mouse embryonic fibroblasts[50]. Our analysis looks at the function of UBC9 in planarians, which contain large pools of adult pluripotent stem cells (neoblasts). UBC9 RNAi led to rapid depletion of neoblasts across the AP body axis (Fig 5A). This may be due to its effect on the cell cycle dynamics as knockdown of UBC9 causes an accumulation of cells in G1 phase and a reduction in G2/M phase (Fig 6B). Previous studies have suggested knockdown of UBC9 is a key regulator of cell cycle transition through various mechanisms of action[55,130]. Additional findings suggest UBC9 knockdown induces DNA damage and chromosomal abnormalities, which would block cells from passing the critical cell cycle checkpoints (Fig 14B). As a consequence, this blockage in G1 phase could also impair the progression of post-mitotic progeny that will negatively impact the maintenance of differentiated tissues. Our findings in planarians are consistent with these observations and support a conserved role for SUMOylation in cell cycle control and adult stem cell maintenance.

Collective regulation of cellular decisions along the AP axis is subject to mechanisms that remain poorly understood. Earlier studies have demonstrated that downregulation of UBC9 induces regional cell death that precede lethality during embryonic development in *D. melanogaster* and zebrafish[24,25]. In accordance, our results demonstrate consistent regional cell death followed by lethality, supporting functional conservation across metazoans and developmental stages (Fig 9A). Additionally, we provide mechanistic insights behind the cell death-driven regional loss of tissue after UBC9 RNAi. Deregulation of Hh pathway by UBC9 knockdown is evident through the steady increase of Ptc expression, which is detected early in the phenotype (Fig 11B). Previous work has determined that Ptc ultimately controls the hedgehog pathway, as high levels of Ptc serve to sequester any free Hh and limit its activity as an activator[178]. Our findings about a role for SUMOylation in regulating Hh signaling are also supported by several recent studies observations in Drosophila[179–182]. For example, Hh stimulates Smo sumoylation by dissociating it from a desumoylation enzyme PIAS1. SUMOylated Smo prevents its ubiquitination and degradation, leading to Smo accumulation on the membrane and elevated Hh pathway activity. Furthermore, downregulation of Hh signaling via agonists or Ptc upregulation has been linked to control tissue sculpting through selective cell death and even accumulation of DNA damage in several models[183–187]. Taken together, these data suggest UBC9 control of Hh signaling is well conserved and the regional defects we observed are in line with Hh downregulation.

The striking lack of tail regeneration highlights SUMOylation as a region-specific requirement for tissue repair by affecting transcription of Hh genes and through regulation of yet to be identified molecular signals (Fig 11B). This result is consistent with previous observations in planarians where repression of Hh signaling results in lack of tail regeneration[109,110]. Nonetheless, it will be interesting

to determine whether 1) other mechanisms besides Ptc signaling also affect SUMOylation-mediated cell death or 2) if increased Ptc expression is involved in regional non-canonical Hh signaling related to cell death. Our findings also highlight the importance of UBC9 as an early requirement for neoblast-driven injury response and suggest that depending on the circumstances SUMOylation may play synergistic/parallel roles or even act as an upstream component of the Hh pathway. The UBC9 downregulation also extend to Hh-mediated impairment of neurogenesis, revealing UBC9 also controls behavior of neural progenitors and brain function[141,188]. Hh signaling is also associated with planarian glial cells and future studies will aim to determine whether UBC9 loss-of-function affects the function of glial cells through its regulation of Hh signaling[142]. Altogether, our results demonstrate that SUMOylation, in the context of the whole adult body, regulates important aspects of cellular proliferation and cell death at regional and systemic levels.

4.2 A novel role for UBC9 and SUMOylation in regeneration

So far, no link has been established between SUMOylation and regeneration as this pathway has mostly been studied in the context of early development and regeneration-deficient models. Here, we establish that loss of SUMOylation through UBC9 knockdown leads to impaired regeneration in the otherwise robust regenerative planarian model *Schmidtea mediterranea*. The ability to restore tissue integrity following wounding and to subsequently repair damaged or lost structures is fundamental to the survival of all multicellular organisms. This task requires a robust and well-coordinated mechanism for rapid induction of factors that are needed for faithful regeneration of the damaged structures. Wounds trigger entry into mitosis at long distances (body wide) and induction of cell cycle changes distant from the site of injury. Neoblasts are then signaled to migrate and divide near the wound and commit to production of cells at the wound that will exit the cell cycle and differentiate[93,172]. With this in mind, we hypothesize that UBC9 RNAi attenuates regeneration in two possible ways.

First, loss of UBC9 reduces the capacity for neoblasts to enter M phase and complete mitosis to maintain proper tissue homeostasis (Fig 6B). Since the planarians are already exhausted of their neoblast population, this makes them unable to respond properly to the missing tissue stimulus and mount the proper mitotic response. We know from previously established literature that the planarian wounding response involves an increase in mitotic activity 6 and 48 hours post amputation. This suggest that lack of UBC9 activity may be stopping the animals from properly generating this initial burst in mitotic activity due their inability to enter M phase. Second, it's possible that UBC9 is responsible for maintaining the transcriptional network that is associated with planarian regeneration initiation[90,172]. Data gathered from the single cell RNA seq analysis suggests that UBC9 expression is massively upregulated within hours after amputation,

signifying its importance in initiating regeneration (Fig 12A). Previously, it has been suggested that several key genes are of absolute importance to initiating and maintain the wounding response in planarians[172,189]. It is possible that these genes may be subject to SUMOylation and without UBC9 function, they are unable to respond to the wounding stimulus and mount a proper regenerative response. Whether or not these are affected by UBC9 knockdown is to be determined and is subject to further experimentation.

Second, the UBC9 phenotype displays some resemblances in intact and regenerating animals. Specifically, during homeostasis, UBC9(RNAi) animals lose their tail and during regeneration, worms are unable to form posterior blastema. In the anterior region, we show that intact animals develop anterior abnormalities over time, which leads to loss of tissue in the anterior region but only at very late stages of the phenotype when they start dying (>25 days post-RNAi). The regenerating worms also show defective anterior regeneration that is associated with a small blastema and defective neurogenesis and brain formation. These examples demonstrate that anterior and posterior defects are present in both the intact and the regenerating animals. However, differences in the manifestation of these defects are visualized depending on the timeline in which the animals are analyzed (Fig 4C). Our work suggests that SUMO targets in the posterior regions are more sensitive to changes in their SUMOylation state when compared to the anterior counterpart and this is likely the reason for the early posterior defect. This is further exacerbated by the loss of Hh signaling, where posterior tissues can no longer be specified and are not created initially following amputation. One way to test this hypothesis is to generate anterior and posterior fragments from normal planarians and subject them to the spectomycin B1 or ginkgolic acid, both of which are known to inhibit SUMOylation. We can then assess the regeneration of each fragment and if we see a marked difference in blastema formation, it would give credence to this idea of differential SUMOylation. Taken together, our data shows the first definitive link between SUMOylation and regeneration and future studies will be needed to elucidate how this regulated in planarians.

4.3 UBC9 and RAD51 knockdown models to study genomic instability and cancer

So far, we have developed two independent DNA damage models in planarians by disrupting gene function via RNAi of RAD51 and UBC9, both of which surprisingly manifested with phenotypes resembling regional defects along the AP axis[11,49]. Both knockdown models present with important patterns of regional and molecular defects along the AP axis and displayed loss of genomic integrity, specifically via accumulation of DSBs throughout the planarian body[11,49] (Fig 20A-D). Molecular analysis in both models revealed a transient presence of DNA DSBs and chromosomal abnormalities that progressively increased over the time (Fig 14A). This is consistent with the role RAD51 plays in DSBs repair through HR. However, the mechanism driving this phenomenon in the UBC9 phenotype

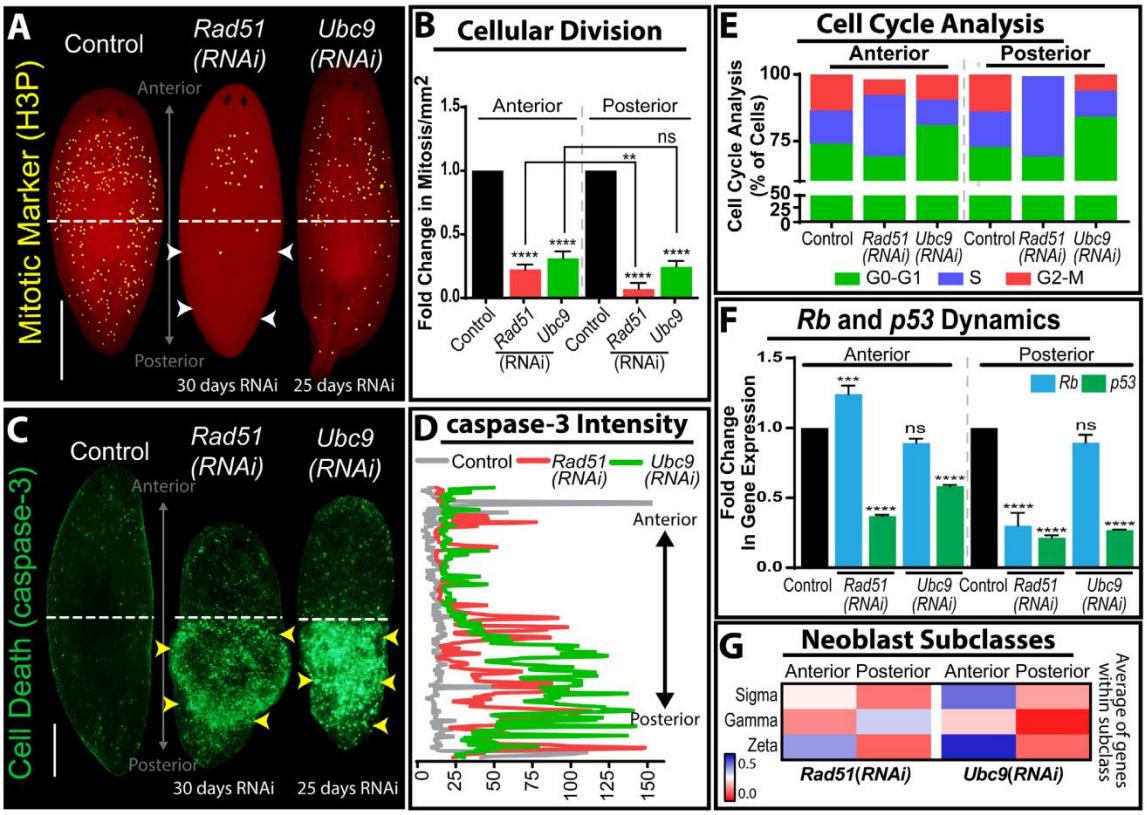

Figure 20: RAD51 and UBC9 knockdown yields high levels of DNA damage, but different neoblast responses. A) Whole mount immunostaining against histone-3 phosphorylated (H3P) in control, Rad51 RNAi and UBC9 RNAi models. Note the difference in mitotic cells along the anteroposterior axis in the Rad51 RNAi group; white arrow heads indicate a severe decrease in mitosis in the posterior versus the anterior. B) Quantification of mitotic activity in control, RAD51 and UBC9 RNAi animals. C) Whole mount immunostaining against caspase-3 antibody in Rad51 and UBC9 RNAi animals. D) Quantification of the fluorescence intensity from caspase-3 stained Rad51 RNAi and UBC9 RNAi animals. Intensity readings were obtained by tracing a line in the middle of the animal from the anterior to the posterior region using ImageJ software. E) Cell cycle analysis using flow cytometry in cells dissociated from the anterior and posterior regions in animals subjected to Rad51 RNAi and UBC9 RNAi. F) Fold change in gene expression of Rb and p53 relative to the control. G) Heat map, representing fold change in the average of gene expression of neoblast subclass (sigma, gamma, zeta) markers in the anterior and posterior regions. Red indicates diminished gene expression and blue increased gene expression. **p < 0.01; ***p < 0.001; ****p < 0.0001; two-way ANOVA. Scale bars = 200 µm.

was less evident. Two observations were critical to relate SUMOylation to DNA damage: 1) the regional defects in animals subjected to UBC9 RNAi were similar to those observed in RAD51 phenotype and 2) late stages of the UBC9 phenotype displayed increase in RAD51 and gamma H2AX protein expression. Additional analysis revealed that DNA damage in UBC9 RNAi is due to the inability of RAD51 to translocate from the cytoplasm to the nucleus to repair DSBs (Fig 15E). This finding links the two models together and additionally explains phenotypic similarities, which altogether supports the idea that HR is the prominent pathway for repair of DSBs in planaria.

Interestingly, we identified that even though DNA damage is ubiquitous, we found certain clusters of cells to be more affected than others in UBC9 RNAi. Why are these cells more prone to DNA damage? Mounting evidence suggests that planarian neoblasts are heterogenous and give rise to lineage-restricted cells that make up differentiated tissues[190–192]. In order to answer this question, we must look to the recently published planarian cell atlas[89,108]. This atlas combines an RNA sequencing approach with *in situ* validation to establish and describe 12 distinct stem cell subclasses within planarians, characterized by a particular transcriptomic prolife[89,193]. Our goal now would be to identify which of these cell populations are most severely affected by UBC9 downregulation. The primary focus would be on the NB2 population of cells, which have been identified as being truly pluripotent since it can single handedly repopulate lethally irradiated animals[194]. Initially, we have to establish whether UBC9 knockdown affects the transcriptomic prolife of these cells, which can be assayed via *in situ* hybridization or qPCR analysis. It has also been identified that these cells express the transmembrane protein tetraspannin -1 (TSPAN-1). Using an antibody against the marker could allow us to track the movement and dynamics of this cell other the time course of UBC9 knockdown. Finally, we can use our previously established markers for DNA damage response such as RAD51 and gamma H2Ax along with TSPAN-1 to specifically identify whether these cells are prone to DNA damage, further validating our initial hypothesis. The approach would help us understand the role of SUMOylation in the process of cellular transformation at the molecular and give context for further investigation.

The induction of DNA damage in most organisms results in a cascade of cell fate decisions leading to cell cycle arrest[195–197]. Cell cycle analysis revealed that while most cells in the RAD51 RNAi were arrested in S phase, cells in UBC9 RNAi animals were primarily arrested in the G1 phase (Fig 20E). p53 and Rb commonly regulate neoblast fate decisions (i.e. apoptosis, proliferation and cell cycle arrest) during tissue renewal, regeneration and the DNA damage response[10,11,198]. We found that p53 gene expression is downregulated uniformly across the AP axis in both RNAi groups (Fig 20F). However, there were stark differences in Rb expression. Specifically, there is an increase in Rb expression in the anterior region of RAD51 RNAi animals whereas there is no significant change in UBC9 RNAi group (Fig 20F). Although our knowledge of Rb dynamics relies on

gene expression data, it is tempting to link increased Rb expression with an ability to bypass cell cycle. Canonically, Rb is thought to be an important regulator of the G1/S checkpoint and studies suggest that overexpression of Rb can increase rates of cellular survival and predispose cells to become more cancerous[199,200]. Furthermore, the genomic instability driven cell cycle arrest in both knockdown models lead to interesting changes in tissue homeostasis and cellular turnover, specifically in terms of cell survival and death (Fig 20A-D). While both models coincide in a significant decrease in the cycling neoblasts (Fig 20G), the RAD51 model reveals a marked difference across the AP axis, specifically loss of survival in the posterior region (Fig 20A). This is likely due to the differential expression regulation of Rb, acting as switch for allowing cell survival in the anterior but not the posterior. On the other hand, both models show a massive increase in cell death in the tail region with significantly less cells dying in the anterior. Experimentation in the UBC9 RNAi model led to us to understand that the cell death is partially attributed to attenuation of Hh signaling and MADD regulation, which will be discussed later. Whether the same mechanism is driving cellular death in the RAD51 model requires further experimentation.

4.4 Rescue of UBC9 phenotype by MADD highlights long-range neural control of cell fate

A remarkable finding from RAD51 and UBC9 knockdown models is that some neoblasts in the anterior region are able to overcome intrinsic surveillance mechanisms and continue proliferating with genomic instability. In the RAD51 model, this may be in part due to increased expression of Rb and neural inputs in the anterior region[11] as it was shown that ectopic induction of brain tissue in the posterior region induced neoblast proliferation[11]. These findings highlight the possibility of intercellular effects, whereby neural signals alter fate decisions of neoblasts with DSBs. Likewise, these results also prompt future studies about possible neural regulation of Rb signaling that facilitate proliferation of neoblasts with DSBs. Alternatively, it is possible that a subset of neoblasts is endowed with proliferative capacity to give rise to cancer-like cells in the anterior. Multiple neoblast subtypes have been characterized[191]. We found that gene expression of markers associated with zeta neoblasts are increased in the anterior for both UBC9 and RAD51 RNAi animals (Fig 20G). Recent research demonstrates the intriguing possibility that inhibition of Hippo signaling triggers dedifferentiation of postmitotic progenitors and reemergence of potency[201]. We speculate that the increasing load of genomic instability may act as a switch for zeta neoblasts to circumvent intrinsic controls and undergo cellular transformation into cancer-like state. Additional experiments are required to dissect the mechanisms driving cells to withstand excessive DNA dam-age and continue to proliferate. Nonetheless, the results obtained with RAD51 and Ubc9 downregulation supports the notion that cellular decisions in the presence of DNA damage are also influenced by regional signals that may involve crosstalk among tissues and organs. This is an important finding as a more comprehensive focus on the regional signals driving proliferation of cells

with genomic instability may help in understand the mechanisms facilitating cancer formation and progression.

Unfortunately, this explanation does not extend to the UBC9 model as Rb expression is depleted uniformly across the body axis (Fig 20F). Since UBC9 and SUMOylation in general affects a wide range of signaling pathways, we needed to develop an alternate strategy to answer this question of how the anterior region persists despite the presence of DNA damage. Our answer to this question came in the form of RNA sequencing. With the ability to bisect planarians via simple amputation, we can extract only the transcripts that are differentially expressed in the anterior in order to find out which one of them is acting as a beacon for cell survival. This analysis eventually resulted in the identification of MADD, which is a newly discovered gene thought to be regulator of cell death through TNF alpha and TRAIL mediating signaling (Fig 17D)[157,158,162,163]. Our data suggests that MADD RNAi is able to rescue all UBC9 related abnormalities, specifically through negative regulation of cell death that follows UBC9 RNAi (Fig 19H). MADD is highly upregulated after UBC9 knockdown, suggesting UBC9 is negatively regulating MADD and it is the ectopic increase in MADD expression that leads to posterior cell death. However, this finding contradicts previous studies in cancer cell lines where attenuation of MADD signaling leads to an increase in cell death[160,163]. One possibility is that MADD function in planarians is different from its function in humans, which is often the case in invertebrate models with various signaling pathways[202–204]. Another possible explanation is that MADD expression may be at a maximum at the end stage of the UBC9 phenotype but may actually be lower in the early stages leading up to tail loss. We have already demonstrated waves of fast gene expression changes is possible in UBC9 knockdown model with Hh and Ptc, but whether this is actually happening with MADD begets further study.

So far, the functional links of MADD established in our study are novel as the previously established literature is scant in identifying the role of MADD in cell proliferation and tissue maintenance. In order to find clues behind the actual mechanism, we once again looked to the literature in the planarian field. Our data as well as the published single cell RNA seq database suggests that MADD expression is vastly restricted to the cephalic ganglia, meaning it could be responsible for proper brain function (Fig 17F). Regeneration data suggests MADD is responsible for proper specification of the cephalic ganglia post amputation. Next, we know that MADD RNAi leads to excessive fissioning (Fig 17B-C). Canonically, fissioning in planarians has been linked to a signal(s) released from the brain and experiments suggest that this signal is actually expressed in the AP gradient along the planarian body axis[165,167–169]. Though we don't know what these signals are, it is possible to suggest they may be certain neurotransmitters and neuropeptides previously described that originate from the cephalic ganglia and ventral nerve cords[141,188]. Some of these secreted neural molecules are under the control of Hh signaling, which we have already established is regulated by UBC9[141]. It is possible that long range regulation may be possible by control of

these signaling factors by Hh and/or MADD to establish and regulate cell fate in the posterior.

Furthermore, a previously identified planarian *Dugesia japonica* gene, P2X-A, also leads to increased fissioning[205]. P2X-A belongs to a family of ATP binding cation-permeable ion channels that involved in functions ranging from cardiac rhythm modulation, transduction of apoptosis and maintenance of muscular tone[205]. We identified a putative *Smed* homolog of P2X and found it to superficially expressed in one single neural linage within the entire gamut of neural progenitors that exist in planarians[90,205]. With these facts in mind, it is possible to speculate that MADD is either directly or indirectly responsible for release of a signaling molecule(s) that interacts with P2X-A to regulate fissioning behavior. It may even be possible for MADD/P2X-A signaling axis to work in tandem with Hh signaling to act as long-range neuronal regulation of fissioning, AP polarity and cell fate. Future studies will be crucial to elucidate how these signaling pathways cooperate to maintain tissue integrity and what role UBC9 plays regulating this complex molecular system.

4.5 Final remarks and future direction

My work has highlighted the importance of SUMOylation as a regulator of various essential cell functions required for organismal integrity (Fig 21). The planarian model system has allowed us to identify novel functions of UBC9 in the context of the adult tissues and in regeneration, something which has remained unknown until now. Though much of the focus of this study has been on UBC9, we have yet to fully characterize the other SUMO components such as SUMO1/SUMO2, SAE1/SAE2, SENPs and E3 ligases within planarians. We know that many of these genes recapitulate the UBC9 phenotype to some extent, but the pathways through which they reach this stage may not be the same for all cases (Fig 8A, E). As a powerful regulator of the DNA damage response, the SUMO pathway remains a prime candidate for drug studies to identify possible therapeutic targets to help stem the onset of cancer. Moving forward, there are still many questions that remain in regard to SUMOylation and planarians. Some of these questions include: 1) what other signaling mechanisms other than Hh is regulated by SUMOylation to control region specific tissue survival? 2) What extent is the SUMO pathway responsible for faithful regeneration of lost tissues in planarians 3) Are the other differentially identified genes specific to the anterior of UBC9 RNAi animals important for regional regulation of tissue maintenance? I will try to provide context and potential outlooks to understand each of these questions in this final section.

We know from experiments involving double knockdown of UBC9 and Hh pathway components that it was not possible to fully rescue the posterior defects associated with UBC9 dysfunction (Fig 11E). It may be possible that SUMOylation controls other signaling pathways that may be responsible for maintaining proper

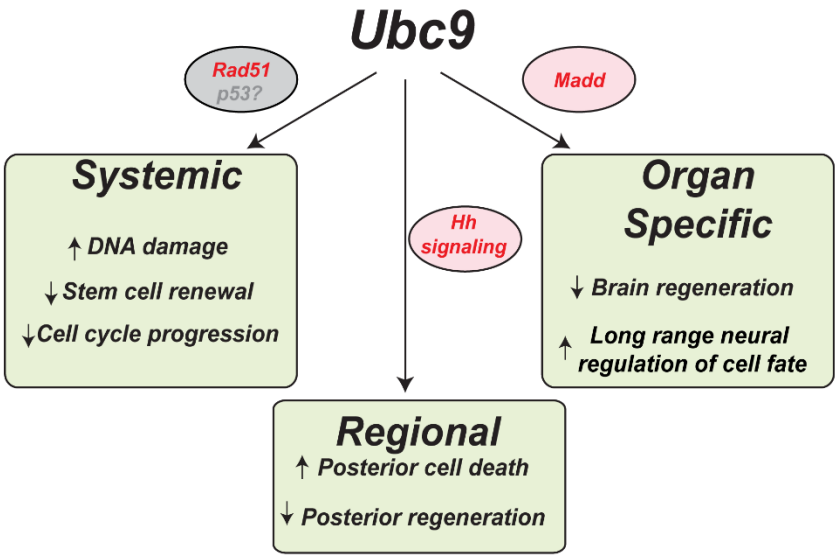

Figure 21: Schematic summary representing UBC9 acts as an upstream regulator of various essential functions in the planarian *Schmidtea mediterranea.* At the organismal level, downregulation of UBC9 lead to a systemic increase in DNA damage due to RAD51 dysfunction, leading to a decrease in both stem cell renewal and cell cycle progression. However, it remains unclear whether inhibition of p53 signaling is associated with any of the systemic effects. Regionally, dysfunctional UBC9 triggers collective cell death and posterior specific abrogation of tissue regeneration, which are mediated through Hh signaling. At the organ level, UBC9 is responsible for proper brain regeneration, likely through regulation of MADD signaling. These experiments establish there may be a long range neural signaling axis that specifies and regulates regional tissue integrity within the planarian body.

AP polarity across the body axis. Previous literature describes a host of signals, specifically Wnt/Beta-catenin and extracellular signaling-related kinase (ERK), that are also instrumental to maintaining proper proportionality by controlling gradient signals[206–209]. For example, knockdown of four Wnt components (wnt1,wnt11-1,wnt11-2 and wnt11-5) have shown to generate phenotype similar to that of UBC9 knockdown[206]. Further double RNAi experiments between SUMO components and these newly identified AP polarity targets will shed light on the exact mechanism through which UBC9 exerts its control over body plan specification. qPCR analysis targeting these polarity genes over the course of UBC9 knockdown will give insight into the dynamics of polarity change that could help us fully characterize the loss of tail phenotype. This would be extremely useful as some of these genes could prove to be potential therapeutic targets when confronted with cancers that follow AP gradients and are more aggressive in the posterior.

In addition, we know very little about the role of SUMOylation in the context of tissue repair and regeneration outside of the observations made in this study. Planarians are prime candidates to study regeneration and we know much about this process, allowing for complete dissection of any and all molecular mechanisms. We know that a regenerative response occurs after the animal sustains, but this response is fluid and heavily dependent on the type of injury[172]. For example, a simple incision to the side of the animal does cause a large increase in cell proliferation, but rather tissue closure and remodeling via cell death. As SUMOylation is a dynamic process, we know that cell responses to different amputations would unique under UBC9 knockdown (Fig 12A). In addition, studies have also demonstrated that changes in gene expression occur shortly after amputation, leading to wave-like changes[93,118,175,210,211]. RNA seq analysis shows that UBC9 expression is mostly upregulated during the early stages of regeneration, coinciding with the mitotic peaks that are commonly observed 2 days after injury (Fig 12A). This is in line with role of SUMOylation in regulating stem cell fate in planarians as well as other models. But how does SUMOylation control other early responders to injury? Genes such as fos-1, egr-3 and jun-1 are expressed by differentiated cells near the wound site within minutes and are overexpressed within the first hour. Is UBC9 involved in the immediate upregulation of these genes? Once again, double RNAi experiments along with qPCR analysis would provide novel insights into the extent of SUMO regulation of the planarian regenerative process. This can be extrapolated among all four identified wound response categories of genes to give a clearer picture of the role of SUMO in regeneration. In addition, we can test how these responses change in regard to different types of injury such as sagittal amputations or incisions. Combined together, these experiments will provide a more complete understanding of the role of SUMOylation in regeneration and could one day provide useful context for regenerative studies in other animal systems.

Finally, we established that SUMOylation and UBC9 are required for the faithful maintenance of genomic integrity in planarians. The role of the SUMO

pathway in regulating components of DNA damage and repair is well established in the scientific literature, but we are the first to demonstrate the dynamics of this regulation in the context of the entire adult body. Using immunofluorescence and karyotyping techniques, we know that cells in the anterior continue to proliferate with ever increasing DNA damage after UBC9 knockdown. RNA sequencing allowed us to identify 37 differentially regulated genes specific to the anterior. So far, we have only characterized MADD and explored its relationship to UBC9. Studying the other candidates may give greater insight into the role of regional signals in regulating tissue homeostasis, specifically genes such as ERCC6L, KMT2A, SPEN and ARIH1, which have been linked to cell proliferation and cell survival (Fig 17C). Specifically, candidates associated with the cephalic ganglia would provide the mechanistic details that underlie the signaling pathway that eventually form a long-range signaling stream that regulates posterior cell fate from the anterior. In addition, our RNA sequencing data can also help identify differentially regulated genes in the posterior of UBC9 RNAi animals, which can further our understanding of how positional and local cues affect regional maintenance of tissues. With this approach, we hope to understand and establish the larger molecular landscape driving regional cell fate decisions and uncover signaling pathways required for circumvention of intrinsic cellular control mechanisms to continue proliferating with DNA damage.

REFERENCES

1. Orford, K. W. & Scadden, D. T. Deconstructing stem cell self-renewal: genetic insights into cell-cycle regulation. *Nat. Rev. Genet.* **9**, 115–128 (2008).
2. Simons, B. D. & Clevers, H. Strategies for Homeostatic Stem Cell Self-Renewal in Adult Tissues. *Cell* **145**, 851–862 (2011).
3. Keller, G. & Snodgrass, R. Life span of multipotential hematopoietic stem cells in vivo. *J. Exp. Med.* **171**, 1407–1418 (1990).
4. Scott, E. W. Stem Cell Reviews and Reports: Adult Stem Cells and Tissue Regeneration Section. *Stem Cell Rev.* **13**, 2 (2017).
5. Alenzi, F. Q., Lotfy, M., Tamimi, W. G. & Wyse, R. K. H. Review: Stem cells and gene therapy. *Lab. Hematol. Off. Publ. Int. Soc. Lab. Hematol.* **16**, 53–73 (2010).
6. Gopinath, S. D. & Rando, T. A. Stem cell review series: aging of the skeletal muscle stem cell niche. *Aging Cell* **7**, 590–598 (2008).
7. Sylvester, K. G. & Longaker, M. T. Stem cells: review and update. *Arch. Surg. Chic. Ill 1960* **139**, 93–99 (2004).
8. Seruya, M. *et al.* Clonal population of adult stem cells: life span and differentiation potential. *Cell Transplant.* **13**, 93–101 (2004).
9. Auerbach, R. & Auerbach, W. Regional differences in the growth of normal and neoplastic cells. *Science* **215**, 127–34 (1982).
10. Auerbach, R., Morrissey, L. W. & Sidky, Y. A. Regional differences in the incidence and growth of mouse tumors following intradermal or subcutaneous inoculation. *Cancer Res* **38**, 1739–44 (1978).
11. Peiris, T. H. *et al.* Regional signals in the planarian body guide stem cell fate in the presence of genomic instability. *Development* **143**, 1697–709 (2016).
12. Petersen, C. P. & Reddien, P. W. Smed-betacatenin-1 is required for anteroposterior blastema polarity in planarian regeneration. *Science* **319**, 327–30 (2008).
13. Oviedo, N. J., Pearson, B. J., Levin, M. & Sanchez Alvarado, A. Planarian PTEN homologs regulate stem cells and regeneration through TOR signaling. *Model Mech* **1**, 131–43; discussion 141 (2008).
14. Kubai, L. & Auerbach, R. Regional differences in the growth of skin transplants. *Transplantation* **30**, 128–131 (1980).
15. Morrissey, L. W., Sidky, Y. A. & Auerbach, R. Regional differences in the growth of tumor cells injected intraperitoneally into syngeneic adult mice. *Cancer Res.* **40**, 2197–2201 (1980).
16. Newmark, P. A. & Alvarado, A. S. NOT YOUR FATHER'S PLANARIAN: A CLASSIC MODEL ENTERS THE ERA OF FUNCTIONAL GENOMICS. *Nat. Rev. Genet.* **3**, 210–219 (2002).
17. Lachiewicz, A. M., Berwick, M., Wiggins, C. L. & Thomas, N. E. Survival differences between patients with scalp or neck melanoma and those with

melanoma of other sites in the Surveillance, Epidemiology, and End Results (SEER) program. *Arch. Dermatol.* **144**, 515–521 (2008).
18. Tseng, W. H. & Martinez, S. R. Tumor Location Predicts Survival in Cutaneous Head and Neck Melanoma. *J. Surg. Res.* **167**, 192–198 (2011).
19. Park, S., Hong, B., Kim, C.-S. & Ahn, H. The impact of tumor location on prognosis of transitional cell carcinoma of the upper urinary tract. *J. Urol.* **171**, 621–625 (2004).
20. Dutta, R. *et al.* Effect of tumor location on survival in urinary bladder adenocarcinoma: A population-based analysis. *Urol. Oncol. Semin. Orig. Investig.* **34**, 531.e1-531.e6 (2016).
21. Ahmed, S. *et al.* Primary Tumor Location and Survival in the General Population With Metastatic Colorectal Cancer. *Clin. Colorectal Cancer* **17**, e201–e206 (2018).
22. Aoyama, T. *et al.* Clinical impact of tumor location on the colon cancer survival and recurrence: analyses of pooled data from three large phase III randomized clinical trials. *Cancer Med.* **6**, 2523–2530 (2017).
23. Artinyan, A. *et al.* The anatomic location of pancreatic cancer is a prognostic factor for survival. *HPB* **10**, 371–376 (2008).
24. Nowak, M. & Hammerschmidt, M. Ubc9 regulates mitosis and cell survival during zebrafish development. *Mol Biol Cell* **17**, 5324–36 (2006).
25. Epps, J. L. & Tanda, S. The Drosophila semushi mutation blocks nuclear import of bicoid during embryogenesis. *Curr. Biol. CB* **8**, 1277–1280 (1998).
26. Jones, D., Crowe, E., Stevens, T. A. & Candido, E. P. Functional and phylogenetic analysis of the ubiquitylation system in Caenorhabditis elegans: ubiquitin-conjugating enzymes, ubiquitin-activating enzymes, and ubiquitin-like proteins. *Genome Biol* **3**, RESEARCH0002 (2002).
27. Flotho, A. & Melchior, F. Sumoylation: a regulatory protein modification in health and disease. *Annu Rev Biochem* **82**, 357–85 (2013).
28. Wang, Y. & Dasso, M. SUMOylation and deSUMOylation at a glance. *J Cell Sci* **122**, 4249–52 (2009).
29. Pichler, A., Fatouros, C., Lee, H. & Eisenhardt, N. SUMO conjugation - a mechanistic view. *Biomol. Concepts* **8**, 13–36 (2017).
30. Johnson, E. S. Protein modification by SUMO. *Annu. Rev. Biochem.* **73**, 355–382 (2004).
31. Gareau, J. R. & Lima, C. D. The SUMO pathway: emerging mechanisms that shape specificity, conjugation and recognition. *Nat. Rev. Mol. Cell Biol.* **11**, 861–871 (2010).
32. Moschos, S. J. & Mo, Y.-Y. Role of SUMO/Ubc9 in DNA damage repair and tumorigenesis. *J. Mol. Histol.* **37**, 309–319 (2006).
33. Shen, Z., Pardington-Purtymun, P. E., Comeaux, J. C., Moyzis, R. K. & Chen, D. J. UBL1, a human ubiquitin-like protein associating with human RAD51/RAD52 proteins. *Genomics* **36**, 271–279 (1996).
34. Thomson, T. M. & Guerra-Rebollo, M. Ubiquitin and SUMO signalling in DNA repair. *Biochem. Soc. Trans.* **38**, 116–131 (2010).

35. Shrivastava, V., Pekar, M., Grosser, E., Im, J. & Vigodner, M. SUMO proteins are involved in the stress response during spermatogenesis and are localized to DNA double-strand breaks in germ cells. *Reprod. Camb. Engl.* **139**, 999–1010 (2010).
36. Ross, S., Best, J. L., Zon, L. I. & Gill, G. SUMO-1 modification represses Sp3 transcriptional activation and modulates its subnuclear localization. *Mol Cell* **10**, 831–42 (2002).
37. Geiss-Friedlander, R. & Melchior, F. Concepts in sumoylation: a decade on. *Nat Rev Mol Cell Biol* **8**, 947–56 (2007).
38. Hay, R. T. SUMO: a history of modification. *Mol Cell* **18**, 1–12 (2005).
39. Gill, G. Something about SUMO inhibits transcription. *Curr Opin Genet Dev* **15**, 536–41 (2005).
40. Eifler, K. & Vertegaal, A. C. O. Mapping the SUMOylated landscape. *FEBS J.* **282**, 3669–3680 (2015).
41. Tatham, M. H., Matic, I., Mann, M. & Hay, R. T. Comparative proteomic analysis identifies a role for SUMO in protein quality control. *Sci. Signal.* **4**, rs4 (2011).
42. Castorálová, M. *et al.* SUMO-2/3 conjugates accumulating under heat shock or MG132 treatment result largely from new protein synthesis. *Biochim. Biophys. Acta* **1823**, 911–919 (2012).
43. Bernier-Villamor, V., Sampson, D. A., Matunis, M. J. & Lima, C. D. Structural basis for E2-mediated SUMO conjugation revealed by a complex between ubiquitin-conjugating enzyme Ubc9 and RanGAP1. *Cell* **108**, 345–356 (2002).
44. Wilkinson, K. A. & Henley, J. M. Mechanisms, regulation and consequences of protein SUMOylation. *Biochem. J.* **428**, 133–145 (2010).
45. Kota, V. *et al.* SUMO Modification of the RNA-Binding Protein La Regulates Cell Proliferation and STAT3 Protein Stability. *Mol. Cell. Biol.* **38**, (2018).
46. Liu, X. *et al.* Hypothermia inhibits the proliferation of bone marrow-derived mesenchymal stem cells and increases tolerance to hypoxia by enhancing SUMOylation. *Int. J. Mol. Med.* **40**, 1631–1638 (2017).
47. Lv, X. *et al.* SUMO regulates somatic cyst stem cell maintenance and directly targets the Hedgehog pathway in adult Drosophila testis. *Development* **143**, 1655–62 (2016).
48. Du, L. *et al.* Role of SUMO activating enzyme in cancer stem cell maintenance and self-renewal. *Nat. Commun.* **7**, 12326 (2016).
49. Thiruvalluvan, M., Barghouth, P. G., Tsur, A., Broday, L. & Oviedo, N. J. SUMOylation controls stem cell proliferation and regional cell death through Hedgehog signaling in planarians. *Cell. Mol. Life Sci. CMLS* **75**, 1285–1301 (2018).
50. Tahmasebi, S., Ghorbani, M., Savage, P., Gocevski, G. & Yang, X. J. The SUMO conjugating enzyme Ubc9 is required for inducing and maintaining stem cell pluripotency. *Stem Cells* **32**, 1012–20 (2014).

51. Nacerddine, K. *et al.* The SUMO pathway is essential for nuclear integrity and chromosome segregation in mice. *Dev Cell* **9**, 769–79 (2005).
52. Saracco, S. A., Miller, M. J., Kurepa, J. & Vierstra, R. D. Genetic analysis of SUMOylation in Arabidopsis: conjugation of SUMO1 and SUMO2 to nuclear proteins is essential. *Plant Physiol* **145**, 119–34 (2007).
53. Yuan, H. *et al.* Small ubiquitin-related modifier paralogs are indispensable but functionally redundant during early development of zebrafish. *Cell Res* **20**, 185–96 (2010).
54. al-Khodairy, F., Enoch, T., Hagan, I. M. & Carr, A. M. The Schizosaccharomyces pombe hus5 gene encodes a ubiquitin conjugating enzyme required for normal mitosis. *J Cell Sci* **108 (Pt 2)**, 475–86 (1995).
55. Seufert, W., Futcher, B. & Jentsch, S. Role of a ubiquitin-conjugating enzyme in degradation of S- and M-phase cyclins. *Nature* **373**, 78–81 (1995).
56. Hayashi, T. *et al.* Ubc9 is essential for viability of higher eukaryotic cells. *Exp Cell Res* **280**, 212–21 (2002).
57. Demarque, M. D. *et al.* Sumoylation by Ubc9 regulates the stem cell compartment and structure and function of the intestinal epithelium in mice. *Gastroenterology* **140**, 286–96 (2011).
58. Saracco, S. A., Miller, M. J., Kurepa, J. & Vierstra, R. D. Genetic Analysis of SUMOylation in Arabidopsis: Conjugation of SUMO1 and SUMO2 to Nuclear Proteins Is Essential. *Plant Physiol.* **145**, 119–134 (2007).
59. Bialik, P. & Woźniak, K. SUMO proteases as potential targets for cancer therapy. *Postepy Hig. Med. Doswiadczalnej Online* **71**, 997–1004 (2017).
60. Han, Z.-J., Feng, Y.-H., Gu, B.-H., Li, Y.-M. & Chen, H. The post-translational modification, SUMOylation, and cancer (Review). *Int. J. Oncol.* **52**, 1081–1094 (2018).
61. Seeler, J.-S. & Dejean, A. SUMO and the robustness of cancer. *Nat. Rev. Cancer* **17**, 184–197 (2017).
62. Seeler, J. S., Bischof, O., Nacerddine, K. & Dejean, A. SUMO, the three Rs and cancer. *Curr. Top. Microbiol. Immunol.* **313**, 49–71 (2007).
63. Yang, X.-J. & Chiang, C.-M. Sumoylation in gene regulation, human disease, and therapeutic action. *F1000prime Rep.* **5**, 45 (2013).
64. Morris, J. R. & Garvin, A. J. SUMO in the DNA Double-Stranded Break Response: Similarities, Differences, and Cooperation with Ubiquitin. *J. Mol. Biol.* **429**, 3376–3387 (2017).
65. Garvin, A. J. & Morris, J. R. SUMO, a small, but powerful, regulator of double-strand break repair. *Philos. Trans. R. Soc. Lond. B. Biol. Sci.* **372**, (2017).
66. Schwertman, P., Bekker-Jensen, S. & Mailand, N. Regulation of DNA double-strand break repair by ubiquitin and ubiquitin-like modifiers. *Nat. Rev. Mol. Cell Biol.* **17**, 379–394 (2016).
67. Nie, M. & Boddy, M. N. Cooperativity of the SUMO and Ubiquitin Pathways in Genome Stability. *Biomolecules* **6**, (2016).
68. Pastink, A., Eeken, J. C. & Lohman, P. H. Genomic integrity and the repair of double-strand DNA breaks. *Mutat. Res.* **480**–**481**, 37–50 (2001).

69. McKinnon, P. J. Genome integrity and disease prevention in the nervous system. *Genes Dev.* **31**, 1180–1194 (2017).
70. Papamichos-Chronakis, M. & Peterson, C. L. Chromatin and the genome integrity network. *Nat. Rev. Genet.* **14**, 62–75 (2013).
71. Kovalenko, O. V. *et al.* Mammalian ubiquitin-conjugating enzyme Ubc9 interacts with Rad51 recombination protein and localizes in synaptonemal complexes. *Proc. Natl. Acad. Sci. U. S. A.* **93**, 2958–2963 (1996).
72. Shen, Z., Pardington-Purtymun, P. E., Comeaux, J. C., Moyzis, R. K. & Chen, D. J. Associations of UBE2I with RAD52, UBL1, p53, and RAD51 proteins in a yeast two-hybrid system. *Genomics* **37**, 183–186 (1996).
73. Ryu, H. *et al.* PIASy mediates SUMO-2/3 conjugation of poly(ADP-ribose) polymerase 1 (PARP1) on mitotic chromosomes. *J. Biol. Chem.* **285**, 14415–14423 (2010).
74. Sarangi, P. & Zhao, X. SUMO-mediated regulation of DNA damage repair and responses. *Trends Biochem Sci* **40**, 233–42 (2015).
75. Morris, J. R. *et al.* The SUMO modification pathway is involved in the BRCA1 response to genotoxic stress. *Nature* **462**, 886–890 (2009).
76. Park, M. A., Seok, Y.-J., Jeong, G. & Lee, J.-S. SUMO1 negatively regulates BRCA1-mediated transcription, via modulation of promoter occupancy. *Nucleic Acids Res.* **36**, 263–283 (2008).
77. Luo, K., Zhang, H., Wang, L., Yuan, J. & Lou, Z. Sumoylation of MDC1 is important for proper DNA damage response. *EMBO J.* **31**, 3008–3019 (2012).
78. Cremona, C. A., Sarangi, P. & Zhao, X. Sumoylation and the DNA Damage Response. *Biomolecules* **2**, 376–388 (2012).
79. Ouyang, K. J. *et al.* SUMO modification regulates BLM and RAD51 interaction at damaged replication forks. *PLoS Biol.* **7**, e1000252 (2009).
80. Shima, H. *et al.* Activation of the SUMO modification system is required for the accumulation of RAD51 at sites of DNA damage. *J Cell Sci* **126**, 5284–92 (2013).
81. Gentile, L., Cebrià, F. & Bartscherer, K. The planarian flatworm: an in vivo model for stem cell biology and nervous system regeneration. *Dis. Model. Mech.* **4**, 12–19 (2011).
82. Alvarado, A. The freshwater planarian Schmidtea mediterranea: embryogenesis, stem cells and regeneration. *Curr. Opin. Genet. Dev.* **13**, 438–444 (2003).
83. Roberts-Galbraith, R. H. & Newmark, P. A. On the organ trail: insights into organ regeneration in the planarian. *Curr. Opin. Genet. Dev.* **32**, 37–46 (2015).
84. Reddien, P. W. & Sanchez Alvarado, A. Fundamentals of planarian regeneration. *Annu Rev Cell Dev Biol* **20**, 725–57 (2004).
85. Rink, J. C. Stem cell systems and regeneration in planaria. *Dev Genes Evol* **223**, 67–84 (2013).
86. Oviedo, N. J., Nicolas, C. L., Adams, D. S. & Levin, M. Planarians: a versatile and powerful model system for molecular studies of regeneration, adult stem cell regulation, aging, and behavior. *CSH Protoc.* **2008**, pdb.emo101 (2008).

87. Eisenhoffer, G. T., Kang, H. & Sanchez Alvarado, A. Molecular analysis of stem cells and their descendants during cell turnover and regeneration in the planarian Schmidtea mediterranea. *Cell Stem Cell* **3**, 327–39 (2008).
88. Peiris, T. H., Garcia-Ojeda, M. E. & Oviedo, N. J. Alternative flow cytometry strategies to analyze stem cells and cell death in planarians. *Regen. Oxf* **3**, 123–35 (2016).
89. Zeng, A. *et al.* Prospectively Isolated Tetraspanin+ Neoblasts Are Adult Pluripotent Stem Cells Underlying Planaria Regeneration. *Cell* **173**, 1593-1608.e20 (2018).
90. Wurtzel, O. *et al.* A generic and cell-type-specific wound response precedes regeneration in planarians. *Dev. Cell* **35**, 632–645 (2015).
91. Solana, J. *et al.* Defining the molecular profile of planarian pluripotent stem cells using a combinatorial RNAseq, RNA interference and irradiation approach. *Genome Biol* **13**, R19 (2012).
92. Salo, E. *et al.* Planarian regeneration: achievements and future directions after 20 years of research. *Int J Dev Biol* **53**, 1317–27 (2009).
93. Wenemoser, D. & Reddien, P. W. Planarian regeneration involves distinct stem cell responses to wounds and tissue absence. *Dev Biol* **344**, 979–91 (2010).
94. Gurley, K. A. *et al.* Expression of secreted Wnt pathway components reveals unexpected complexity of the planarian amputation response. *Dev Biol* **347**, 24–39 (2010).
95. Peiris, T. H. *et al.* TOR signaling regulates planarian stem cells and controls localized and organismal growth. *J Cell Sci* **125**, 1657–65 (2012).
96. Newmark, P. A. & Sanchez Alvarado, A. Bromodeoxyuridine specifically labels the regenerative stem cells of planarians. *Dev Biol* **220**, 142–53 (2000).
97. King, R. S. & Newmark, P. A. In situ hybridization protocol for enhanced detection of gene expression in the planarian Schmidtea mediterranea. *BMC Dev Biol* **13**, 8 (2013).
98. Reddien, P. W., Oviedo, N. J., Jennings, J. R., Jenkin, J. C. & Sanchez Alvarado, A. SMEDWI-2 is a PIWI-like protein that regulates planarian stem cells. *Science* **310**, 1327–30 (2005).
99. Sanchez Alvarado, A. & Newmark, P. A. Double-stranded RNA specifically disrupts gene expression during planarian regeneration. *Proc Natl Acad Sci U A* **96**, 5049–54 (1999).
100. Rawls, S. M., Shah, H., Ayoub, G. & Raffa, R. B. 5-HT(1A)-like receptor activation inhibits abstinence-induced methamphetamine withdrawal in planarians. *Neurosci. Lett.* **484**, 113–117 (2010).
101. Raffa, R. B. & Valdez, J. M. Cocaine withdrawal in Planaria. *Eur. J. Pharmacol.* **430**, 143–145 (2001).
102. Farrell, M. S., Gilmore, K., Raffa, R. B. & Walker, E. A. Behavioral characterization of serotonergic activation in the flatworm Planaria. *Behav. Pharmacol.* **19**, 177–182 (2008).

103. Pagán, O. R. *et al.* Planarians in pharmacology: parthenolide is a specific behavioral antagonist of cocaine in the planarian Girardia tigrina. *Int. J. Dev. Biol.* **56**, 193–196 (2012).
104. Rawls, S. M. *et al.* Nicotine behavioral pharmacology: clues from planarians. *Drug Alcohol Depend.* **118**, 274–279 (2011).
105. Sacavage, S. *et al.* Withdrawal-like behavior in planarians is dependent on drug exposure duration. *Neurosci. Lett.* **439**, 84–88 (2008).
106. Robb, S. M., Ross, E. & Sanchez Alvarado, A. SmedGD: the Schmidtea mediterranea genome database. *Nucleic Acids Res* **36**, D599-606 (2008).
107. Robb, S. M., Gotting, K., Ross, E. & Sanchez Alvarado, A. SmedGD 2.0: The Schmidtea mediterranea genome database. *Genesis* **53**, 535–46 (2015).
108. Fincher, C. T., Wurtzel, O., Hoog, T. de, Kravarik, K. M. & Reddien, P. W. Cell type transcriptome atlas for the planarian Schmidtea mediterranea. *Science* eaaq1736 (2018). doi:10.1126/science.aaq1736
109. Rink, J. C., Gurley, K. A., Elliott, S. A. & Sanchez Alvarado, A. Planarian Hh signaling regulates regeneration polarity and links Hh pathway evolution to cilia. *Science* **326**, 1406–10 (2009).
110. Yazawa, S., Umesono, Y., Hayashi, T., Tarui, H. & Agata, K. Planarian Hedgehog/Patched establishes anterior-posterior polarity by regulating Wnt signaling. *Proc. Natl. Acad. Sci. U. S. A.* **106**, 22329–22334 (2009).
111. Oviedo, N. J., Nicolas, C. L., Adams, D. S. & Levin, M. Establishing and maintaining a colony of planarians. *CSH Protoc* **2008**, pdb prot5053 (2008).
112. Sánchez Alvarado, A. Stem cells and the Planarian Schmidtea mediterranea. *C. R. Biol.* **330**, 498–503 (2007).
113. Kang, H. & Sánchez Alvarado, A. Flow cytometry methods for the study of cell-cycle parameters of planarian stem cells. *Dev. Dyn. Off. Publ. Am. Assoc. Anat.* **238**, 1111–1117 (2009).
114. Pearson, B. J. *et al.* Formaldehyde-based whole-mount in situ hybridization method for planarians. *Dev Dyn* **238**, 443–50 (2009).
115. Peiris, T. H., Ramirez, D., Barghouth, P. G. & Oviedo, N. J. The Akt signaling pathway is required for tissue maintenance and regeneration in planarians. *BMC Dev Biol* **16**, 7 (2016).
116. Collins, A. R. The comet assay for DNA damage and repair: principles, applications, and limitations. *Mol. Biotechnol.* **26**, 249–261 (2004).
117. Sinha, M. *et al.* Restoring Systemic GDF11 Levels Reverses Age-Related Dysfunction in Mouse Skeletal Muscle. *Science* **344**, 649–652 (2014).
118. Guedelhoefer, O. C. & Sánchez Alvarado, A. Amputation induces stem cell mobilization to sites of injury during planarian regeneration. *Dev. Camb. Engl.* **139**, 3510–3520 (2012).
119. Brandl, H. *et al.* PlanMine--a mineable resource of planarian biology and biodiversity. *Nucleic Acids Res.* **44**, D764-773 (2016).
120. Broday, L. *et al.* The small ubiquitin-like modifier (SUMO) is required for gonadal and uterine-vulval morphogenesis in Caenorhabditis elegans. *Genes Dev.* **18**, 2380–2391 (2004).

121. Tanaka, K. *et al.* Characterization of a Fission Yeast SUMO-1 Homologue, Pmt3p, Required for Multiple Nuclear Events, Including the Control of Telomere Length and Chromosome Segregation. *Mol. Cell. Biol.* **19**, 8660–8672 (1999).
122. Wang, L. *et al.* SUMO2 is essential while SUMO3 is dispensable for mouse embryonic development. *EMBO Rep.* **15**, 878–885 (2014).
123. Apionishev, S., Malhotra, D., Raghavachari, S., Tanda, S. & Rasooly, R. S. The Drosophila UBC9 homologue lesswright mediates the disjunction of homologues in meiosis I. *Genes Cells Devoted Mol. Cell. Mech.* **6**, 215–224 (2001).
124. Andreou, A. M. & Tavernarakis, N. SUMOylation and cell signalling. *Biotechnol J* **4**, 1740–52 (2009).
125. Broday, L. The SUMO system in Caenorhabditis elegans development. *Int. J. Dev. Biol.* **61**, 159–164 (2017).
126. Sawicka, A. & Seiser, C. Histone H3 phosphorylation - a versatile chromatin modification for different occasions. *Biochimie* **94**, 2193–2201 (2012).
127. Hans, F. & Dimitrov, S. Histone H3 phosphorylation and cell division. *Oncogene* **20**, 3021–3027 (2001).
128. Hendzel, M. J. *et al.* Mitosis-specific phosphorylation of histone H3 initiates primarily within pericentromeric heterochromatin during G2 and spreads in an ordered fashion coincident with mitotic chromosome condensation. *Chromosoma* **106**, 348–360 (1997).
129. Meng, F., Qian, J., Yue, H., Li, X. & Xue, K. SUMOylation of Rb enhances its binding with CDK2 and phosphorylation at early G1 phase. *Cell Cycle* **15**, 1724–32 (2016).
130. Bellail, A. C., Olson, J. J. & Hao, C. SUMO1 modification stabilizes CDK6 protein and drives the cell cycle and glioblastoma progression. *Nat Commun* **5**, 4234 (2014).
131. Labbé, R. M. *et al.* A comparative transcriptomic analysis reveals conserved features of stem cell pluripotency in planarians and mammals. *Stem Cells Dayt. Ohio* **30**, 1734–1745 (2012).
132. Pellettieri, J. *et al.* Cell death and tissue remodeling in planarian regeneration. *Dev Biol* **338**, 76–85 (2010).
133. Tu, K. C., Pearson, B. J. & Sanchez Alvarado, A. TORC1 is required to balance cell proliferation and cell death in planarians. *Dev Biol* **365**, 458–69 (2012).
134. Beane, W. S., Morokuma, J., Adams, D. S. & Levin, M. A chemical genetics approach reveals H,K-ATPase-mediated membrane voltage is required for planarian head regeneration. *Chem Biol* **18**, 77–89 (2011).
135. Beane, W. S., Morokuma, J., Lemire, J. M. & Levin, M. Bioelectric signaling regulates head and organ size during planarian regeneration. *Development* **140**, 313–22 (2013).
136. McIlwain, D. R., Berger, T. & Mak, T. W. Caspase functions in cell death and disease. *Cold Spring Harb. Perspect. Biol.* **5**, a008656 (2013).

137. Elmore, S. Apoptosis: a review of programmed cell death. *Toxicol. Pathol.* **35**, 495–516 (2007).
138. Riedl, S. J. & Shi, Y. Molecular mechanisms of caspase regulation during apoptosis. *Nat. Rev. Mol. Cell Biol.* **5**, 897–907 (2004).
139. Porter, A. G. & Jänicke, R. U. Emerging roles of caspase-3 in apoptosis. *Cell Death Differ.* **6**, 99–104 (1999).
140. Lu, Z., Wu, H. & Mo, Y. Y. Regulation of bcl-2 expression by Ubc9. *Exp Cell Res* **312**, 1865–75 (2006).
141. Currie, K. W., Molinaro, A. M. & Pearson, B. J. Neuronal sources of hedgehog modulate neurogenesis in the adult planarian brain. *eLife* **5**, (2016).
142. Wang, I. E., Lapan, S. W., Scimone, M. L., Clandinin, T. R. & Reddien, P. W. Hedgehog signaling regulates gene expression in planarian glia. *eLife* **5**,
143. Dong, Z., Yang, T., Yang, Y., Dou, H. & Chen, G. DjhnRNPA2/B1-like gene is required for planarian regeneration and tissue homeostasis. *Gene* **633**, 9–16 (2017).
144. Barghouth, P. G., Thiruvalluvan, M., LeGro, M. & Oviedo, N. J. DNA damage and tissue repair: What we can learn from planaria. *Semin. Cell Dev. Biol.* (2018). doi:10.1016/j.semcdb.2018.04.013
145. Mladenov, E. & Iliakis, G. Induction and repair of DNA double strand breaks: the increasing spectrum of non-homologous end joining pathways. *Mutat. Res.* **711**, 61–72 (2011).
146. Rübe, C. E. *et al.* DNA double-strand break rejoining in complex normal tissues. *Int. J. Radiat. Oncol. Biol. Phys.* **72**, 1180–1187 (2008).
147. Sirbu, B. M. *et al.* ATR-p53 restricts homologous recombination in response to replicative stress but does not limit DNA interstrand crosslink repair in lung cancer cells. *PloS One* **6**, e23053 (2011).
148. Ammazzalorso, F., Pirzio, L. M., Bignami, M., Franchitto, A. & Pichierri, P. ATR and ATM differently regulate WRN to prevent DSBs at stalled replication forks and promote replication fork recovery. *EMBO J.* **29**, 3156–3169 (2010).
149. Rodríguez, J. A. Interplay between nuclear transport and ubiquitin/SUMO modifications in the regulation of cancer-related proteins. *Semin. Cancer Biol.* **27**, 11–19 (2014).
150. Ptak, C. & Wozniak, R. W. SUMO and Nucleocytoplasmic Transport. *Adv. Exp. Med. Biol.* **963**, 111–126 (2017).
151. Gareau, J. R., Reverter, D. & Lima, C. D. Determinants of small ubiquitin-like modifier 1 (SUMO1) protein specificity, E3 ligase, and SUMO-RanGAP1 binding activities of nucleoporin RanBP2. *J. Biol. Chem.* **287**, 4740–4751 (2012).
152. Mahajan, R., Gerace, L. & Melchior, F. Molecular characterization of the SUMO-1 modification of RanGAP1 and its role in nuclear envelope association. *J. Cell Biol.* **140**, 259–270 (1998).
153. Reverter, D. & Lima, C. D. Insights into E3 ligase activity revealed by a SUMO-RanGAP1-Ubc9-Nup358 complex. *Nature* **435**, 687–692 (2005).
154. Kurtzman, A. L. & Schechter, N. Ubc9 interacts with a nuclear localization signal and mediates nuclear localization of the paired-like homeobox protein

Vsx-1 independent of SUMO-1 modification. *Proc Natl Acad Sci U A* **98**, 5602–7 (2001).
155. Wu, C. S. *et al.* SUMOylation of ATRIP potentiates DNA damage signaling by boosting multiple protein interactions in the ATR pathway. *Genes Dev* **28**, 1472–84 (2014).
156. Li, P. *et al.* Akt-phosphorylated mitogen-activated kinase-activating death domain protein (MADD) inhibits TRAIL-induced apoptosis by blocking Fas-associated death domain (FADD) association with death receptor 4. *J. Biol. Chem.* **285**, 22713–22722 (2010).
157. Mo, Y., Williams, C. & Miller, C. A. DENN/MADD/IG20 alternative splicing changes and cell death in Alzheimer's disease. *J. Mol. Neurosci. MN* **48**, 97–110 (2012).
158. Del Villar, K. & Miller, C. A. Down-regulation of DENN/MADD, a TNF receptor binding protein, correlates with neuronal cell death in Alzheimer's disease brain and hippocampal neurons. *Proc. Natl. Acad. Sci. U. S. A.* **101**, 4210–4215 (2004).
159. Jayarama, S. *et al.* MADD is a downstream target of PTEN in triggering apoptosis. *J. Cell. Biochem.* **115**, (2014).
160. Turner, A. *et al.* MADD knock-down enhances doxorubicin and TRAIL induced apoptosis in breast cancer cells. *PloS One* **8**, e56817 (2013).
161. Bi, W. *et al.* MADD promotes the survival of human lung adenocarcinoma cells by inhibiting apoptosis. *Oncol. Rep.* **29**, 1533–1539 (2013).
162. Schievella, A. R., Chen, J. H., Graham, J. R. & Lin, L. L. MADD, a novel death domain protein that interacts with the type 1 tumor necrosis factor receptor and activates mitogen-activated protein kinase. *J. Biol. Chem.* **272**, 12069–12075 (1997).
163. Mulherkar, N., Prasad, K. V. & Prabhakar, B. S. MADD/DENN splice variant of the IG20 gene is a negative regulator of caspase-8 activation. Knockdown enhances TRAIL-induced apoptosis of cancer cells. *J. Biol. Chem.* **282**, 11715–11721 (2007).
164. Wang, S. & El-Deiry, W. S. TRAIL and apoptosis induction by TNF-family death receptors. *Oncogene* **22**, 8628–8633 (2003).
165. Child, C. M. Physiological isolation of parts and fission in planaria. *Arch. Für Entwicklungsmechanik Org.* **30**, 159–205 (1910).
166. Sakurai, T. *et al.* The planarian P2X homolog in the regulation of asexual reproduction. *Int. J. Dev. Biol.* **56**, 173–182 (2012).
167. Best, J. B., Goodman, A. B. & Pigon, A. Fissioning in planarians: control by the brain. *Science* **164**, 565–566 (1969).
168. Best, J. B., Abelein, M., Kreutzer, E. & Pigon, A. Cephalic mechanism for social control of fissioning in planarians: III. Central nervous system centers of facilitation and inhibition. *J. Comp. Physiol. Psychol.* **89**, 923–932 (1975).
169. Malinowski, P. T. *et al.* Mechanics dictate where and how freshwater planarians fission. *Proc. Natl. Acad. Sci. U. S. A.* **114**, 10888–10893 (2017).
170. Cochet-Escartin, O., Mickolajczyk, K. J. & Collins, E.-M. S. Scrunching: a novel escape gait in planarians. *Phys. Biol.* **12**, 056010 (2015).

171. Cochet-Escartin, O., Carter, J. A., Chakraverti-Wuerthwein, M., Sinha, J. & Collins, E.-M. S. Slo1 regulates ethanol-induced scrunching in freshwater planarians. *Phys. Biol.* **13**, 055001 (2016).
172. Wenemoser, D., Lapan, S. W., Wilkinson, A. W., Bell, G. W. & Reddien, P. W. A molecular wound response program associated with regeneration initiation in planarians. *Genes Dev* **26**, 988–1002 (2012).
173. Currie, K. W. *et al.* HOX gene complement and expression in the planarian Schmidtea mediterranea. *EvoDevo* **7**, 7 (2016).
174. Giribet, G. Assembling the lophotrochozoan (=spiralian) tree of life. *Philos. Trans. R. Soc. Lond. B. Biol. Sci.* **363**, 1513–1522 (2008).
175. Gehrke, A. R. & Srivastava, M. Neoblasts and the evolution of whole-body regeneration. *Curr. Opin. Genet. Dev.* **40**, 131–137 (2016).
176. Yukita, A. *et al.* Ubc9 negatively regulates BMP-mediated osteoblastic differentiation in cultured cells. *Bone* **50**, 1092–9 (2012).
177. Myatt, S. S. *et al.* SUMOylation inhibits FOXM1 activity and delays mitotic transition. *Oncogene* **33**, 4316–29 (2014).
178. Chen, Y. & Struhl, G. Dual roles for patched in sequestering and transducing Hedgehog. *Cell* **87**, 553–563 (1996).
179. Ma, G. *et al.* Regulation of Smoothened Trafficking and Hedgehog Signaling by the SUMO Pathway. *Dev. Cell* **39**, 438–451 (2016).
180. Han, L., Pan, Y. & Wang, B. Small ubiquitin-like Modifier (SUMO) modification inhibits GLI2 protein transcriptional activity in vitro and in vivo. *J. Biol. Chem.* **287**, 20483–20489 (2012).
181. Cox, B., Briscoe, J. & Ulloa, F. SUMOylation by Pias1 regulates the activity of the Hedgehog dependent Gli transcription factors. *PloS One* **5**, e11996 (2010).
182. Zhang, J., Liu, Y., Jiang, K. & Jia, J. SUMO regulates the activity of Smoothened and Costal-2 in Drosophila Hedgehog signaling. *Sci. Rep.* **7**, 42749 (2017).
183. Wang, X. *et al.* Anti-proliferation of breast cancer cells with itraconazole: Hedgehog pathway inhibition induces apoptosis and autophagic cell death. *Cancer Lett.* **385**, 128–136 (2017).
184. Lu, F. L. *et al.* Sonic hedgehog antagonists induce cell death in acute myeloid leukemia cells with the presence of lipopolysaccharides, tumor necrosis factor-α, or interferons. *Invest. New Drugs* **31**, 823–832 (2013).
185. Thibert, C. *et al.* Inhibition of neuroepithelial patched-induced apoptosis by sonic hedgehog. *Science* **301**, 843–846 (2003).
186. Mazumdar, T., DeVecchio, J., Agyeman, A., Shi, T. & Houghton, J. A. Blocking Hedgehog survival signaling at the level of the GLI genes induces DNA damage and extensive cell death in human colon carcinoma cells. *Cancer Res.* **71**, 5904–5914 (2011).
187. Guerrero, I. & Ruiz i Altaba, A. Development. Longing for ligand: hedgehog, patched, and cell death. *Science* **301**, 774–776 (2003).

188. Currie, K. W. & Pearson, B. J. Transcription factors lhx1/5-1 and pitx are required for the maintenance and regeneration of serotonergic neurons in planarians. *Development* **140**, 3577–88 (2013).
189. Wurtzel, O., Oderberg, I. M. & Reddien, P. W. Planarian Epidermal Stem Cells Respond to Positional Cues to Promote Cell-Type Diversity. *Dev. Cell* **40**, 491-504.e5 (2017).
190. Zhu, S. J. & Pearson, B. J. (Neo)blast from the past: new insights into planarian stem cell lineages. *Curr. Opin. Genet. Dev.* **40**, 74–80 (2016).
191. Molinaro, A. M. & Pearson, B. J. In silico lineage tracing through single cell transcriptomics identifies a neural stem cell population in planarians. *Genome Biol.* **17**, 87 (2016).
192. van Wolfswinkel, J. C., Wagner, D. E. & Reddien, P. W. Single-cell analysis reveals functionally distinct classes within the planarian stem cell compartment. *Cell Stem Cell* **15**, 326–39 (2014).
193. Rozario, T. & Newmark, P. A. Prospecting for Planarian Pluripotency. *Cell* **173**, 1566–1567 (2018).
194. Wagner, D. E., Wang, I. E. & Reddien, P. W. Clonogenic neoblasts are pluripotent adult stem cells that underlie planarian regeneration. *Science* **332**, 811–6 (2011).
195. Hsieh, Y.-H. *et al.* Induction of cell cycle arrest, DNA damage, and apoptosis by nimbolide in human renal cell carcinoma cells. *Tumour Biol. J. Int. Soc. Oncodevelopmental Biol. Med.* **36**, 7539–7547 (2015).
196. Yedjou, C. G., Tchounwou, H. M. & Tchounwou, P. B. DNA Damage, Cell Cycle Arrest, and Apoptosis Induction Caused by Lead in Human Leukemia Cells. *Int. J. Environ. Res. Public. Health* **13**, ijerph13010056 (2015).
197. Kastan, M. B. & Kuerbitz, S. J. Control of G1 arrest after DNA damage. *Environ. Health Perspect.* **101 Suppl 5**, 55–58 (1993).
198. Zhu, S. J. & Pearson, B. J. The Retinoblastoma pathway regulates stem cell proliferation in freshwater planarians. *Dev Biol* **373**, 442–52 (2013).
199. Davis, J. N., McCabe, M. T., Hayward, S. W., Park, J. M. & Day, M. L. Disruption of Rb/E2F Pathway Results in Increased Cyclooxygenase-2 Expression and Activity in Prostate Epithelial Cells. *Cancer Res.* **65**, 3633–3642 (2005).
200. Vyas, R. *et al.* RNF4 is required for DNA double-strand break repair *in vivo*. *Cell Death Differ.* **20**, 490–502 (2013).
201. de Sousa, N., Rodríguez-Esteban, G., Rojo-Laguna, J. I., Saló, E. & Adell, T. Hippo signaling controls cell cycle and restricts cell plasticity in planarians. *PLoS Biol.* **16**, e2002399 (2018).
202. Jordan, D. M., Ramensky, V. E. & Sunyaev, S. R. Human allelic variation: perspective from protein function, structure, and evolution. *Curr. Opin. Struct. Biol.* **20**, 342–350 (2010).
203. Zhang, J., Webb, D. M. & Podlaha, O. Accelerated protein evolution and origins of human-specific features: Foxp2 as an example. *Genetics* **162**, 1825–1835 (2002).

204. Lopez-Bigas, N., De, S. & Teichmann, S. A. Functional protein divergence in the evolution of Homo sapiens. *Genome Biol.* **9**, R33 (2008).
205. Sakurai, T. *et al.* The planarian P2X homolog in the regulation of asexual reproduction. *Int. J. Dev. Biol.* **56**, 173–182 (2012).
206. Sureda-Gómez, M., Martín-Durán, J. M. & Adell, T. Localization of planarian β-CATENIN-1 reveals multiple roles during anterior-posterior regeneration and organogenesis. *Dev. Camb. Engl.* **143**, 4149–4160 (2016).
207. Reuter, H. *et al.* B-catenin-dependent control of positional information along the AP body axis in planarians involves a teashirt family member. *Cell Rep.* **10**, 253–265 (2015).
208. Sureda-Gómez, M., Pascual-Carreras, E. & Adell, T. Posterior Wnts Have Distinct Roles in Specification and Patterning of the Planarian Posterior Region. *Int. J. Mol. Sci.* **16**, 26543–26554 (2015).
209. Scimone, M. L., Cote, L. E., Rogers, T. & Reddien, P. W. Two FGFRL-Wnt circuits organize the planarian anteroposterior axis. *eLife* **5**, (2016).
210. Adler, C. E. & Sánchez Alvarado, A. Types or States? Cellular Dynamics and Regenerative Potential. *Trends Cell Biol.* **25**, 687–696 (2015).
211. Elliott, S. A. & Sanchez Alvarado, A. The history and enduring contributions of planarians to the study of animal regeneration. *Wiley Interdiscip Rev Dev Biol* **2**, 301–26 (2013).